





This is to certify that the

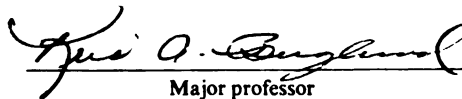
dissertation entitled

A Study of the Applicability of Fluorescence  
Spectroscopy in the Development of A  
Supersaturation Sensor and in Measuring Kinetic  
Parameters in Batch Crystallization Processes  
presented by

Sanjay K. Yedur

has been accepted towards fulfillment  
of the requirements for

Ph.D. degree in Chemical Engineering

  
Major professor

Date June 13, 1996



**PLACE IN RETURN BOX to remove this checkout from your record.  
TO AVOID FINES return on or before date due.**

DATE DUE	DATE DUE	DATE DUE
_____	_____	_____
_____	_____	_____
_____	_____	_____
_____	_____	_____
_____	_____	_____
_____	_____	_____
_____	_____	_____

**MSU is An Affirmative Action/Equal Opportunity Institution**

c:\crl\data\due.pm3-p.1

**A STUDY OF THE APPLICABILITY OF FLUORESCENCE  
SPECTROSCOPY IN THE DEVELOPMENT OF A SUPERSATURATION  
SENSOR AND IN MEASURING KINETIC PARAMETERS IN BATCH  
CRYSTALLIZATION PROCESSES**

**By**

**Sanjay Krishnamurthy Yedur**

**A DISSERTATION**

**Submitted to  
Michigan State University  
in partial fulfillment of the requirements for the degree of**

**DOCTOR OF PHILOSOPHY**

**Department of Chemical Engineering**

**1996**



# **ABSTRACT**

## **A STUDY OF THE APPLICABILITY OF FLUORESCENCE SPECTROSCOPY IN THE DEVELOPMENT OF A SUPERSATURATION SENSOR AND IN MEASURING KINETIC PARAMETERS IN BATCH CRYSTALLIZATION PROCESSES**

By

Sanjay Krishnamurthy Yedur

The main parameters of interest in a crystallization process are the crystal size distribution (CSD) and the purity of the product. These parameters depend upon the supersaturation in the crystallizer. A novel technique is presented that uses fluorescence spectroscopy to measure the supersaturation in crystallizing solutions. In its most fundamental terms, supersaturation is dependent on the activity of the solute in solution which is a strong function of the solution structure. Fluorescence spectroscopy depends on the solution structure and provides a more accurate measurement of supersaturation than current techniques that assume ideality of the crystallizing solution.

The fluorescent properties of a probe, pyranine, were used to provide supersaturation measurements in aqueous citric acid solutions. The solvatochromic nature of the emission of pyranine provides an excellent calibration curve for supersaturation measurements. While pyranine performs very satisfactorily, its use in food and pharmaceutical processes is limited since it is not listed as food grade. For such applications, all dyes listed as food grade were screened for their potential use. Three of the seven, brilliant blue, fast green, and allura red were found suitable for use. Fluorescence spectra of these dyes in sucrose solutions are presented and calibration curves drawn to show their ability to measure supersaturation.

For use as an *in situ* sensor, it is desirable to immobilize the probes onto a surface so that an immersible sensor can be constructed. Brilliant blue is immobilized on anionic cellulose acetate membranes for this purpose. However, the chemistry involved in the immobilization causes some loss of sensitivity of the probes that potentially reduces their effectiveness.

The desupersaturation curves of crystallizing solutions yield information on the kinetic parameters involved during the nucleation and growth of the crystals. The fluorescence of pyranine was used to generate such curves for citric acid during seeded isothermal desupersaturation experiments. A model is described that can be used to fit these curves and provide the kinetic constants of nucleation and growth.

Future research objectives involve the development of an apparatus that can contact the probe with the crystallizing solution in an *ex situ* manner, to alleviate any concerns of contamination of the crystals by the probe. Some basic experiments along with other recommendations for further investigations are provided.

**To my family, for their support through the years**

# Acknowledgments

First and foremost, thanks are due to my mentor, Dr. Kris Berglund, for the encouragement, support and guidance he has provided to me over the last few years. My association with him provided me not only with a greater appreciation of engineering research, but also gave me valuable insight into the workings of a university.

Thanks are also due to the members of my dissertation committee, Drs. Daina Briedis, Alec Scranton, and Gary Blanchard for their time and the interest that they took in my project.

Special thanks are due to my colleagues and friends Laurie Ruiz, Dilum Dunuwila, Everson Miranda, Marketta Uusi-Penttilä and numerous others present in Kris's lab at different times during my tenure. Out of the many, I would like to mention some special people. Laurie Ruiz, always a great friend, provided a smooth way out of all the red tape that I had to go through in my years here. A pleasant chat with her would help put all the pitfalls I encountered while conducting research into proper perspective. Dilum, my colleague and friend since I came here to graduate school, has always been the person I call with any problem in my research, and he has never disappointed me! And finally Everson, now a faculty member in Brazil, whose most notable achievement, in my opinion, was to get me involved in running!

A special word about my cousin Anupama, presently at UC, San Diego. Over the years, she has provided me with many unforgettable anecdotes from her own chaotic life and that of those around her. Her frequent misadventures, which invariably resulted in a frantic phone call for support and advice, provided me with much needed respites from the tedium of graduate school. A self confessed drama queen, she constantly

courts non-traditional situations that get her into trouble and results in a great source of entertainment for me. Anu - thanks for everything.

My friends Sam Larson and Jim Dearing deserve special mention too. Sam was the first person that I interacted with here at Michigan State University. She helped me tremendously while I was suffering through a culture shock and has been a great friend all these years. In their household, I am treated as a member of the family, and I tremendously appreciate their friendship.

Many other people influenced me in different ways. My good friends Arvind Mathur, Himanshu Asthana, and Sanjay Padaki deserve special thanks for their help and support whenever I needed them. James 'Moe' Benda introduced me to, among other things, the beautiful Upper Peninsula of Michigan. In my first term here, we spent many a philosophical hour over coffee while ostensibly at work! Rik ter Veen and Marketta Uusi-Penttilä are completely responsible for getting me interested in the game of bridge. Shalini Mathur and Savi Dunuwila provided me with sound non-technical advice (since they were smart enough never to be afflicted with an engineering education) whenever I needed it, and I am most grateful to them for that. Astrid Baviere, Raul Tomas, Takayo Sugimoto, and Grigoris Papakostas are among the special people I met during the Foreign Teaching Assistant Program, and remain good friends.

To all these people -a big thank you from the bottom of my heart.

# Table of Contents

List of Tables.....	x
List of Figures.....	xi
Chapter 1	
INTRODUCTION.....	1
1.1 Background.....	1
1.2 The role of supersaturation in crystallization.....	2
1.3 Fluorescence spectroscopy.....	9
1.4 Overview of this work.....	13
1.5 References .....	17
Chapter 2	
USE OF FLUORESCENCE SPECTROSCOPY IN CONCENTRATION AND SUPERSATURATION MEASUREMENTS IN CITRIC ACID SOLUTIONS.....	19
2.1 Background.....	19
2.2 Materials and Methods.....	22
2.3 Results and Discussion.....	25
2.4 Conclusions.....	34
2.5 References .....	36
Chapter 3	
A NOVEL ANALYTICAL USE OF FOOD GRADE COLORS: SPECTROSCOPIC MEASUREMENT OF CONCENTRATION AND SUPERSATURATION IN SUCROSE SOLUTIONS .....	38
3.1 Background.....	38
3.2 Materials and Methods.....	42
3.2.1 Absorption experiments.....	43
3.2.2 Fluorescence experiments .....	43
3.2.3 Immobilization of the probes.....	43

3.3 Results and Discussion.....	44
3.3.1 Results with the ‘free’ dye in solution .....	44
3.3.2 Results with the immobilized dyes .....	54
3.4 Conclusions.....	58
3.5 References .....	58

## Chapter 4

A SOL-GEL BASED FLUORESCENCE SENSOR FOR CONCENTRATION MEASUREMENTS IN SUCROSE SOLUTIONS.....	60
4.1 Background.....	60
4.2 Materials and Methods.....	61
4.2.1 Film preparation .....	63
4.2.2 Entrapment of the chlorin .....	63
4.3 Results and Discussion.....	64
4.3.1 Sol-gel films.....	64
4.3.2 Free chlorin in aqueous solutions.....	64
4.3.3 Entrapment of the chlorin .....	64
4.4 References .....	70

## Chapter 5

ON THE APPLICATION OF FLUORESCENCE SPECTROSCOPY TO MEASURE THE DESUPERSATURATION OF CITRIC ACID SOLUTIONS.....	72
5.1 Background.....	72
5.2 Materials and Methods.....	73
5.3 Results and Discussion.....	75
5.3.1 The desupersaturation curve.....	78
5.3.2 Effect of seed weight.....	82
5.3.3 Effect of temperature .....	85
5.3.4 Effect of probe concentration.....	87

5.3.5 Measurement of kinetic parameters.....	88
5.4 Conclusions.....	90
5.5 References .....	92
<b>Chapter 6</b>	
MODELS FOR THE EXTRACTION OF KINETIC PARAMETERS FROM THE DESUPERSATURATION CURVES.....	93
6.1 Background.....	93
6.2 Development of the model .....	96
6.3 Conclusions.....	100
6.4 References .....	101
<b>Chapter 7</b>	
CONTINUING INVESTIGATIONS AND RECOMMENDATIONS FOR FUTURE WORK.....	102
7.1 Background.....	102
7.2 Continuing Investigations.....	103
7.2.1 Estimation of kinetic parameters .....	103
7.2.2 <i>Ex situ</i> monitoring of concentration .....	103
7.3 Recommendations for future work.....	107
7.3.1 ATR Fluorescence .....	111
7.4 Conclusions.....	112
7.5 References .....	112
<b>Chapter 8</b>	
CONCLUSIONS.....	114
APPENDIX.....	116



## List of Tables

Table 3.1	Selected physical properties of FD&C colors.....	41
Table A1	Raw data for Figure 2.4.....	116
Table A2	Raw data for Figure 2.5.....	116
Table A3	Raw data for Figure 2.6.....	117
Table A4	Raw data for Figure 2.7.....	117
Table A5	Raw data for Figure 2.8.....	118
Table A6	Raw data for Figure 3.6.....	118
Table A7	Raw data for Figure 3.7.....	119
Table A8	Raw data for Figure 3.9.....	119
Table A9	Raw data for Figure 4.4.....	120
Table A10	Raw data for Figure 5.2.....	121
Table A11	Raw data for Figure 5.3.....	123
Table A12	Raw data for Figure 5.4.....	125
Table A13	Raw data for Figure 5.5.....	129
Table A14	Raw data for Figure 5.6.....	133

# List of Figures

Figure 1.1 Information feedback diagram illustrating the importance of supersaturation and the interaction between size distribution and kinetics resulting from the constraint of the mass balance. ....	4
Figure 1.2 Schematic energy level diagram showing the potential energy wells of the ground state and the first electronic state for a diatomic molecule. ....	11
Figure 1.3 Schematic Energy Level (Jablonski) diagram for a diatomic molecule.....	12
Figure 2.1 Molecular structure of Pyranine (trisodium salt of 8-hydroxy-1,3,6-pyrenetrisulfonic acid) .....	21
Figure 2.2 Excited state kinetics of pyranine .....	23
Figure 2.3. Emission spectra of pyranine in citric acid solutions of 10, 30, 50, and 70 weight percents; taken at 25 °C. ....	27
Figure 2.4 Peak Intensity Ratio (ratio of emission peak intensities at 440 nm and 510 nm) as a function of citric acid concentration.....	29
Figure 2.5 Peak Intensity Ratio (ratio of peak intensities at 440 nm and 510 nm) versus the supersaturation $S$ (defined as $S=(c-c^*)/c^*$ , where $c$ and $c^*$ are the actual concentration and the saturation concentration respectively). ....	30
Figure 2.6 pH of aqueous citric acid solutions as a function of citric acid concentration. .	32
Figure 2.7 Comparison of PIR's (ratio of peak intensities at 440 nm and 510 nm) obtained from pyranine emission in citric acid solutions as a function of pH of the solutions to the PIR's obtained from pyranine emission in HCl-NaOH solutions of varying pH's. Closed circles: Citric acid solutions; open circles: HCl-NaOH solutions.....	33
Figure 2.8 Corrected PIR (corrected for pH effects) versus citric acid concentration (wt%). The arrow indicates the solubility at 25 °C. ....	35

Figure 3.1 Molecular structures of the seven FD&C colors. ....	40
Figure 3.2 Schematic diagram of the apparatus used to measure the fluorescence from the immobilized sensor that is immersed in a crystallizer. 1) Source. 2) Collimating lens. 3) Monochromators. 4) Jacketed crystallizer. 5) Immobilized probe assembly. 6) Bifurcated fiber optic. 7) Stirrer. 8) PMT Detector. 9) Computer. ....	45
Figure 3.3 Absorption spectra of the FD&C colors. The concentrations of each in aqueous solution are: FD&C Blue No. 1 and FD&C Green No. 3: 5 ppm; FD&C Blue No. 2 and FD&C Red No. 40: 10 ppm; FD&C Blue No. 2, FD&C Red No. 3, FD&C Yellow No. 5, and FD&C Yellow No. 6: 20 ppm. ....	47
Figure 3.4 Emission spectra of FD&C Red No. 40 in sucrose solutions of different concentrations (expressed as wt%). All spectra recorded at room temperature (25 °C). Excitation wavelength: 500 nm. ....	49
Figure 3.5 Emission spectra of FD&C Green No. 3 in sucrose solutions of different concentrations (expressed as wt%). All spectra recorded at room temperature (25 °C). Excitation wavelength: 420 nm. ....	50
Figure 3.6 Calibration curve showing the relation between the Peak Intensity Ratio (defined as the ratio of the peak intensities at 662 nm to that at 515 nm) and sucrose concentration for FD&C Green No. 3. ....	52
Figure 3.7 Calibration curve showing the relation between the Peak Intensity Ratio (defined as the ratio of the peak intensities at 587 nm in each sample to the peak intensity at the same wavelength in 0% sucrose solution) and sucrose concentration for FD&C Red No. 40. Inset shows the parameters for an exponential fit to the curve. ....	53
Figure 3.8 Emission spectra of FD&C Blue No.1 in sucrose solutions of different concentrations (expressed as wt%). The dye molecules are immobilized onto an anion exchange membrane. All spectra recorded at room temperature. Excitation wavelength: 400 nm. ....	56
Figure 3.9 Calibration curve showing the relation between the Peak Intensity Ratio (defined as the ratio of the peak intensities at 664 nm to that at 615 nm) and sucrose concentration for the immobilized FD&C Blue No.1. ....	57
Figure 4.1 Chemical structure of Octaethyl chlorin diol. ....	62

Figure 4.2 Emission spectrum of free chlorin in solution in different sucrose solutions. All spectra collected at room temperature. ....	65
Figure 4.3 Changes in emission spectra of chlorin embedded in a titanium carboxylate thin film in various aqueous sucrose solutions; all spectra collected at room temperature.....	67
Figure 4.4 Calibration curve showing a linear relationship between the Peak Intensity Ratio (defined as the ratio of the intensities of the peaks at 646 nm and 673 nm) and sucrose concentration. ....	69
Figure 5.1 Emission spectra of pyranine over the course of a seeded isothermal (25 °C) citric acid batch crystallization. Ten spectra are shown here, each at an interval of 10 minutes from t = 0 minute to t=90 minutes. These ten are culled from the ninety spectra collected at intervals of 1 minute.....	77
Figure 5.2 Typical desupersaturation curve of a seeded citric acid batch crystallization experiments. The experimental conditions were as follows: Temperature = 25 °C, initial supersaturation ( $c/c^*$ ) = 1.2, agitator speed = 400 rpm, probe (pyranine) concentration = $1.0\text{e-}05$ M, seeds (average size 660 microns) = 3 gms, excitation wavelength = 365 nm. ....	79
Figure 5.3 Backscattered excitation light during the desupersaturation experiment as a function of time. The experimental conditions are exactly the same as those described in Figure 5.2. ....	81
Figure 5.4 Effect of seed amount on the desupersaturation curve of seeded citric acid batch crystallization experiments. The ordinate are normalized so that all curves start at the same point, since initial supersaturation ( $c/c^* = 1.2$ ), is the same in all three cases. Other experimental conditions: Temperature = 25 °C, agitator speed = 400 rpm, probe (pyranine) concentration = $1.0\text{e-}05$ M, seeds (average size 660 microns) = 3 gms, excitation wavelength = 365 nm.....	83
Figure 5.5 Effect of temperature on the desupersaturation curve of seeded citric acid batch crystallization experiments. The ordinate are normalized so that all curves start at the same point, since initial supersaturation ( $c/c^* = 1.2$ ), is the same in all three cases. Other experimental conditions: agitator speed = 400 rpm, probe (pyranine) concentration = $1.0\text{e-}05$ M, seeds (average size 660 microns) = 3 gms, excitation wavelength = 365 nm. ....	86

Figure 5.6 Effect of varying the probe (pyranine) concentration on the desupersaturation curve of seeded citric acid batch crystallization experiments. The ordinate shows the relative supersaturation  $\{(c/c^*)-1\}$  that is the same in all three cases. Other experimental conditions: temperature = 25 °C, agitator speed = 400 rpm, seeds (average size 660 microns) = 3 gms, excitation wavelength = 365 nm.. 89

Figure 5.7 Control policy projected to maximize the mean size of a crystal size distribution from a cooling batch crystallization process [7]. The policy is based on maintaining a constant supersaturation during the course of the crystallization. The supersaturation is defined by either of the following two equations:

$$\text{Supersaturation} = \Delta \text{PIR} = \text{PIR} - \text{PIR}^*$$

$$\text{Supersaturation} = \sigma = \frac{\Delta \text{PIR}}{\text{PIR}^*}$$

where PIR is the ratio of emission peaks of a probe such as pyranine in a supersaturated solution, and PIR\* is the same ratio in a saturated solution. ... 91

Figure 7.1 Schematic of a conventional Flow Injection System. C = carrier stream, R = reagent stream, S = sample, D = detector, P = pump, and W = waste stream. 104

Figure 7.2 Schematic of a reverse Flow Injection System. C = carrier stream, R = reagent stream, S = sample, D = detector, P = pump, and W = waste stream. .... 104

Figure 7.3 Schematic of the apparatus used to measure the concentration of a crystallizing solution *ex situ*. The top view of the flow cell is shown on the upper left hand corner. .... 106

Figure 7.4 Typical desupersaturation curve of a seeded citric acid batch crystallization experiment using the apparatus shown in Figure 7.3. The experimental conditions were as follows: Temperature = 25 °C, initial supersaturation ( $c/c^*$ ) = 1.2, agitator speed = 400 rpm, probe (pyranine) concentration = 1.0e-05 M, seeds (average size 660 microns) = 3 gms, excitation wavelength = 365 nm. The ordinate shows the Peak Intensity Ratio, defined as the ratio of the intensities of the emission peaks of pyranine at 449 nm and 520 nm. .... 108

# **Chapter 1**

## **INTRODUCTION**

### **1.1 Background**

Crystallization from solution is one of the most widely used unit operations in the chemical process industry. It ranks second behind distillation in use as a separation process. Almost all processes that require a final purification step involve a crystallization operation. While crystallization is quite common in many food and fine chemical industries, it is especially important in the pharmaceutical industry, where almost all products are crystallized. Purity of the product is the primary concern in the manufacture of drugs. Besides separation and purification, the production of a specified crystal size distribution is another important consideration of any crystallization operation.

To obtain the desired product purity and the specified crystal size distribution, careful control of the whole process is essential. However, the current control schemes used in industrial crystallizers suffer from numerous drawbacks. Control of batch industrial crystallization process is generally done manually by operators. As with most manually controlled processes, the success of a given batch crystallization relies on the skill of a single individual. To overcome this drawback, there is a need to implement control strategies that provide a quantitative output that can be either used by an operator without any risk of error, or implemented in an automatic control scheme. A primary impetus for improved control comes from the pharmaceutical industry wherein nearly all products are

crystallized at some point in their production. Pharmaceutical processing is usually done in a batch mode, which is often more difficult to control than continuous processes due to the relatively short time constants present in batch processes. Another consideration is batch to batch fluctuations, which can cause considerable variation in the crystallization process resulting in final product divergence. Such variation is simply unacceptable to the Food and Drug Administration. Reworking a batch that does not meet specifications incurs additional costs and provides an opportunity for additional contamination.

The need for control of large scale, continuous crystallizers is also a problem for the food and chemical industries. Typical applications of crystallization include the production of sugars (sucrose, glucose, lactose, and fructose), carboxylic acids (citric and itaconic), and amino acids (glycine and lysine). As in pharmaceutical crystallization, often there is no attempt at automatic control of the crystallization process. All the various products listed and many commodity chemicals are crystallized from aqueous solution at high concentrations and generally very high process throughput. In contrast to pharmaceutical processing, the longer time constants of large continuous crystallization processes require careful control of supersaturation since process upsets cause departure from steady state that may take a long time to re-establish. During the departure from steady state the process is probably making an off specification product that is unacceptable.

Therefore, both batch and continuous crystallization processes require the precise measurement and control of the process, although for quite different reasons.

## **1.2 The role of supersaturation in crystallization**

The most important parameter that defines the crystallization process is supersaturation. Supersaturation is defined as the amount of solute in excess of the equilibrium solubility that is present in solution at a given temperature and is the driving force for the crystallization. The process of crystallization can be divided into two parts: nucleation and growth. Nucleation refers to the birth of nuclei in solution and growth is the

subsequent deposition of solid mass onto the nuclei. Supersaturation is the driving force for both crystal nucleation and growth and as such controls the overall rate of crystallization.

Figure 1.1 shows the role of supersaturation on a continuous crystallization process by means of an information feedback diagram. A similar diagram with different balance equations can be drawn for a batch crystallization process. Supersaturation affects both the nucleation rate and the growth rate. A high supersaturation results in a larger nucleation rate that causes a large number of nuclei to be formed. On the other hand, a lower supersaturation favors a higher growth rate that results in fewer crystals that grow to a larger size. As shown in the illustration, the final crystal size distribution also determines the surface area of the crystals in the crystallizer that, in turn, affects the supersaturation. Secondary nucleation, also affected by the CSD, is responsible for additional mass to come out of solution. The specific equations describing the various processes are described in detail in Chapter 6. The role played by supersaturation is therefore paramount in the design and operation of the crystallizer. Thus, to develop a control strategy for any crystallizer, either batch or continuous, an accurate measurement of supersaturation is a primary requirement.

In spite of its importance, an accurate *in situ* measurement of supersaturation is still cited as one of the most important needs of industry [1]. A number of analytical techniques have been proposed and are in use for the measurement of solubility and supersaturation [2,3]. These cover a broad range of techniques from simple residual weight determinations to radioactive tracer methods. Conventional techniques that are currently used include refractometry, interferometry, viscometry, and density calibrations. The primary difficulty in using any of these is the procurement of a sample that accurately reflects the dynamic conditions in the crystallizer. Generally, the separation of the crystals from the liquid phase is a prerequisite for these techniques. While filtration and decantation are commonly used for the separation, it is practically impossible to preserve the actual conditions that were



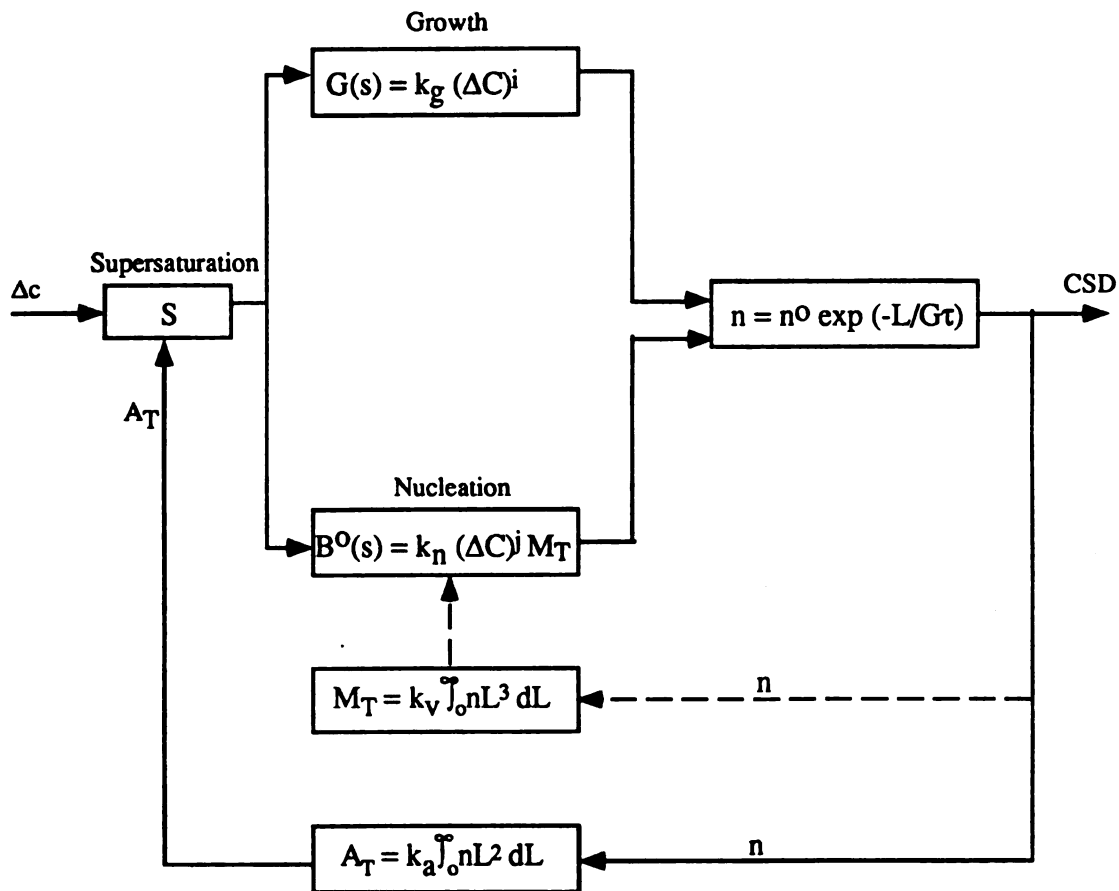


Figure 1.1 Information feedback diagram illustrating the importance of supersaturation and the interaction between size distribution and kinetics resulting from the constraint of the mass balance.

prevailing in the crystallizer when the sample was withdrawn. Refractometry is one of the more common techniques and involves the measurement of small differences in the refractive indices of the solution with a change in the solute concentration. Invariably, these differences appear in the fourth or fifth decimal place that makes the sensitivity and reliability of this technique suspect.

Apart from these procedural complications, there is a fundamental problem with all conventional techniques that makes the measurement of supersaturation at best an approximation.

The fundamental driving force for crystallization is the difference between the chemical potential of the crystallizing substance in the transferring and the transferred state [4]. For an anhydrous solute crystallizing from a binary solution, the driving force may be written as

$$\Delta \mu = \mu_2 - \mu_1 \quad (1.1)$$

where  $\mu_2$  and  $\mu_1$  are the chemical potentials in the crystal and in the solution respectively. This quantity being negative in a crystallizing system, it is convenient to describe it in terms of an 'affinity of reaction' to make the driving force a positive quantity [4]. The 'affinity of reaction' is defined as

$$\phi = -\Delta \mu = \mu_1 - \mu_2 \quad (1.2)$$

The chemical potential  $\mu$  is defined as

$$\mu = \mu_0 - RT \ln a \quad (1.3)$$

where  $\mu_0$  is the standard potential and 'a' is the solute activity.

The supersaturation  $S$  can then be expressed [5] in dimensionless terms by

$$S = \frac{\phi}{RT} = \frac{\mu_1 - \mu_2}{RT} \quad (1.4)$$

This equation can be further simplified to

$$S = v \ln \left[ \frac{a_1}{a_2} \right] \quad (1.5)$$

$$= v \ln \left[ \frac{\gamma_1 c_1}{\gamma_2 c_2} \right] \quad (1.6)$$

where the  $\gamma$ 's are the activity coefficients,  $c$ 's are a measure of the concentration, and ' $v$ ' is the number of ions in a molecular unit.

However, due to the inherent difficulty in measuring the activities and the relative lack of literature data on activities, three very distinct and questionable assumptions are made:

a) the activity coefficients in the solution and in the crystal are assumed to be independent of concentration, i.e.,  $\gamma \neq f(c)$ , so that the ratios of the activity coefficients are unity.

b) the number of ions ' $v$ ' is taken to be unity. These approximations reduce equation (1.6) to

$$S = \ln \left( \frac{c_1}{c_2} \right) = \ln (S_c + 1) \quad (1.7)$$

$$\text{where } S_c = \left( \frac{c_1 - c_2}{c_2} \right) \quad (1.8)$$

c)  $S_c$  is taken to be much less than unity in which case equation (1.7) reduces to

$$S = S_c = \left( \frac{c_1 - c_2}{c_2} \right) \quad (1.9)$$

This definition of supersaturation (equation 1.9) is the most widely used expression because of the relative ease of the measurement of concentration as compared to the activity.

In these previous equations, the concentrations can be expressed in any units, although the preferred one would be that for which the activity coefficient varies the least over the range of concentrations of interest [5].

As mentioned before, there is considerable question over the validity of each of the assumptions. Numerous workers have attempted to estimate the errors involved and the effects on different systems due to the three assumptions [4, 6, 7, 8, 9, 10].

Mullin and Söhnel [4] have calculated errors involved in anhydrous solids when the activity coefficients are taken to be independent of concentrations (assumption 'a'). They found that the larger the deviation of the ratio of the activities from unity, the greater is the error involved. They report serious errors when this ratio deviates from unity by more than  $\pm 1\%$ . The assumption is valid only for very dilute solutions which, of course, is unlikely to occur in the majority of crystallizing solutions. Also, for crystallization of electrolytes from aqueous solution, it is imperative not to neglect the number of ions 'v' (assumption 'b'). The errors involved due to neglecting 'v' may be greater than that due to the use of concentrations in place of activities.

Söhnel and Mullin [6] have extended the study of the errors involved to more complex systems like hydrates, partially dissociated electrolytes, and to systems of mixed electrolytes. For hydrates, the errors involved due to assumption 'a' are as important as for anhydrous solids and that the larger the deviation of the ratio of the activities from unity, the greater is the error involved. However, they conclude that any partial dissociation of electrolyte in solution need not be taken into account to calculate the driving force. Other electrolytes present in the system can significantly affect the driving force calculations and as such should be taken into consideration.

Söhnel and Garside [7] have compared different methods of calculating the activity coefficients of solutes and have concluded that irrespective of the method used, the deviation of the ratio of activity coefficients from the true value is greater at higher supersaturation. Van Leeuwen [8] has developed relations between theoretical and experimental measures for the crystallization driving force. For numerous systems including growth from aqueous solution and melt growth, it has been shown that the ratio of the activity coefficients is much different from unity.

Söhnel and Garside [9] have calculated errors involved by using concentrations instead of activities and have found that for the crystallization of  $K_2SO_4$  and  $KH_2PO_4$ , the differences are comparatively small. This result is explained by the fact that for the two particular systems under study, the activity coefficient is a weak function of concentration.

Cardew and Davey [10] have discussed various ways of calculating the supersaturation using both activities and concentrations. This distinction is shown to have a significant role in the determination of constants in crystal growth rate models.

All the articles cited highlight the importance of using activity and activity coefficients in the measurements of supersaturation. However, as mentioned, for practical reasons, it is quite impossible to obtain the activity coefficients for all systems. The working definition of supersaturation based on concentrations (equation 1.9) is invariably used in all techniques currently available for supersaturation measurement.

Another technique employed for the measurement of supersaturation is the use of Dühring's rule that states that the boiling point of a solution is a linear function of the boiling point of the pure solvent at the same pressure. This technique has been used to measure the supersaturation of sucrose solutions and for the development of an automatic method for controlling the degree of supersaturation [11].

The point to be noted about the supersaturation measurement techniques that are currently in use is that all of them rely on the measurement of mass based concentration.

The errors introduced due to the neglect of activity coefficients has already been discussed. In spite of the awareness to the problem, there is no technique yet to measure the supersaturation based on the activities of the solutes. The practical inability to measure the activities (that inherently depend on the molecular interactions of the solute with the solution), is a major obstacle in the development of a sensor to measure supersaturation. In this work, it is proposed that since activity is a strong function of solution structure, techniques that are sensitive to solution structure will be more likely to reflect changes in activity thereby providing a more direct method of estimation of supersaturation.

Optical spectroscopic techniques such as fluorescence and infra-red spectroscopy offer tremendous potential in this respect. Fourier Transform InfraRed Spectroscopy has already been proven to be well suited for the *in situ* measurement of supersaturation in maleic acid [12]. In this work, the emphasis is on using the numerous advantages of *fluorescence spectroscopy* to develop a sensor that can be utilized *in situ* in a crystallizer for the measurement of supersaturation.

### 1.3 Fluorescence Spectroscopy

Optical spectroscopy is based upon the interaction of light with matter. Every molecule possesses a series of closely spaced energy levels. By the absorption of a discrete quantum of light, the molecule can jump from a lower energy level to a higher one. The energy of the quanta of light has to be equal to the energy difference between the two energy states in order for the system to obey the fundamental equation (1.10) that defines the relation between energy and a quantum of light.

$$E = h\nu = \frac{hc}{\lambda} \quad (1.10)$$

E is the energy, h is Planck's constant,  $\nu$  is the frequency, c is the speed of light in vacuum, and  $\lambda$  is the wavelength of light. This process of absorption is depicted in Figure

1.2. Each electronic state of the molecule is composed of various vibrational states, denoted in the figure as 0, 1, 2, and 3 for the curve depicting the first excited state. The schematic energy level diagram, the Jablonski diagram, for a diatomic molecule is shown in Figure 1.3. The ground state is indicated by  $S_0$ , the first excited electronic state by  $S_1$ , and the first excited triplet state by  $T_1$ . The multiplicity of the state, one or three, defines whether a particular state is a singlet or a triplet. When a quantum of light impinges on a molecule, it is absorbed in about  $10^{-15}$  seconds, and a transition to a higher electronic level takes place. This absorption of radiation is extremely specific, and radiation of a particular wavelength of light is absorbed only by a characteristic structure of the molecule. These ground to singlet state transitions are responsible for the absorption spectra of the molecules.

The molecule spends an average of about  $10^{-10}$  seconds in the excited state, during which time, some energy in excess of the lowest vibrational energy level is dissipated. If the remaining energy is not further dissipated by collisions with other molecules, the molecule returns from the lowest singlet excited state to the ground electronic state with the emission of energy. This phenomenon is called *fluorescence*. Since some of the energy is lost in the brief period before emission can occur, the fluorescence is always of a longer wavelength than the energy that was initially absorbed.

Another pathway for the dissipation of energy is phosphorescence, in which an intersystem crossing from the singlet to the triplet state occurs. When the energy from this state is released, the molecule returns to the ground state. This phenomenon appears as a delayed response at a much longer wavelength. While the lifetime for fluorescence is in the order of nanoseconds, it is of the order of milliseconds or longer for phosphorescence.

The highly selective nature of fluorescence makes it an ideal tool to be used in an analytical sensor. In this investigation, the focus is on using fluorescent molecules as analytical probes of their immediate environment. The overall objective is to be able to

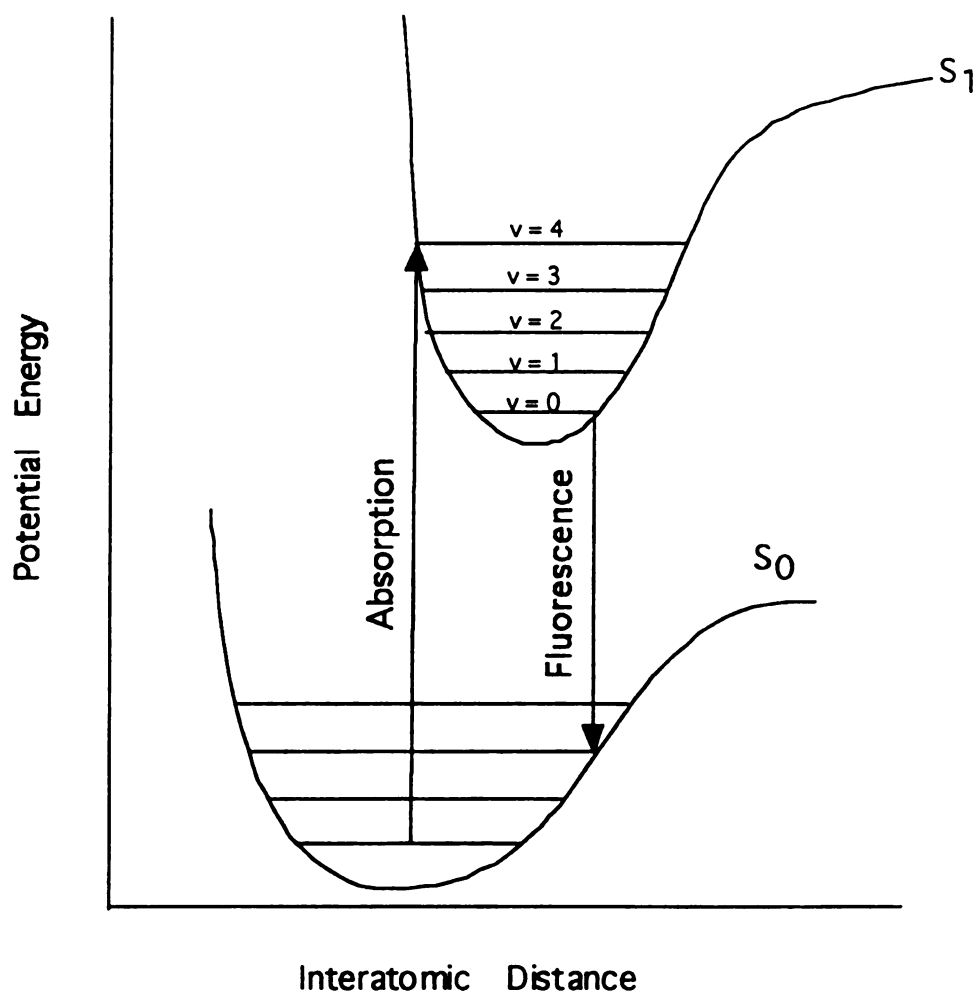


Figure 1.2 Schematic energy level diagram showing the potential energy wells of the ground state and the first electronic state for a diatomic molecule.



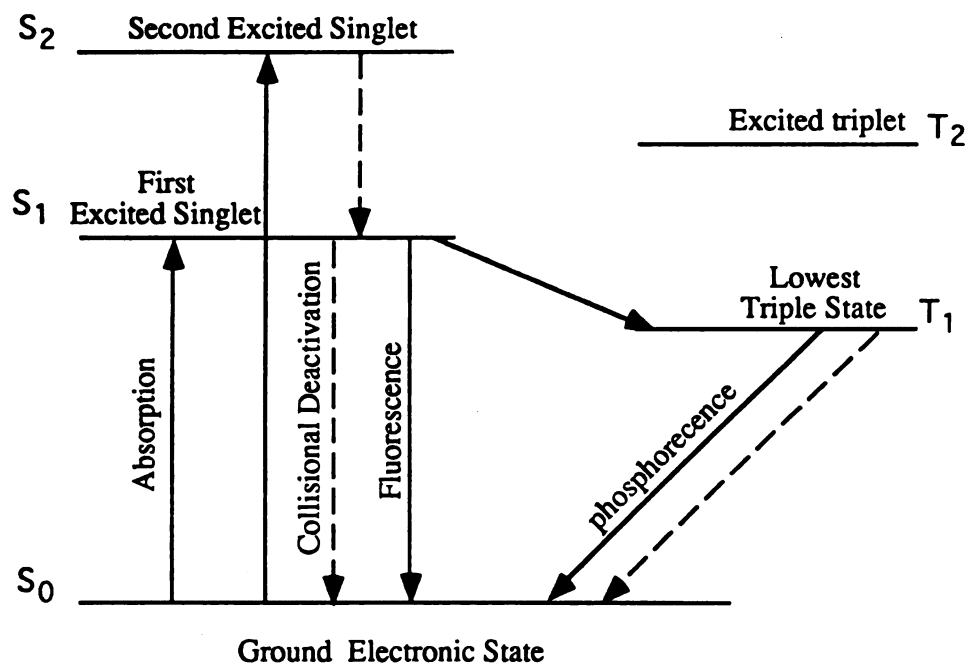


Figure 1.3 Schematic Energy Level (Jablonski) diagram for a diatomic molecule.

exploit this technique for use not only as probes of supersaturation, but also to use the fluorescent probe technique as a tool to extract kinetic parameters that describe a batch crystallization process.

## 1.4 Overview of this work

In Chapter 2, results are presented on the use of a fluorescent dye pyranine, (essentially the trisodium salt of 8-hydroxy, 1, 3, 6 -pyrene trisulfonic acid), that is introduced into undersaturated and supersaturated citric acid solutions. This work is an extension of earlier work done on similar lines with various sugar solutions [13, 14]. It is evident that the change in the fluorescence spectrum of pyranine with a change in the citric acid solution concentration can be correlated with a highly non-linear curve that serves as a calibration curve. It is also shown that the fluorescence spectrum of pyranine is a function not only of the pH of the solution, but is also strongly dependent on the solution concentration. The high degree of non-linearity in concentrated solutions indicates the high sensitivity of the technique in the supersaturated region, which is of interest in all crystallization operations. The calibration curve so generated can then be used as the standard curve to be compared with when this technique is used in a crystallizer *in situ*.

The drawback of using pyranine as the trace fluorescent probe is that it is listed only as a Drug and Cosmetic (D&C) grade color by the FDA and as such may not be appropriate for use in some food and pharmaceutical applications for fear of contamination. In an attempt to circumvent this problem, all colors that have been approved as Food, Drug, and Cosmetic (FD&C) grade colors were screened to test their efficacy for use as a concentration and supersaturation sensor in food applications. There are seven colors currently listed by the FDA as FD&C grade. The results of these investigations are presented in Chapter 3.

While the use of these probes in solution provides very satisfactory results, in some cases, it is necessary to immobilize or contain the probe in some fashion. This necessity may arise, for example, in pharmaceutical crystallizations, where the highest degree of purity is desired. Having the probe freely in the crystallizing solution may not be appropriate because of the probability of incorporation of the probe molecules into the crystal lattice, thereby reducing the purity of the final product.

In recent years, a vast amount of research has been conducted in the area of optically based chemical sensors. A common feature of all these sensors is the presence of an immobilized reagent phase that reacts with an analyte to produce a change in the optical properties. This change is picked up by appropriate sensing devices. The optical indicator phase sensors are sometimes referred to as 'optrodes' or 'optodes' by an analogy to electrodes [15]. An optrode is defined as a device used at the interface between an optical fiber and a solution under study. These devices are discussed in more detail elsewhere [16, 17, 18]. Depending on the nature of the signal, optical sensors are generally classified as fluorescence, absorbance, Raman, or IR sensors. Out of these, the fluorescent sensors are the most widely used. Optical sensors provide a number of advantages over conventional chemical sensors, some of which are listed below [15, 16, 17, 18, 19]:

- a) Optical sensors do not require a reference signal as in potentiometric methods. Also, stability is improved with respect to calibration.
- b) The ease of miniaturization allows the development of light, small, and flexible fiber sensors.
- c) Since the primary signal is optical, it is not subject to electrical interferences like static electricity or surface potentials.
- d) The revolution in communications has provided optical fibers which can transmit light to and from remote locations without large intensity losses.

e) Much more information can be transmitted through an optical fiber than an electrical lead. The signals can differ in wavelength, phase, decay profile, polarization, or intensity modulation.

f) Optical sensors can offer significant cost advantages over conventional sensors, particularly if one spectrometer is used with several sensors.

Notwithstanding these advantages, there are certain limitations to optical sensors:

a) Interference from ambient light is probable. The sensor must therefore be used in the dark or the signal has to be encoded so that it can be separated from the ambient signal.

b) Sensors with immobilized indicator phases may not have long term stability due to photobleaching.

c) Since the indicator and the analyte are in different phases, a mass transfer resistance is necessarily involved, thus limiting the response time of the sensor.

d) Sensors with immobilized indicator phases have a limited dynamic range when compared to electrodes.

Optical sensors have found widespread use specially in the biomedical area where commercial systems are already available for the measurement of pH,  $p\text{CO}_2$ , and  $p\text{O}_2$  in blood. Besides these applications, these sensors have found use in an extremely wide variety of cases, including the sensing of alkali metal ions, glucose, methane, trinitrotoluene, antigens, enzyme activity, ammonia, halide ions, non-alkali metal ions, chlorinated hydrocarbons, albumin, and in analytical measurements such as ionic strength, potential, adsorption sensing, humidity, temperature, radiation, sound, magnetism, titrations, and substrate analysis [16, 20].

In the latter half of Chapter 3, results of experiments involving the immobilization of the FD&C colors on anion exchange membranes are presented. It is shown that

although the fluorescent spectrum is altered because of the chemistry involved in the immobilization, the essential emission properties of the probe molecules are still maintained and that such a membrane can be used as a concentration and supersaturation sensor.

Chapter 4 deals with a new fluorescent probe - chlorin, and a new technology for the construction of the sensor. While with FD&C colors, ion exchange membranes were used to immobilize the dyes, here, a  $\text{TiO}_2$  sol-gel film is created on a glass surface. This film has an extremely porous structure and allows for the incorporation of guest molecules. Chlorin was introduced into the film and trapped inside the sol-gel matrix. When such a modified glass strip was introduced into aqueous sucrose solutions, the fluorescence spectra of the chlorin changed markedly with the amount of sucrose in solution. The suitability of a sol-gel based sensor is discussed in Chapter 4.

After establishing the feasibility of a fluorescence based sensor for measurement of concentration and supersaturation in crystallizing solutions, other possibilities for using this technique were explored. The measurement of kinetic parameters in a crystallization process is an important task that affects not only the operating conditions of the crystallizer, but is quite important in establishing any kind of a control strategy for the optimal operation of the crystallizer. Isothermal desupersaturation experiments were conducted on aqueous citric acid solutions and the change in concentration with time was tracked with a fluorescent probe that was added to the crystallizing solution. The ability of the fluorescent probe to measure the desupersaturation characteristics is discussed in Chapter 5.

The desupersaturation experiments provide a wealth of information about the process of crystallization. The kinetics of nucleation and growth, including their rates and kinetic constants can be extracted from the desupersaturation curves by solving the appropriate balance equations. Chapter 6 deals with these issues and provides a methodology for estimating the kinetic parameters for citric acid solutions.

Chapter 7 introduces the concept of Reverse Flow Injection Analysis (rFIA) and offers some ideas for future implementation. Results of preliminary experiments with rFIA are presented and its potential to enhance the advantages of the fluorescence probe technique is discussed. It is expected that future research will attempt to use these modifications to the fluorescent probe technique to make it a much more practical analytical tool. Ideas are presented about the direction this research should take in the future and the anticipated benefits.

## 1.5 References

1. *Proceedings of the Workshop on Opportunities & Challenges in Crystallization Research*, Iowa State University, Ames, Iowa. March 4-6, (1991).
2. H. K. Zimmerman, *Chemical Reviews*, The Experimental Determinations of Solubilities. **51**, 25-65, (1952).
3. J. W. Mullin, In: *Crystallization*, Butterworth Heinemann, Oxford, England, (1993).
4. J. W. Mullin, O. Söhnel, *Chemical Engineering Science*, Expressions of supersaturation in crystallization studies. **32**, 683-686, (1977).
5. J. Garside, *Chemical Engineering Science*, Industrial Crystallization from Solution. **40**, 3-26, (1985).
6. O. Söhnel, J. W. Mullin, *Chemical Engineering Science*, Expressions of supersaturation for systems containing hydrates, partially dissociated electrolytes and mixtures of electrolytes. **33**, 1535-1538, (1978).
7. O. Söhnel, J. Garside, *Journal of Crystal Growth*, The Thermodynamic Driving Force for Crystallization from Solution. **46**, 238-240, (1979).
8. C. Van Leeuwen, *Journal of Crystal Growth*, On the driving force for crystallization: The growth affinity. **46**, 91-95, (1979).
9. O. Söhnel, J. Garside, *Journal of Crystal Growth*, On Supersaturation Evaluation for Solution Growth. **54**, 358-360, (1981).
10. P. T. Cardew, R. J. Davey, and J. Garside, *Journal of Crystal Growth*, Evaluation of Supersaturation in Crystal Growth From Solution. **46**, 534-538, (1979).

11. A. L. Holven, *Industrial and Engineering Chemistry*, Supersaturation in Sugar Boiling Operations. **34**, 1234-1240, (1942).
12. D. D. Dunuwila, An Investigation of the Feasibility of Using In Situ ATR FTIR Spectroscopy in the Measurement of Crystallization Phenomenon for Research and Development of Batch Crystallization Processes. PhD Thesis, Michigan State University. (1996).
13. R. Chakraborty, K. A. Berglund, *Journal of Crystal Growth*, Steady State Fluorescence Spectroscopy of Pyranine as a Trace Extrinsic Probe to study structure in aqueous sugar solutions. **125**, 81-96, (1992).
14. R. Chakraborty, K. A. Berglund, *AIChE Symposium Series No. 284*, The Use of Pyranine as a Trace Fluorescent probe to Study Structure in Aqueous Sucrose Solutions. **83**, 114-123, (1991).
15. O. S. Wolfbeis, *Trends in Analytical Chemistry*, Fluorescence Optical Sensors in Analytical Chemistry. **4**, 184-188, (1985).
16. W. R. Seitz, *CRC Critical Reviews in Analytical Chemistry*, Chemical Sensors Based on Immobilized Indicators and Fiber Optics. **19**, 135-173, (1988).
17. S. A. Borman, *Analytical Chemistry*, **53:14**, 1616A-1618A, (1981).
18. J. Janata, In: *Principles of Chemical Sensors*, Plenum Press, New York, 241-284, (1989).
19. W. R. Seitz, *Analytical Chemistry*, Chemical Sensors based on Fiber Optics. **56**, 16A-34A, (1984).
20. U. J. Krull, R. S. Brown, in *Laser Remote Chemical Analysis*, R. M. Measures, Eds. John Wiley and Sons, Vol. 94, 505-532, (1988).

## **Chapter 2**

# **USE OF FLUORESCENCE SPECTROSCOPY IN CONCENTRATION AND SUPERSATURATION MEASUREMENTS IN CITRIC ACID SOLUTIONS\***

## **2.1 Background**

The study of solution structure is critical for a complete understanding of the behavior of crystallizing solutions, especially in the supersaturated region. In this work, we show that since optical techniques involving spectroscopy are dependent on solution structure, they are well suited to reflect changes in activity, thereby providing a more direct method of estimation of supersaturation.

Numerous workers have attempted to study solution structure using a wide variety of techniques. Frank and Wen [1] first proposed a theory involving a cluster model for water molecules. Since then, numerous studies have been conducted to understand the role of the solvent molecules and their interaction with the solute molecules. The solvent-solute and the solute-solute interactions are relatively more complex to study, especially in concentrated solutions, and therefore have been studied mainly for undersaturated solutions.

A variety of means have been used for studying the nature of molecular association and solute organization. Mullin and Leci [2] found that an isothermal column of a

---

\* Yedur, S. K., and K. A. Berglund. *Applied Spectroscopy*. In print. 1996.



supersaturated solution of citric acid generated a concentration gradient over a period of several days. It was suggested that solute clusters were being formed and the concentration gradient developed as a result of the density difference between the clusters and the solution. The large degree of hydrogen bonding possible between the citric acid molecules and the solvent water molecules was thought to be the cause of cluster formation. Cussler [3] conducted diffusion studies in the triethylamine-water and other binary systems and showed that the diffusion in the systems studied could be predicted much better by using a model that allowed for cluster diffusion as well as molecular diffusion. Myerson and co-workers [4,5] observed the decrease in the diffusivities of urea, glycine, KCl, and NaCl solutions which provided evidence for molecular aggregation. Hussman *et al.* [6] and McMahon *et al.* [7] also confirmed cluster formation with Raman spectroscopy on alkali nitrate solutions. Larson and Garside [8,9] measured density gradients in columns of citric acid, urea, sodium nitrate, and potassium nitrate solutions, confirming the formation of solute clusters in supersaturated solutions. Ohgaki *et al.* [10] have observed solute clusters and their aggregations in citric acid solutions using scanning electron microscopy.

Although many investigations have demonstrated microscopic solvent interactions using techniques such as NMR, X-ray diffraction, and Raman [11,12,13], a novel method using the fluorescence properties of a probe molecule was developed by Chakraborty and Berglund[14,15]. In their work, the authors have demonstrated that relative amounts of associated and bulk water can be estimated by monitoring the relative peak intensities of the steady state fluorescence of a probe molecule such as trisodium 8-hydroxy-1,3,6-pyrenetrisulfonate (pyranine). The molecular structure of pyranine is shown in Figure 2.1.

Pyranine is a non-toxic D&C dye and as such is approved for use in drug and cosmetic applications. It is listed by the FDA as D&C Green No. 8. Pyranine has been widely applied to the study of reverse micelles [16, 17, 18], sols [19], sol-gels [20], and as a source of protons for pH jump experiments [21, 22, 23].

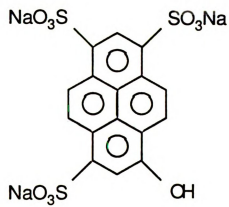


**Figure 2.1** Molecular structure of Pyranine (trisodium salt of 8-hydroxy-1,3,6-pyrenetrisulfonic acid)

The emission properties of pyranine have been well characterized [16, and references therein]. In aqueous solution, pyranine exists with the sulfonate groups dissociated. Upon excitation with light at a wavelength of around 355 nm, it has two excited states. One, emitting at 440 nm, is due to the protonated form of the molecule, whereas the other, emitting at 510 nm, is due to the deprotonated form. These kinetics are shown in Figure 2.2. Whether the observed emission is from the protonated form or from the deprotonated form depends on the molecular environment in its immediate vicinity. Thus, solute-solvent interactions in solution can be studied by observing the emission of the probe molecule.

In this work, the concentration of citric acid solutions has been measured by using pyranine, both in undersaturated and supersaturated conditions, to get an accurate estimation of the supersaturation.

The pH of citric acid solutions decreases linearly with concentration. As has been noted [17], the emission properties of pyranine are affected by the pH of the solution. In this work, however, we show that the pyranine molecule's response to the citric acid solution is more than a pH effect alone and that it is possible to get an estimate of the supersaturation by using this fluorescence technique.

## **2.2 Materials and Methods**

A stock solution of pyranine (obtained from Eastman Kodak, Rochester, NY) was prepared by dissolving 0.0264 grams of pyranine in 50 mL of spectroscopic grade methanol. Citric acid solutions of 10, 20, 30, 40, 50, 60, and 70 weight percent were prepared by dissolving the appropriate amount of citric acid monohydrate (obtained from Columbus Chemical Industries Inc., Columbus, WI) in distilled water. The 70% supersaturated solution was prepared by mildly heating the solution in a water bath until all the solute was dissolved and subsequent cooling to room temperature. The solutions were

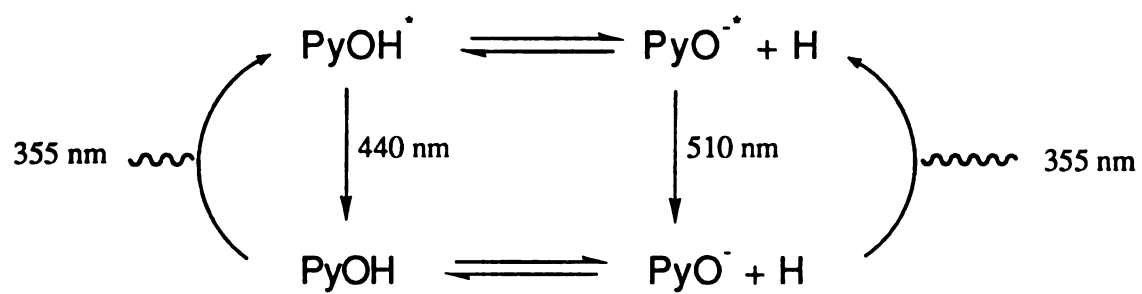


Figure 2.2 Excited state kinetics of pyranine

used as prepared without any degassing. The pH of the solutions was measured using a pH electrode with an Orion Research digital ionalyzer/501.

Ten microliters of the pyranine stock solution was taken in a vial and the methanol allowed to evaporate. Ten milliliters of the citric acid solution was added. This procedure was repeated for each of the citric acid solutions prepared. A  $1.0 \times 10^{-6}$  M pyranine concentration was thus achieved in each case. A similar protocol was followed to obtain pyranine concentrations of  $1.0 \times 10^{-5}$  M and  $1.0 \times 10^{-7}$  M.

Fluorescence spectra of the pyranine in each of the citric acid solutions were collected within a couple of hours of the preparation of the solutions. All spectra were taken in a controlled environment set at 25 °C with a SPEX 1681 FLUOROLOG spectrometer equipped with an Xenon lamp source and a PMT detector. A quartz cuvette was used in all cases. Based on the absorption behavior of pyranine, an excitation wavelength of 342 nm was used. The emission was recorded over a range from 400 to 600 nm. The quantum efficiency of pyranine is close to unity so a very small amount of excitation light is required. Copious amounts of emitted light are generated which prompted the excitation monochromator slits to be 0.5 mm open while the emission monochromator slits were opened to 1 mm. The response of the PMT detector in the range of wavelengths studied was constant which precluded the need for corrections to be made for PMT response.

The fluorescence spectra of pyranine in solutions of different pH's were also obtained. Solutions with pH's of below 3 were studied. These solutions were prepared by adding appropriate amounts of hydrochloric acid and ammonium hydroxide. A similar procedure to that described earlier was used to prepare  $1.0 \times 10^{-6}$  M pyranine concentration solutions at different pH's.

## 2.3 Results and Discussion

The quantum yield of pyranine is very close to unity under all experimental conditions [23]. This property was one of the strongest points behind choosing pyranine as the probe. Although it is unclear whether the yield is unity for both emitting species, the change would be the same for both the species. This is evidenced by the fact that the emission spectra show a very consistent relative change in the two peaks. Any possible variation in the individual quantum efficiencies will be factored out during the ratioing of the two peaks.

Even though the probe may be affected by oxygen quenching, in this case it is not a potential problem as the purpose of the experiments is to monitor the performance of the probe in a real-life crystallizing solution. For this purpose, the aqueous solutions prepared are assumed to be saturated with oxygen and so any quenching would not adversely affect the behavior of the probe during the course of the experiment.

From previous literature [14,15], it was known that the emission properties of pyranine do not change from a range of 10 to 100 ppm in aqueous sucrose solutions. To test any possible effect in citric acid solutions, experiments were conducted with three pyranine concentrations of  $1.0 \times 10^{-5}$  M,  $1.0 \times 10^{-6}$  M, and  $1.0 \times 10^{-7}$  M. As expected, there are no distinctive changes in the three spectra. Two peaks at 440 nm and at 510 nm appear with an isosbestic point. However, when the concentration is  $1.0 \times 10^{-5}$  M, there appears to be a diminution of emission intensity in highly concentrated citric acid solutions. This might be due to some self-aggregation of the probe in the highly viscous environment. This does not mean that there is any evidence for excimer formation, as no broadening of the peak or bathochromic shifts are noticed. The fact that pyranine is not a planar molecule (due to the presence of the sulfonate groups) also excludes the possibility of excimer formation. As expected, the absolute intensities vary slightly for the lower two concentrations, but identical peak intensity ratio curves are generated. This suggests that

either of these concentrations may be used. However, in this work, we choose to use a pyranine concentration of  $1.0 \times 10^{-6}$  M throughout, as it is a more convenient amount to work with. The relative inexpensiveness of the probe does not justify the use of a lower concentration that is more difficult to measure accurately.

The emission spectra of  $1.0 \times 10^{-6}$  M pyranine in citric acid solutions of four different concentrations are shown in Figure 2.3. The spectra of the other concentrations also followed the trend. As noted previously, the emission spectrum of pyranine in water shows two distinct peaks, one at 440 nm and the other at 510 nm. Pyranine occurs in two excited states in equilibrium: one in which the hydroxyl proton is associated with the molecule and another in which it is dissociated. As is evident from the figure, the intensities of the peaks at 440 and 510 nanometers change with citric acid concentration. An isosbestic point is observed at 495 nm that indicates that the two fluorescing species are in equilibrium. At least three experiments were carried out at the same concentrations and the spectra are quite reproducible.

At low concentrations of citric acid, emission at 510 nm is more intense than that at 440 nm, indicating the presence of deprotonated pyranine in solution. At higher concentrations, the intensity of emission at 440 nm increases with a corresponding decrease in the intensity at 510 nm. This indicates that the equilibrium between the deprotonated and protonated forms of pyranine shifts towards the protonated form with an increase in citric acid concentration. Fully protonated pyranine molecules exist only when there are no proton acceptors (water molecules) available for exchange in the immediate vicinity of the pyranine hydroxyl proton.

The Peak Intensity Ratio (PIR), defined as the ratio of the peak intensity at 440 nm to the intensity at 510 nm is thus a measure of the ratio of water associated with the solute(citric acid) to that not associated with the solute. The use of this ratio also provides an internal correction for intensity fluctuations due to possible variations in the

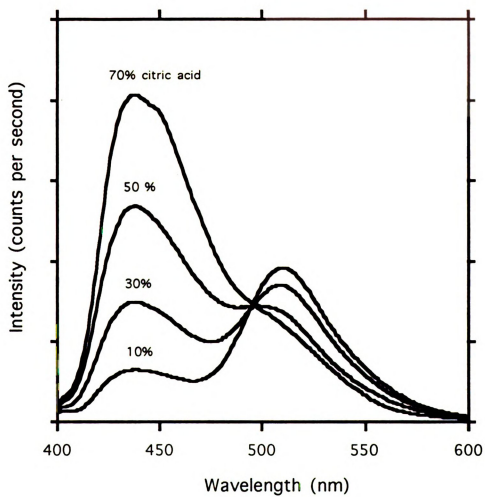


Figure 2.3. Emission spectra of pyranine in citric acid solutions of 10, 30, 50, and 70 weight percents; taken at 25 °C.



spectrophotometer setup. Chakraborty and Berglund [14,15] have put forward a theory based on the work of Birch *et al.* [24] according to which three kinds of exchangeable protons are available in concentrated sugar solutions: bulk water, solvation water, and the sucrose hydroxyl. Here, we propose that a similar environment occurs in the case of concentrated citric acid solutions. Out of the available protons for exchange, the protons associated with the citric acid molecule are unlikely to compete with the water molecules in interacting with the pyranine molecules because the pH of the solutions are generally below the pK's of the carboxylic acid groups. It follows that the pyranine only reacts with the water molecules and not with the citric acid molecules. The pyranine molecule that interacts with a water molecule which is in contact with other water molecules will become deprotonated and will emit at 510 nm. This suggests one microenvironment of the pyranine to be bulk water. On the other hand, a pyranine molecule in the vicinity of solvation water that is already associated with a citric acid molecule would not exchange protons and would be in the protonated state emitting at 440 nm. Thus, the other microenvironment of the pyranine molecule would be water of solvation associated with the citric acid molecules.

The previous discussion suggests that pyranine responds to the available water in its immediate environment. This association with water is, in turn, is related to the amount of citric acid present in solution. Thus, the change in emission properties of pyranine can be related to the concentration of aqueous solutions of citric acid. A graph of the PIR versus concentration is shown in Figure 2.4. The smooth nature of the curve indicates that it can be used to determine the concentration, and also the supersaturation of citric acid solutions. The presence of an upward curvature indicates that the response is highly non-linear. The same data are presented as a plot between the PIR and the supersaturation in Figure 2.5. It has been shown elsewhere [14,15] that the supersaturation measurement

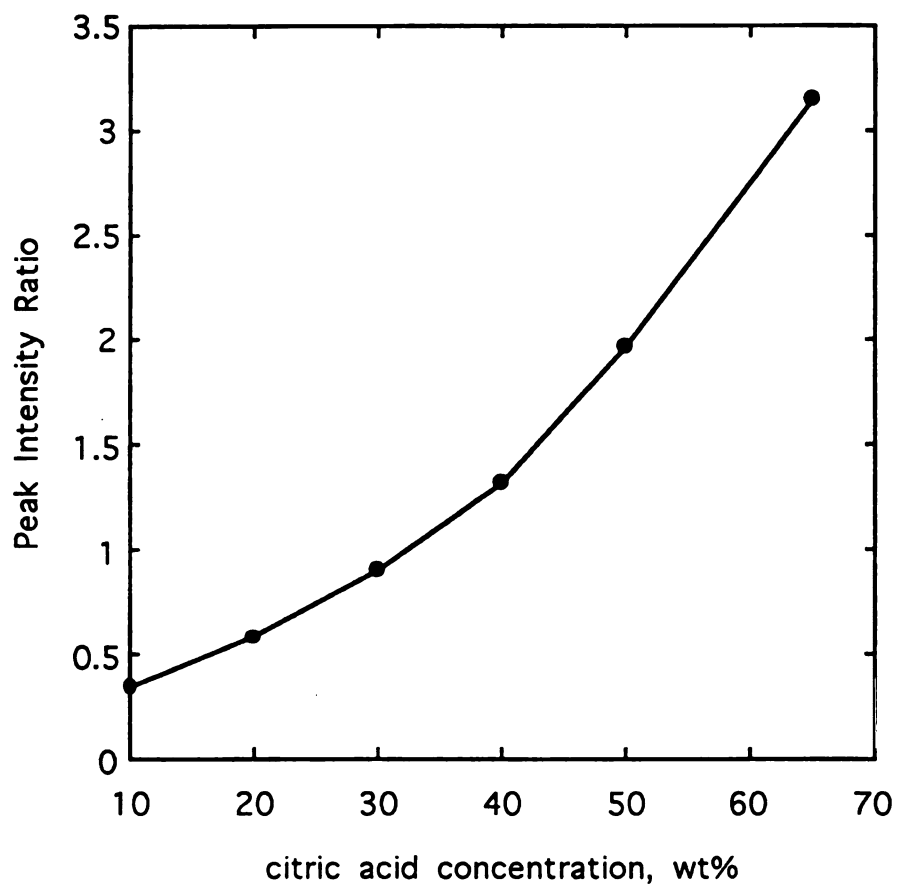
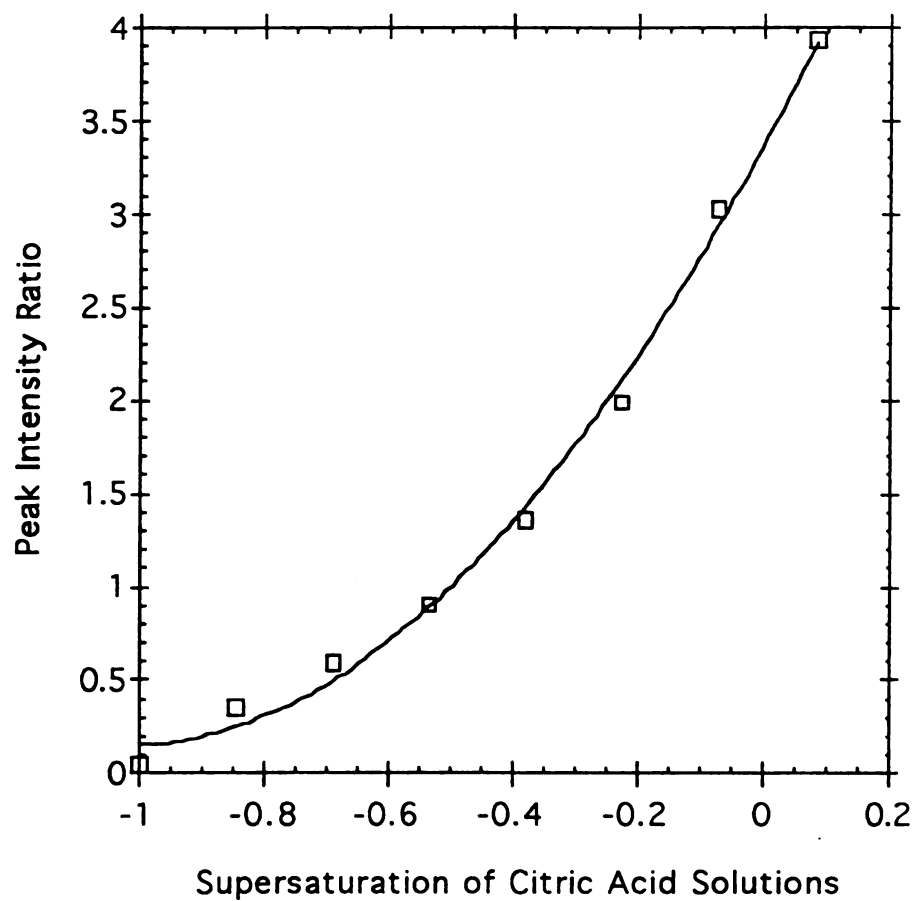


Figure 2.4 Peak Intensity Ratio (ratio of emission peak intensities at 440 nm and 510 nm) as a function of citric acid concentration.



**Figure 2.5** Peak Intensity Ratio (ratio of peak intensities at 440 nm and 510 nm) versus the supersaturation  $S$  (defined as  $S=(c-c^*)/c^*$ , where  $c$  and  $c^*$  are the actual concentration and the saturation concentration respectively).

using the PIR is more sensitive than other techniques, as it is a consequence of the activity rather than just the concentration.

There is, however, a caveat because the pH of citric acid solutions changes dramatically with concentration. It has been found that the effect of varying the pH on the emission of pyranine is also striking. Results of Bardez *et al.* [17] suggests that lowering of the pH also causes an increase in the emission at 440 nm. The question arises as to whether the changes in the PIR seen in the citric acid solutions were just pH effects or were truly the result of changes in the microenvironment of the probe molecule.

Figure 2.6 shows a plot of the pH of citric acid solutions versus the concentration. The plot indicates that as the concentration of the aqueous solution increases, the pH decreases linearly. At extremely high concentrations of near saturation (about 65 wt% at 30°C) and above, the pH falls very close to zero and also dips below zero. A reliable measurement using a pH meter is not possible at these high concentrations.

Experiments were conducted by dissolving pyranine in HCl-NaOH solutions of different pH's. At basic conditions of high pH's, pyranine cannot be excited from the ground state due to its pKa. At such pH's, it is not feasible to study the emission properties and so the emission of pyranine was studied only in solutions of lower pH where it can be excited. This was also the range of the pH of citric acid solutions.

Figure 2.7 shows a comparison of the PIR's obtained from pyranine emission in citric acid solutions to the PIR's in HCl-NaOH solutions of different pH's. As is evident, the emission in the presence of citric acid shows a steeper slope and greater absolute values than the PIR in the absence of citric acid indicating that the pyranine molecule, besides being sensitive to the pH of the solution, also responds to the presence of the citric acid present. Since the relationship between the concentration and the pH is linear, and that between concentration and PIR is highly non-linear, it can be concluded that the PIR

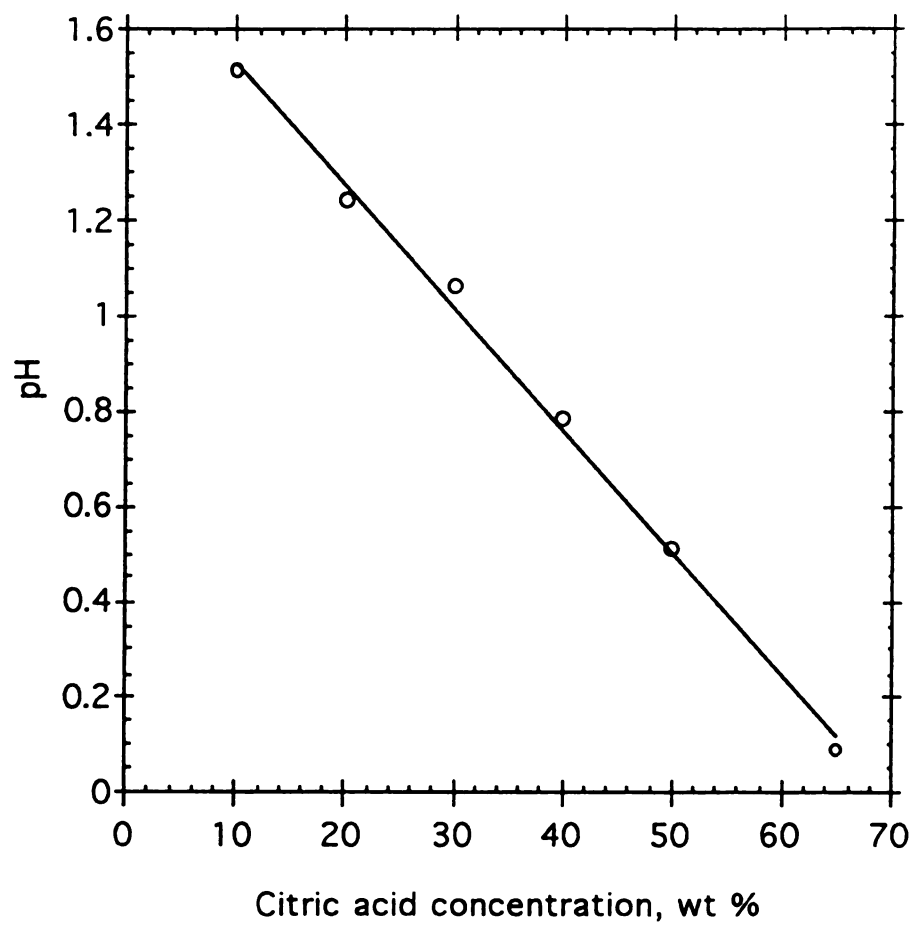


Figure 2.6 pH of aqueous citric acid solutions as a function of citric acid concentration.

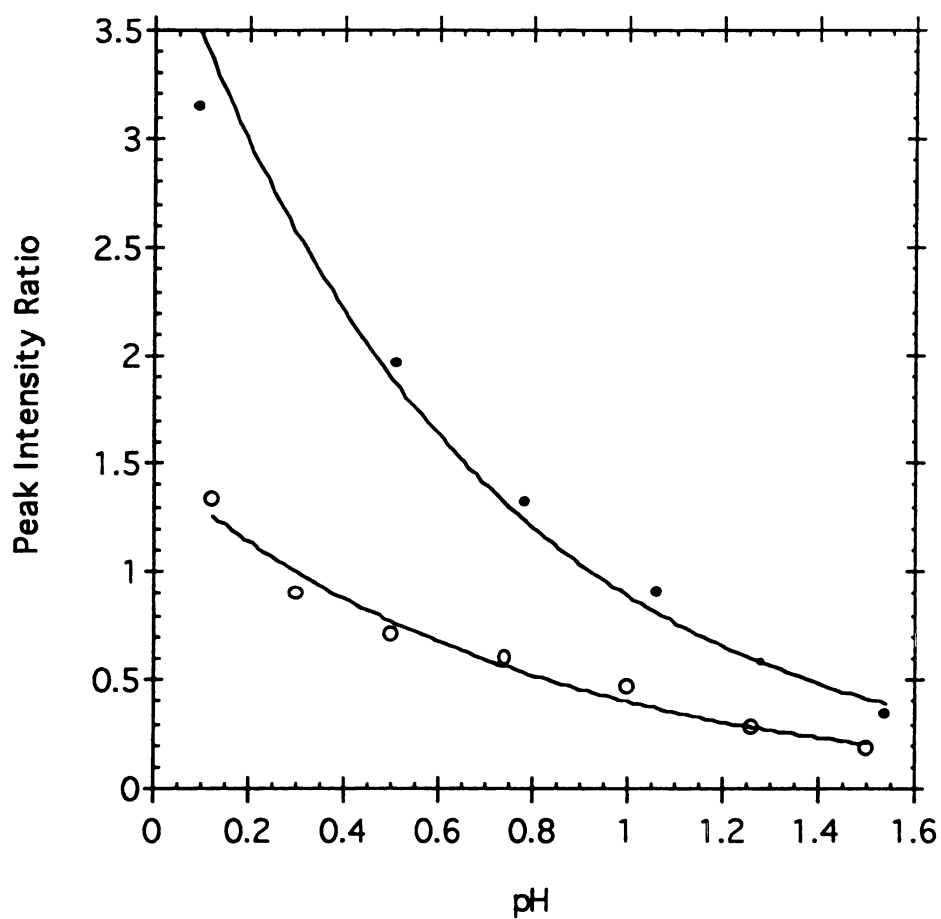


Figure 2.7 Comparison of PIR's (ratio of peak intensities at 440 nm and 510 nm) obtained from pyranine emission in citric acid solutions as a function of pH of the solutions to the PIR's obtained from pyranine emission in HCl-NaOH solutions of varying pH's. Closed circles: Citric acid solutions; open circles: HCl-NaOH solutions.

obtained can be used to measure the supersaturation of citric acid solutions. In an effort to decouple the effect of pH from the effect of the solution on the PIR, both the curves were fit to exponential curves. The curve fits provided significant  $R^2$  values of 0.98 and 0.97 for the overall effect and the pH effect, respectively. Using these fits and the relationship between concentration and pH shown in Figure 2.7, the pH effect was subtracted from the overall effect to generate a corrected PIR curve as a function of citric acid concentration. This corrected calibration curve is shown in Figure 2.8. This plot clearly demonstrates that the non-linear response of the PIR as a function of concentration can be used as a calibration curve for the measurement of supersaturation as the technique works well even in the supersaturated region. Note that the solubility at the experimental temperature of 25 °C is marked on the plot by the arrow.

## 2.4 Conclusions

The emission properties of a fluorescent probe molecule like pyranine in trace amounts can be used to obtain an estimate of the supersaturation of citric acid solutions. The method used, involving the measurement of the Peak Intensity Ratio (PIR), defined as the ratio of the intensity of the emission peak of pyranine at 440 nm to the intensity of the peak at 510 nm gives rise to a parameter - the PIR, that is strongly correlated to the solute concentration. The relationship between the two is highly non-linear and extends into the supersaturated region. Since the emission properties are a function of the solvent microenvironment around the probe molecule, they are strongly dependent upon the activity of the solvent. This technique holds promise for better accuracy than current mass based techniques for supersaturation measurements. It is also shown that the response of the pyranine is not only due to a pH change of the citric acid solution at higher concentrations, but truly reflects the solute and solvent microenvironments.

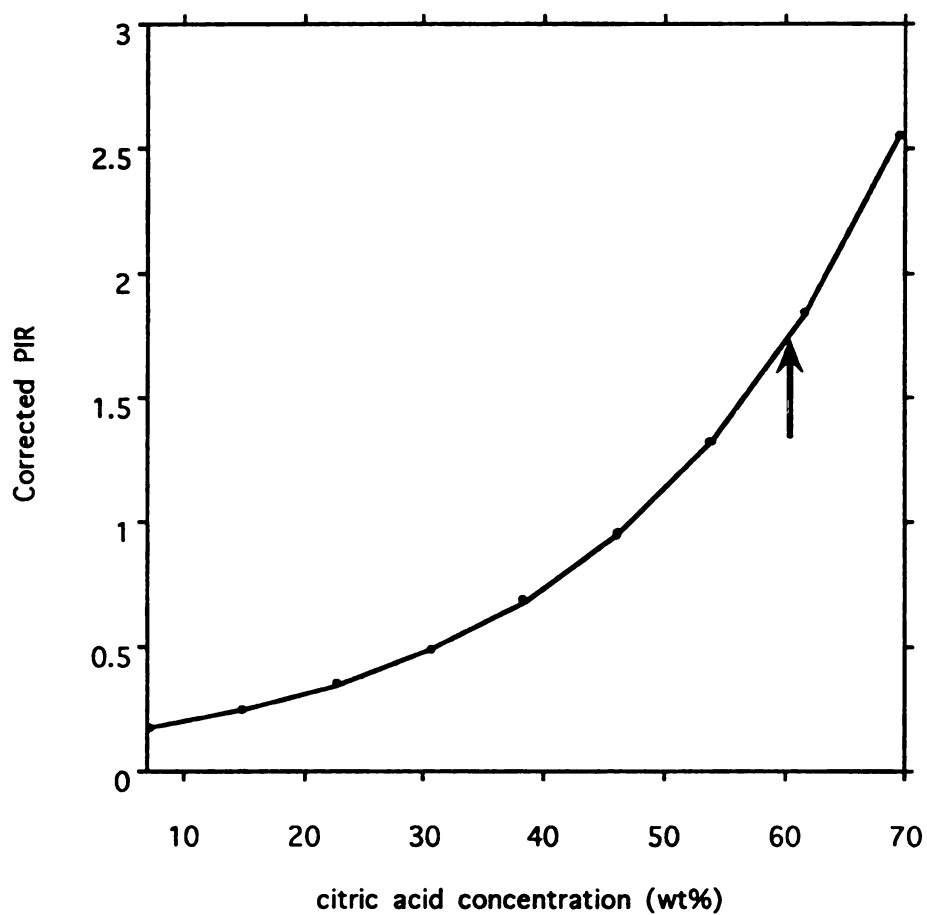


Figure 2.8 Corrected PIR (corrected for pH effects) versus citric acid concentration (wt%). The arrow indicates the solubility at 25 °C.



## 2.5 References

1. W.S. Frank and W.Y. Wen, *Disc. Faraday Soc.* **24**, 1333, (1957).
2. J.W. Mullin and C.L. Leci, *Phil Mag.* **19**, 1075, (1969).
3. E.L. Cussler, *AIChE Journal*. **26:1**, 43, (1980).
4. Y.C. Chang and A.S. Myerson, in: *Industrial Crystallization '84*, S.J. Jancic and E.J. DeJong, Eds. Elsevier, Amsterdam, 27, (1984).
5. L.S. Sorrel and A.S. Myerson, *AIChE Journal*, **28:5**, 772, (1982).
6. G.A. Hussman, M.A. Larson, and K.A. Berglund, in: *Industrial Crystallization '84*, S.J. Jancic and E.J. DeJong, Eds. Elsevier, Amsterdam, 21, (1984)
7. P.M. McMahon, K.A. Berglund, and M.A. Larson, in: *Industrial Crystallization '84*, S.J. Jancic and E.J. DeJong, Eds. Elsevier, Amsterdam, 229, (1984)
8. M.A. Larson and J. Garside, *Chem. Eng. Sci.* **41:5**, 1285, (1986).
9. M.A. Larson and J. Garside, *J. Crystal Growth*. **76**, 88, (1986).
10. K. Ohgaki, N. Hirokawa, and M. Ueda, *Chem. Eng. Sci.* **47:8**, 1819, (1992).
11. M. Mathlouthi and D.V. Luu, *Carbohydrate Research*. **81**, 203, (1980).
12. M. Mathlouthi, C. Luu, A.M. Meffroy-Biget, and D.V. Luu, *Carbohydrate Research*. **81**, 213, (1980).
13. M. Mathlouthi, *Carbohydrate Research*. **91**, 113, (1981).
14. R. Chakraborty and K.A. Berglund, *AIChE Symposium Series no. 284*. **83**, 114, (1991).
15. R. Chakraborty and K.A. Berglund, *J. Crystal Growth*. **125**, 81, (1992).
16. H. Kondo, I. Mlwa, and J. Sunamoto, *J. Phys. Chem.* **86**, 4826, (1982).
17. E. Bardez, B.T. Gougillon, E. Keh, and B. Valeur, *J. Phys. Chem.* **88**, 1909, (1984).
18. G.D. Correll, R.N. Cheser, F. Nome, and J.H. Fendler, *J. Am. Chem. Soc.* **100:4**, 1254, (1978).
19. V.R. Kaufman, D. Anvir, D. Pines-Rojanski, and D. Huppert, *J. Non-Crystalline Solids*. **99**, 379, (1988).

20. J.C. Pouxviel, B. Dunn, and J.I. Zink, *J. Phys. Chem.* **93**, 2134, (1989).
21. K.K. Smith, K.J. Kaufman, D. Huppert, and M. Gutman, *Chem. Phys. Letters.* **64:3**, 522, (1979).
22. E. Pines and D. Huppert, *J. Phys. Chem.* **87**, 4471, (1983).
23. M.J. Politi and J.H. Fendler, *J. Am. Chem. Soc.* **106:2**, 265, (1984).
24. G.G. Birch, J. Grigor and W. Derbyshire, *J. Solution Chem.* **18:8**, 795, (1989).

## **Chapter 3**

# **A NOVEL ANALYTICAL USE OF FOOD GRADE COLORS: SPECTROSCOPIC MEASUREMENT OF CONCENTRATION AND SUPERSATURATION IN SUCROSE SOLUTIONS**

### **3.1 Background**

The use of food colors has traditionally been only as an additive to various food products and cosmetics along with certain very specific uses in medical devices. Colors are applied to fruits, meats, and other foods to improve their desirability and are added to drugs and pharmaceuticals primarily for ease of identification [1]. The utility of these colors is limited to increasing the visual appeal of the final product. Foods and cosmetics are colored basically in two ways - either the free dye is added to the solution, or the dye is added as a lake. A lake is defined as a pigment that is prepared by precipitating a soluble dye onto an approved insoluble reactive or adsorptive substratum or diluent [1]. Currently, alumina is the only approved base for FD&C lakes. While there are a number of colors approved for external drug and cosmetic use, there are only seven colors listed in the United States by the Food and Drug Administration (FDA) as certified for food, drug, and cosmetic (FD&C) use. In the following list, the official designation is as a number, the common names are listed in brackets. The colors are FD&C Blue No. 1 (brilliant blue), FD&C Blue No. 2 (indigo carmine), FD&C Green No. 3 (fast green), FD&C Red No. 3 (erythrosine), FD&C Red No. 40 (allura red), FD&C Yellow No. 5 (tartrazine), and

FD&C Yellow No. 6 (sunset yellow). The chemical structures of the seven FD&C colors are shown in Figure 3.1. Some important physical properties are listed in Table 3.1. Additional basic information about food colors and their application has been reviewed and compiled elsewhere [1, 2, 3].

The combined usage of these colors in all various applications is quite high. In 1990, the total amount of FD&C primary colors and lakes certified by the Food and Drug Administration exceeded 8.5 million pounds [1]. While the use of these colors as visually appealing materials are apparent, their use as analytical probes, however, is a novel approach that has come out of the work done in this laboratory in the last few years on fluorescent compounds [4, 5, 6].

The proposed research utilizes a technique involving a fluorescent probe molecule, that is based on the sensitivity of the probe molecule placed in a crystallizing environment, to the solution structure. It is known that the relative changes in the emission spectra of compounds such as pyranine, carminic acid, nile red, and pyrene butyric acid, when placed in different solutions, can be correlated to the polarity of the solution. The photochemistry of some fluorescent probes like pyranine [7] and carminic acid [8, 9] are well understood, whereas the majority of probes are yet to be studied. The molecular structure of pyranine is shown in Figure 2.1 while Figure 2.2 shows the kinetic diagram for the two-state excited state proton transfer process of pyranine (PyOH). Pyranine is highly soluble in aqueous solutions where it is completely dissociated. The protonated form emits at a wavelength maxima of 440 nm, while the dissociated form emits at a wavelength maxima of 511 nm. Steady-state fluorescence investigations using pyranine as a trace fluorescent probe have demonstrated that the relative amounts of associated and bulk water can be measured by monitoring the relative peak intensities of the steady state fluorescence [4, 5, 6]. This result suggests that pyranine is an excellent probe for measuring bulk concentration of the solution in which it is placed.

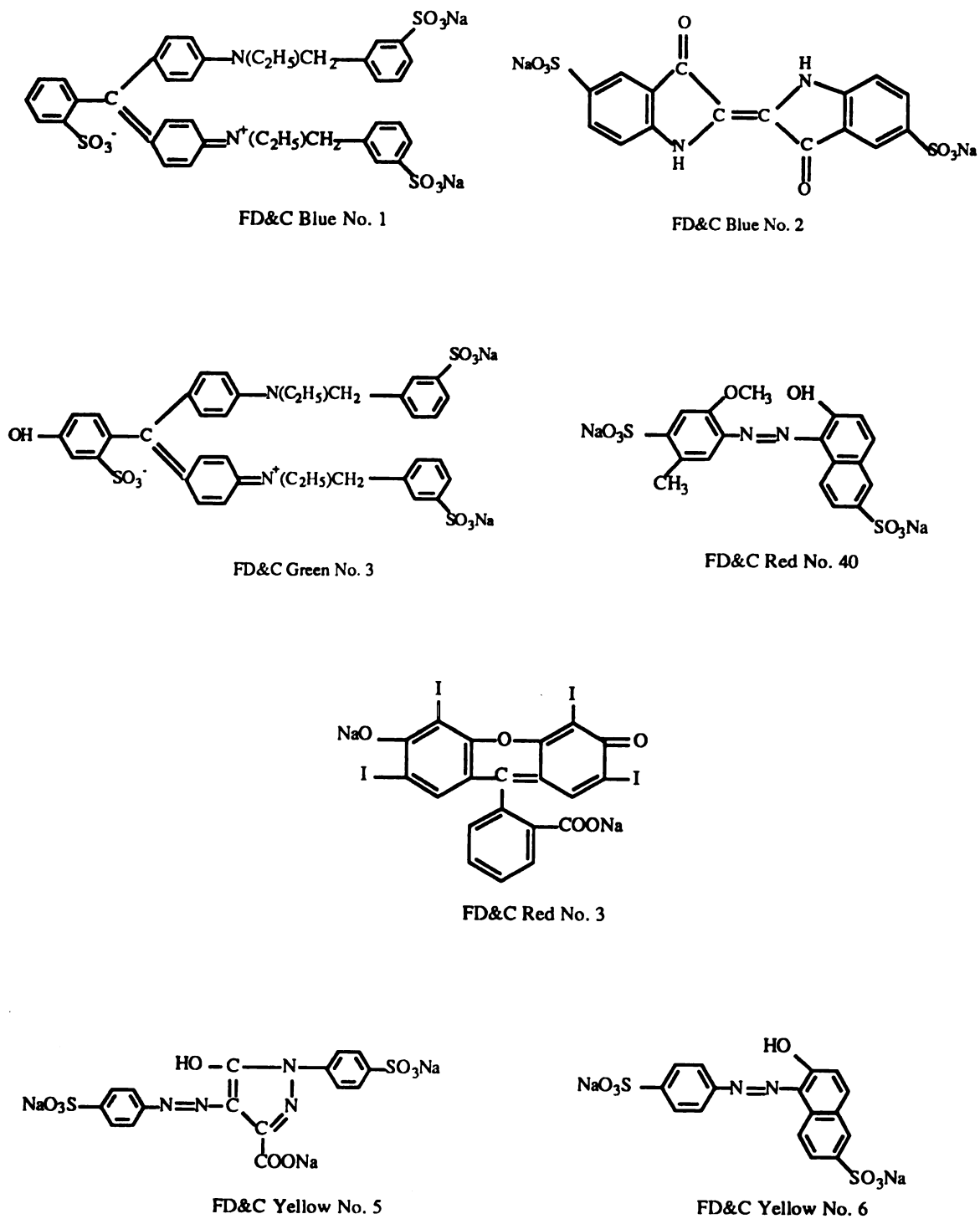


Figure 3.1 Molecular structures of the seven FD&C colors.

Table 3.1 Selected physical properties of the FD&amp;C colors [11].

Property	FD&C Blue No. 1	FD&C Blue No. 2	FD&C Green No. 3	FD&C Red No. 3	FD&C Red No. 40	FD&C Yellow No. 5	FD&C Yellow No. 6
Common Name	Brilliant Blue FCF	Indigo Carmine, Indigotine	Fast Green FCF	Erythrosine	Allura Red, NT Red	Tartrazine	Sunset Yellow FCF
Chemical Class	Triphenylamine	Indigoid	Triphenylmethane	Xanthene	Monoazo	Pyrazolone	Monoazo
Hue	Greenish Blue	Deep Blue	Bluish Green	Bluish Pink	Yellowish Red	Lemon Yellow	Reddish Yellow
Absorption Maxima*, nm	629	610	616	527	505	433	484
Fluorescence Maxima*, nm	664	-	662	550	587	-	-
Solubility in water at 25 °C, (gms/100mL)	20	1.6	20	9	22	20	19
Light Stability	Fair	Very Poor	Fair	Poor	Very Good	Good	Moderate

\* These values are from this work. For the fluorescence maxima, the excitation wavelength for each dye is mentioned in the text. All values are for emission in water, recorded at room temperature.

The drawback of using pyranine is its standing as a D&C grade color only and as such is not appropriate for use in food and pharmaceutical processes for fear of contamination. The present work is an attempt to circumvent this problem by screening dyes that have been approved as FD&C grade colors to test their efficacy for use as a concentration sensor in food and pharmaceutical systems. Although photochemical information other than the absorption spectra about the food grade dyes is not available, it is reasonable to believe, (by a comparison of the structures and properties), that the photochemistry is probably similar to that of pyranine. As discussed in the Results and Discussion section, the emission spectra confirm this assertion.

In this work, we report on the use of FD&C colors as probes for the measurement of the concentrations of the solutions in which they are placed. The impetus for this work is also derived from the fact that these colors are already present during the manufacture of the food items. For example, the FD&C colors are present during the processing of many varieties of candies and sodas. It is possible to use the emission properties of these colors *in situ*, to record concentration differences of the solutions in which they are present. The test crystallizing solute chosen is sucrose. Sucrose is chosen due to its low cost, high solubility, and high viscosity. Furthermore, more sucrose is crystallized worldwide than any other compound.

### 3.2 Materials and Methods

All FD&C colors used in this work were obtained as samples from Warner - Jenkinson Company, Inc. St. Louis, U.S.A. and had purities of 90%. They were used as obtained to confirm the practical utility of the approach. Sucrose (reagent grade) was obtained from Aldrich Chemical Co. Sucrose solutions of different concentrations (wt%) were prepared by dissolving the appropriate weight of sucrose in distilled water. All experiments were conducted at ambient temperature unless otherwise noted. In order to

prepare supersaturated solutions, the mixture was gently heated to a higher temperature so that all solids were dissolved and the solution was cooled back to the ambient temperature.

### **3.2.1 Absorption experiments**

Absorption spectra were collected on a Guided Wave Model 260 spectrophotometer equipped with a tungsten-halogen lamp as the light source and a silicon detector. Fluorescence emission spectra were collected on a SPEX FLUOROLOG spectrophotometer that has a xenon lamp as a source and a PMT detector.

For the absorption spectra, color solutions were prepared to give 5 ppm solutions of FD&C Blue No. 1 and FD&C Green No. 3; 10 ppm of FD&C Blue No. 2 and FD&C Red No. 4; and 20 ppm of the remaining four. The desired concentration was achieved in each case by dissolving 'x' grams of the color in 20 mL of water to make the stock solution. Next, 10  $\mu$ L of the stock solution was pipetted out and dissolved in 5 mL of distilled water. This protocol gave a concentration of '100x' ppm.

### **3.2.2 Fluorescence experiments**

For the fluorescence spectra, the stock solutions were prepared in a similar fashion, but in each case generating a sample sucrose solution that had a dye concentration of 1.0e-05 M. The smaller concentration compared to absorption is a necessity of the fluorescence experiment. A higher concentration causes undesirable effects such as the inner filter effect. The spectra of the free dyes in solution were collected by placing the test solutions in 4 sided 1 cm by 1 cm quartz cuvettes that were placed in the sample compartment of the FLUOROLOG. The excitation wavelengths used were as follows: for FD&C Red No. 40: 500 nm; for FD&C Green No. 3: 420 nm; for FD&C Blue No. 1: 400 nm; for FD&C Yellow No. 5: 433 nm; and for FD&C Yellow No. 6: 484 nm.

### **3.2.3 Immobilization of the probes**

For the experiments with the immobilized dyes, the food colors were immobilized on ion exchange membranes obtained from Schleicher and Schuell, Keene, NH. The specific membrane used was the DEAE cellulose acetate NA45 anion exchange membrane



that had a pore size of 0.45  $\mu\text{m}$ . The dye was immobilized on to the membrane using the following protocol. Five hundredths of a gram of FD&C Blue No. 1 was dissolved in 20 mL of distilled water. From this stock solution, 20  $\mu\text{L}$  was pipetted out and dissolved in 5 mL of distilled water to give a concentrated dye solution. A 2 cm by 0.5 cm strip of the membrane was placed in the solution and manually stirred vigorously for one minute and then thoroughly rinsed with distilled water. The membrane turned from white to a bright blue color. A sensor was constructed by attaching the membranes over the closed end of a 1 cm diameter flat-bottomed glass tube. A bifurcated fiber optic set, manufactured by SPEX, was inserted into the open end and placed flush with the closed end. One end of the bifurcated end was connected to the light source of the FLUOROLOG via a monochromator, whereas the other end was connected to the PMT detector. Thus, the bifurcated fiber optic served a dual purpose by providing the exciting light and collecting the emitted light from the probe. The emission and excitation slits were kept open at 2 mm and 6 mm, respectively. The complete sensor was directly dipped into a crystallizer. This arrangement is shown schematically in Figure 3.2.

### **3.3 Results and Discussion**

#### **3.3.1 Results with the 'free' dye in solution**

Fluorescence spectroscopy is an extremely sensitive technique that involves the study of the emission spectrum of a molecule after it has absorbed energy from an excitation source. Probe molecules absorb light of a specific wavelength and then emit the light at longer wavelengths. If this absorption and/or emission wavelength shifts as a result of the solvent environment that they are placed in, the probes are termed solvatochromic. In addition, some molecules exhibit a simple change in the emission intensities when placed in differing solution environments. Both types of change in the emission spectrum are extremely sensitive to small changes in the solvent concentration and can be used to monitor changes in the solution composition continuously.

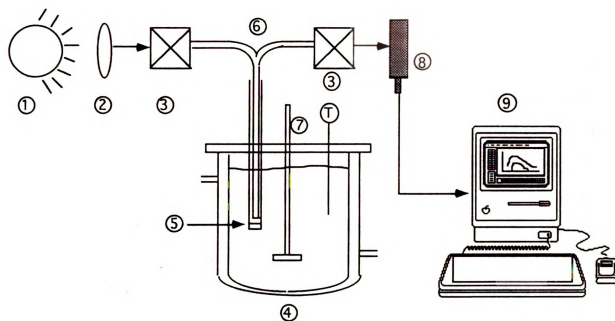


Figure 3.2 Schematic diagram of the apparatus used to measure the fluorescence from the immobilized sensor that is immersed in a crystallizer. 1) Source. 2) Collimating lens. 3) Monochromators. 4) Jacketed crystallizer. 5) Immobilized probe assembly. 6) Bifurcated fiber optic. 7) Stirrer. 8) PMT Detector. 9) Computer.

The main objective of this study was to screen the seven FD&C colors for their suitability to behave as analytical probes of the concentration of the solution in which they were placed.

Figure 3.3 shows the absorption spectra of each of the seven FD&C dyes. The wavelength corresponding to the maximum absorption indicates the wavelength that should be used as the excitation wavelength for fluorescence experiments. Each dye therefore will be excited at a wavelength corresponding to its absorption maximum.

In order to provide an internal standard for the emission measurements, it is necessary to normalize the spectrum. As a result, there would be no variation in data due to any instrumental artifacts. A normalized calibration curve should be the same regardless of any instrumental variations. Normalization can be accomplished in a variety of ways. The most common technique is to take a ratio of the intensities of two of the most intense peaks in a spectrum. Then, a calibration curve can be generated that shows the peak intensity ratio as a function of the solute concentration. Another possible normalization technique involves normalizing all spectra with respect to a standard spectrum, for example, a spectrum in pure water (0% sucrose). This latter technique is especially useful when there are no clear multiple peaks in the spectrum for the ratioing technique to be feasible. Both these techniques have been demonstrated here. The normalized parameter is then plotted against the solution concentration to give rise to a calibration curve that shows the strong dependence of one on the other.

FD&C Blue No. 2 (Indigo carmine) and FD&C Red No. 3 (Erythrosine) do not exhibit good stability towards light. Both colors fade appreciably within a week, that makes them unsuitable for use in a sensor. Hence, these two were not considered any further. Results obtained with the two yellow dyes, FD&C Yellow No. 5 and FD&C Yellow No. 6 showed no reproducible correlation to solute concentration. These, therefore, were also not considered any further as candidates for a concentration sensor. The lack of correlation is probably due to high pKa values of the excited state and

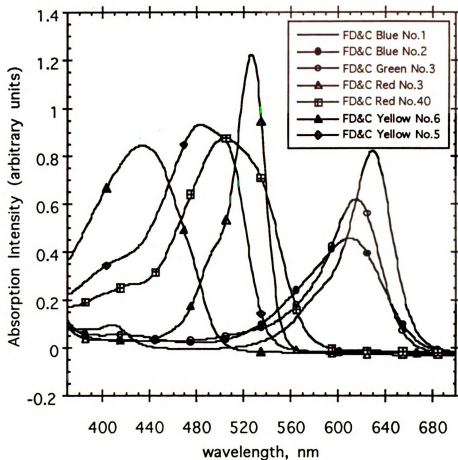


Figure 3.3 Absorption spectra of the FD&C colors. The concentrations of each in aqueous solution are: FD&C Blue No. 1 and FD&C Green No. 3: 5 ppm; FD&C Blue No. 2 and FD&C Red No. 40: 10 ppm; FD&C Blue No. 2, FD&C Red No. 3, FD&C Yellow No. 5, and FD&C Yellow No. 6: 20 ppm.

unfavorable polarization kinetics. The emission spectra of the remaining three dyes showed great promise. Figure 3.4 shows the fluorescence spectrum of FD&C Red No. 40 in differing sucrose solutions of 0, 10, 30, 50, and 65 wt % concentrations while Figure 3.5 shows the same for FD&C Green No. 3 in sucrose solutions of 30, 50, and 65 wt% concentrations. The spectrum for FD&C Blue No. 1 showed a similar response as the FD&C Red No. 40. It is interesting to note that the fluorescence of these dyes in pure water is close to zero but increases dramatically in the presence of the solute. This increase is explained on the basis of the fact that fluorescence is a mechanism for the relaxation of the energy absorbed by the molecules when exposed to an incident light. However, in an aqueous solution, the interactions due to random motion provide a path of lesser resistance for the relaxation to occur than fluorescence emission does. So, the amount of energy that manifests itself in the form of fluorescence is low. However, when the amount of solute in solution increases, there is less mobility of the dye molecules and the energy relaxation occurs more readily by fluorescence. Thus, the increase in solute concentration is responsible for the large increase in fluorescence.

The photochemistry of food colors and the kinetic diagram showing the emission properties is unknown. However, by studying these diagrams for some dyes whose photochemistry is known completely, like pyranine (Figure 2.1, Figure 2.2), it is possible to make some generalizations. In solutions, the dyes occur in the form of dissociated anions. The relative amounts of the anion and cation, which is affected by the amount of solute in solution, gives rise to the change in the emission peaks. In the case of pyranine, the only dissociated cation that can affect the equilibrium is the proton (the dissociated sodium ions do not play a role toward the application being considered); while in the case of the food dyes, it is very likely that there are a number of species in equilibrium in solution. So, while the relative protonation or deprotonation of pyranine gives rise to the two emission peaks; in the food dyes, the combined effect of the emission of all ionic species is responsible for the spectrum that is observed. Thus, theoretically, the broad

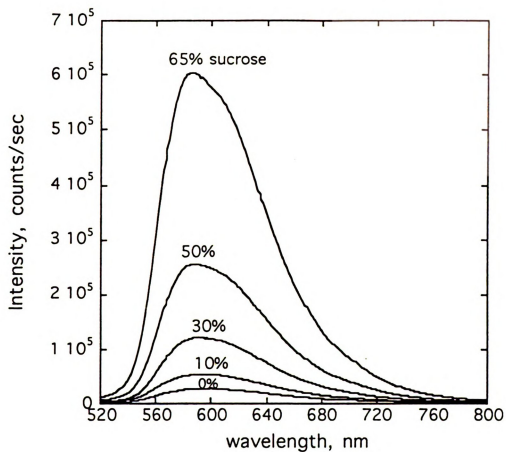


Figure 3.4 Emission spectra of FD&C Red No. 40 in sucrose solutions of different concentrations (expressed as wt%). All spectra recorded at room temperature (25 °C). Excitation wavelength: 500 nm.

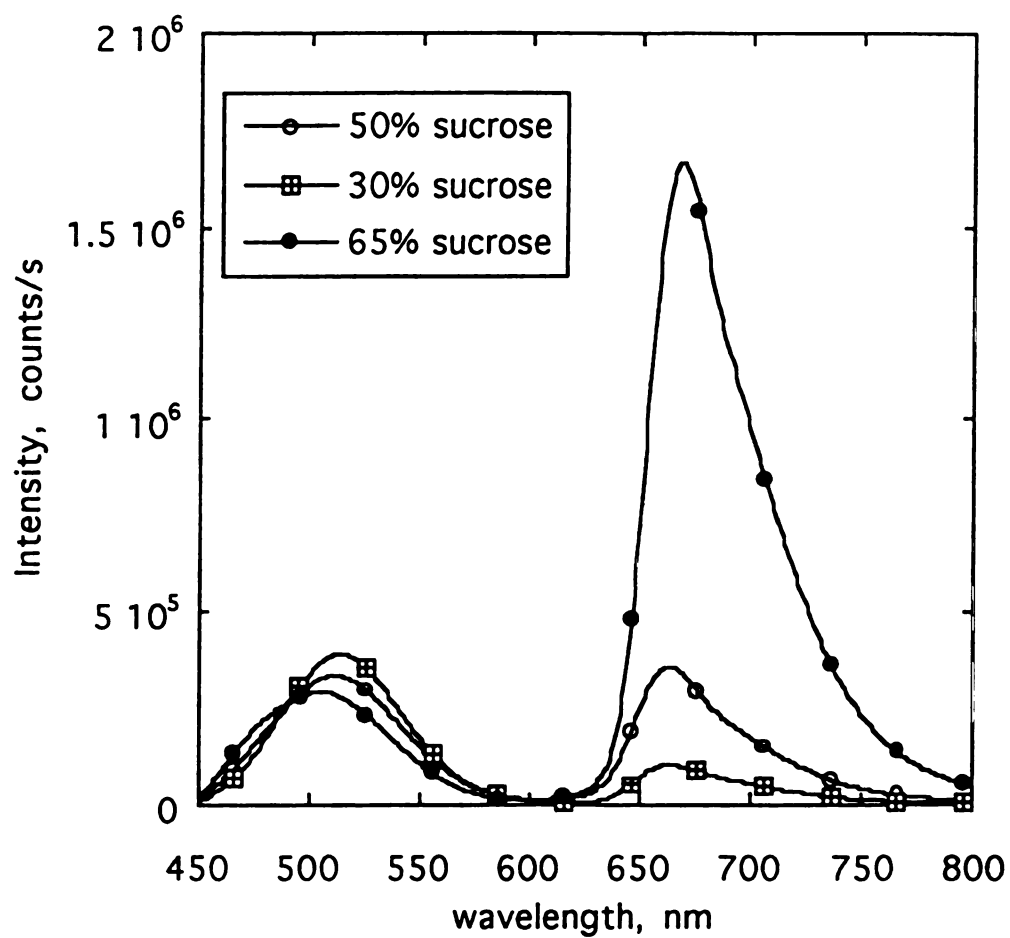


Figure 3.4 Emission spectra of FD&C Green No. 3 in sucrose solutions of different concentrations (expressed as wt%). All spectra recorded at room temperature (25 °C). Excitation wavelength: 420 nm.

peaks in the case of these food colors can be resolved into an appropriate number of peaks corresponding to the number of species in solution once the solution equilibrium is known. However, for the purpose and application in mind, the information available at this time is sufficient to construct a complete probe assembly for measuring concentration and supersaturation of solutions.

Figures 3.6 and 3.7 show the calibration curves obtained for the green and red dyes respectively. In the case of FD&C Green No. 3, the normalization parameter chosen, the Peak Intensity Ratio (PIR), is defined as

$$\text{Peak Intensity Ratio} = \frac{\text{Peak Intensity at 662 nm}}{\text{Peak Intensity at 515 nm}} \quad (3.1)$$

and is plotted against the sucrose concentration in Figure 3.6. For FD&C Red No. 40, the maximum intensity of each spectrum is divided by the maximum intensity of the spectrum at 0 wt% sucrose to give the Peak Intensity Ratio. The calibration curve so generated is shown in Figure 3.7. This calibration curve is also fit to an exponential curve with the parameters shown in the graph. A strong correlation coefficient is obtained that shows that this equation can very well be used for extrapolating the curve.

In both cases, a very strong non-linear dependence of the PIR on solution concentration is apparent. This dependence extends well into the highly concentrated region (above 65%) which is the critical region in crystallization experiments. In this region, the non-linearity of the calibration curve makes this technique especially sensitive, since small changes in solute concentration will be reflected by large changes in the PIR. Compare this to a conventional technique for measuring concentrations in a supersaturated solution such as refractometry, where changes are recorded only in the fourth or higher decimal place of the refractive index. This relatively large gain in signal demonstrates that the fluorescent probe technique is superior to conventional techniques in terms of sensitivity.



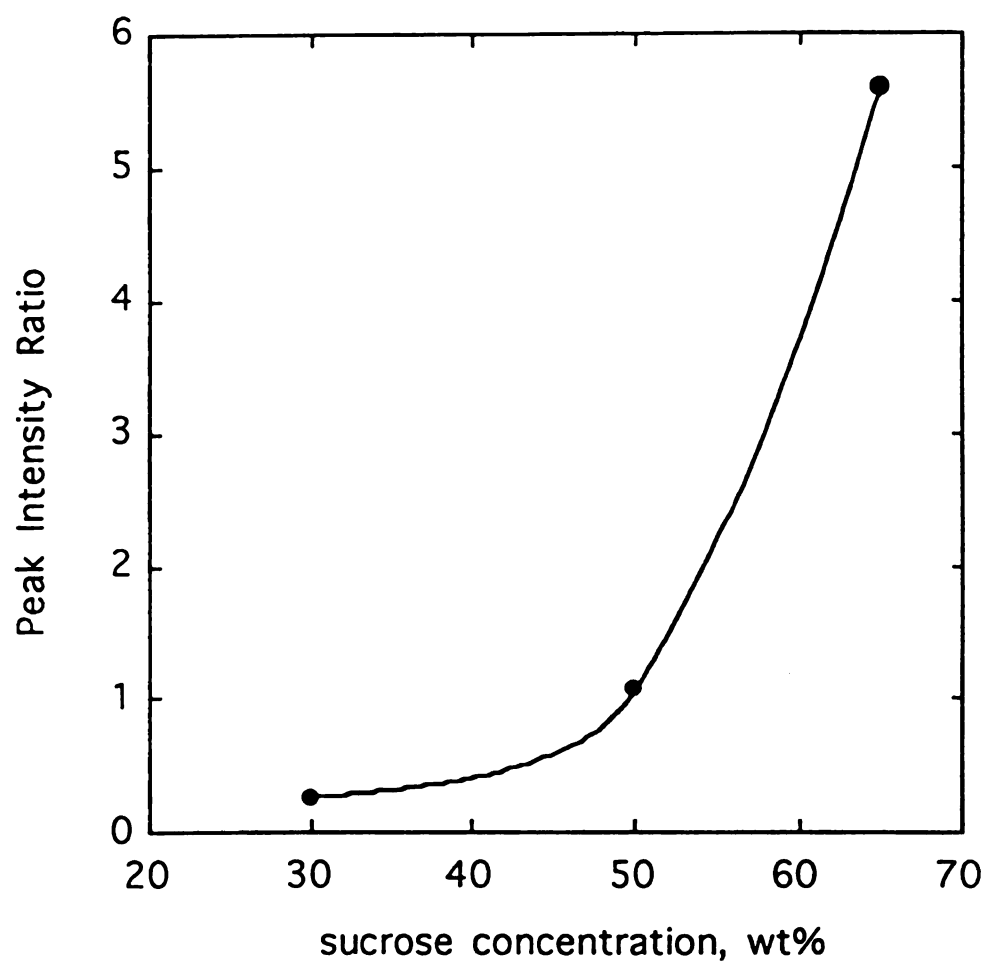


**Figure 3.6** Calibration curve showing the relation between the Peak Intensity Ratio (defined as the ratio of the peak intensities at 662 nm to that at 515 nm) and sucrose concentration for FD&C Green No. 3.

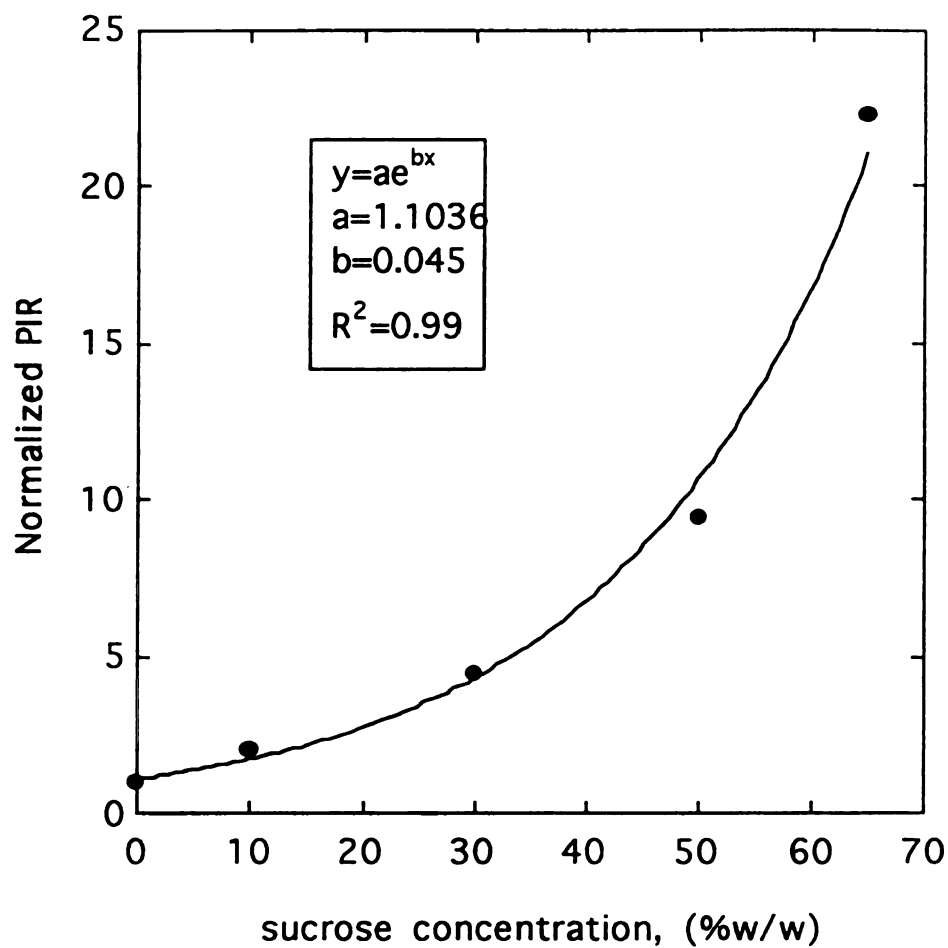


**Figure 3.7** Calibration curve showing the relation between the Peak Intensity Ratio (defined as the ratio of the peak intensities at 587 nm in each sample to the peak intensity at the same wavelength in 0% sucrose solution) and sucrose concentration for FD&C Red No. 40. Inset shows the parameters for an exponential fit to the curve.

### 3.3.2 Results with the immobilized dyes

In the work described so far, the probe was dissolved in water and was present freely in solution during the crystallization process. For use as an analytical sensor, it is desirable that the probe be attached to a surface to avoid concerns of contamination of the crystals by the probe. If a probe is immobilized on a surface, an immersion probe can be constructed that can be dipped into a crystallizer for *in situ* monitoring of concentration during the crystallization process. Also, in an industrial environment, remote sensing of supersaturation would be the preferred method of measurement. It is therefore necessary to immobilize the probe in a way such that its emission properties are preserved and at the same time a fiber optic arrangement be used for remote sensing. Direct coupling to the fiber optic, although a possibility, must be executed in a judicious manner in that it is likely to change the photochemical behavior of the molecule. A better approach is to immobilize the dye molecules on to a membrane and use the fiber optics to collect the emission off the probes taking care that the membrane material chosen is rigid and stable to biological and thermal degradation.

In this work, we report on immobilizing the probes onto an ion exchange membrane. A bifurcated fiber optic was used that served a dual purpose by shining the incident light and collecting the emitted light from the probe. The complete sensor was directly dipped into a crystallizer. This arrangement is shown schematically in Figure 3.2.

An ion exchanger is defined as a substance that is capable of reversible exchanges of its constitutional ions with some other external ionic species bearing the same charge [10]. All ion exchangers have a fundamental matrix that is fixed and chemically insensitive to the surrounding electrolytes. The hydrophilic site of exchange containing ionizable functional groups and mobile counterions is attached to this inert matrix. These counterions can be replaced when brought into contact with a solution containing ions of suitable charge and size.

Ion exchange onto a cellulosic anion exchanger is used for immobilizing the probe as all the FD&C dyes form anions in solution. Ion exchange celluloses are aggregates of glucosidic chains held together by interchain bonding, which provides dimensional stability to the matrix. Cellulosic exchangers can be fibrous or microgranular and are widely used in the purification of biological macromolecules. The microgranular variety is well suited to the study of organic molecules [10]. Some of the common commercially available cellulosic ion exchangers include AE cellulose, DEAE cellulose, TEAE cellulose, GE cellulose, PAB cellulose etc. Here, we use the NA45 DEAE cellulose acetate membrane which serves to immobilize all the FD&C dyes remarkably well without negatively affecting their emission properties. There are, however, some variations in the intensities obtained to that with the free dye in solution. This variation is attributed to the immobilization procedure that is known to cause some enhancement of the signal while also causing a significant increase in the baseline intensity. Furthermore, the presence of the silica fiber optics also causes an increase in the baseline that reflects in a slight loss of sensitivity. In spite of these effects, the immobilized probe shows good performance characteristics.

Figure 3.8 shows the emission response obtained from FD&C Blue No. 1 that is immobilized onto the anion exchange membrane. As is evident, there is a clear correlation between sucrose concentration and the emission spectrum of FD&C Blue No. 1. As an internal standard, we have defined a parameter called the Peak Intensity Ratio that is defined as the ratio of the intensities at wavelengths of 664 nm and 615 nm. Figure 3.9 shows the dependence of PIR on sucrose concentration. As was the case with the free dyes in solution, a marked non-linear change is observed in the PIR with sucrose concentrations over a wide range. This calibration curve can thus be used as an analytical probe for crystallizing sucrose solutions where the concentration is continuously changing. Work is currently in progress in developing immersible probes with the other FD&C colors.

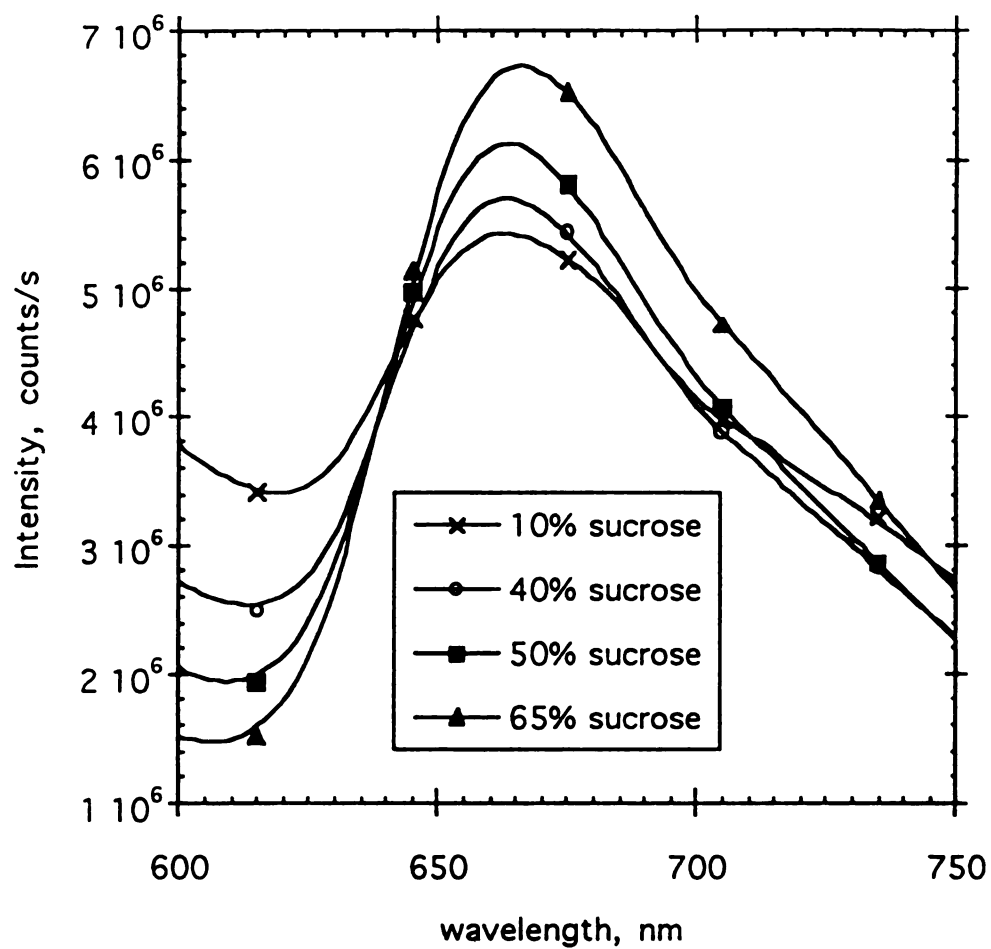


**Figure 3.8** Emission spectra of FD&C Blue No.1 in sucrose solutions of different concentrations (expressed as wt%). The dye molecules are immobilized onto an anion exchange membrane. All spectra recorded at room temperature. Excitation wavelength: 400 nm.

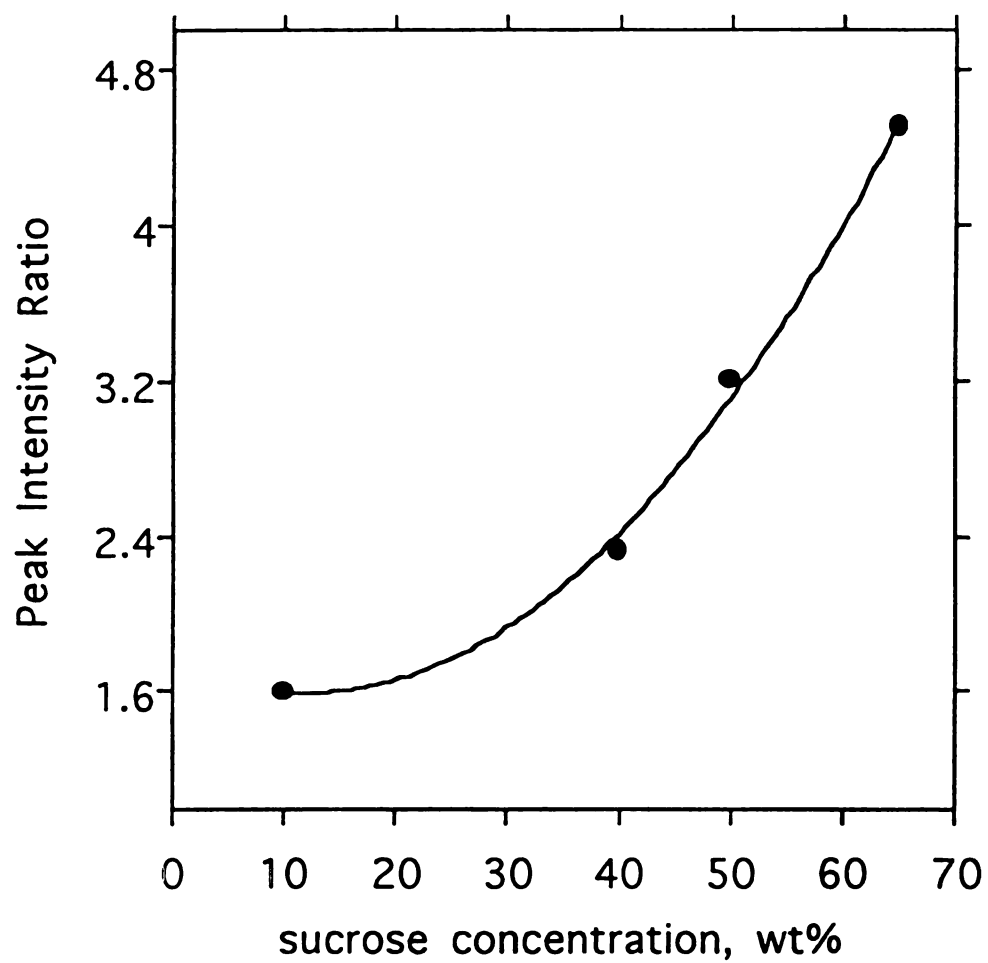


**Figure 3.9** Calibration curve showing the relation between the Peak Intensity Ratio (defined as the ratio of the peak intensities at 664 nm to that at 615 nm) and sucrose concentration for the immobilized FD&C Blue No.1.

### 3.4 Conclusions

The technical feasibility of a fluorescence probe sensor for the measurement of concentration and supersaturation in crystallizing solutions using food grade colors has been established. The use of fluorescence permits development of a sensor that directly measures a property (Peak Intensity Ratio) that is fundamentally related to the activity rather than the concentration of the solute. The major advantage of this technique is that the food colors are already present during the manufacture and processing of the foods, and so can be used *in situ*. Besides, the inherent non-toxicity of these compounds is a major advantage over more conventional probes, most of which would not be approved for use in food products. There are no other known commercial devices on the market based on this concept. Additionally, the use of an optically based system provides many advantages including no interference from electrical noise and low cost resulting from recent developments in fiber optics.

### 3.5 References

1. D. M. Marmion, In: *Handbook of U.S. Colorants*. 3rd. Ed. John Wiley & Sons, Inc. New York. pp 84, (1991).
2. J. D. Dziezak, *Food Technology*, Applications of Food Colorants. **41(4)**, 78-88, (1987).
3. P. Markakis, Food Colors. In: *Encyclopedia of Physical Science and Technology*. Vol. 5. 502-517, (1987).
4. R. Chakraborty, K. A. Berglund, *Journal of Crystal Growth*, Steady State Fluorescence Spectroscopy of Pyranine as a Trace Extrinsic Probe to Study Structure in Aqueous Sugar Solutions. **125**, 81-96, (1992).
5. R. Chakraborty, K. A. Berglund, *AIChE Symposium Series No. 284*, The Use of Pyranine as a Trace Fluorescent probe to Study Structure in Aqueous Sucrose Solutions. **83**, 114-123, (1991).

6. S. K. Yedur and K.A. Berglund, Use of Fluorescence Spectroscopy in Concentration and Supersaturation Measurements in Citric Acid Solutions. Accepted for publication in *Applied Spectroscopy*. (1996).
7. H. Kondo, I. Miwa, and J. Sunamoto, *Journal. Phys. Chem.*, Biphasic Structure Model for Reversed Micelles. Depressed Acid Dissociation of Excited-State pyranine in the Restricted Reaction Field. **86**, 4826-4831, (1982).
8. H. Stapelfelt, H. Jun, and L. H. Skibsted, *Food Chemistry*, Fluorescence properties of carminic acid in relation to aggregation, complex formation and oxygen activation in aqueous food models. **48**, 1-11, (1993).
9. J. P. Rasimas and G. J. Blanchard, *J. Phys. Chem.*, Understanding the Electronic Properties of Glycosylated Chromophores Using AM1 Semiempirical Calculations. **98:49**, 12949-12957, (1994).
10. P. R. Brown and A. M. Krstulovic, In: *Separation and Purification*. 3rd Edition. Eds. Edmond Perry and Arnold Weissberger. Chapter IV, John Wiley & Sons, New York 197-255, (1978).
11. Certified Food Colors. Published by: Warner -Jenkinson Company, Inc. St. Louis, MO, U.S.A. (1995).



## **Chapter 4**

# **A SOL-GEL BASED FLUORESCENCE SENSOR FOR CONCENTRATION MEASUREMENTS IN SUCROSE SOLUTIONS**

### **4.1 Background**

An ideal optical sensor should have the capability to detect fluctuations in analyte concentration continuously; that is, the optical probe should interact with the analyte in a reversible manner for long periods of time. The development of the sol-gel process has enabled the construction of novel materials that are well suited to optical sensing and various detection systems [1, 2]. In addition to providing transparent and porous materials, the sol-gel technique offers a number of modifying techniques that can be used to incorporate molecular probes into the polymer matrix without any loss of optical properties [3]. The primary focus of this investigation was to study the feasibility of using sol-gel derived thin films for sensory applications in aqueous crystallizing solutions, where typically the concentrations are very high. Conventional techniques of measuring concentration and supersaturation in crystallization operations like refractometry, turbidity measurement etc., involve the use of mass concentration measurements that lack the sensitivity required for optimum process control. More accurate measurements can be made by the use of the fluorescent probe technique [4]. In this work, we report on the use of the fluorescent properties of a chlorin incorporated in a sol-gel thin film to measure the

concentration of aqueous sucrose solutions. Sucrose is chosen as the test analyte because of its high solubility, and because of the fact that more sugar is crystallized in the world today than any other chemical.

Under controlled conditions, solution precursors of sol-gel systems can be prevented from forming gels. Stable solutions thus obtained can be used to make thin films supported on various substrates using dipping, spin casting, or deposition techniques. These thin films retain the structural integrity of porous sol-gel glasses along with high internal surface area and favorable optical properties. Thin films that are porous, optically transparent, mechanically stable and resistant to aqueous and organic solvents were produced by controlled hydrolysis of titanium (IV) isopropoxide using valeric acid as the chelating ligand. Ethanol was used for controlling the hydrolysis which is the key to make thin sol-gel films [5]. Spin casting was used exclusively to produce the films while dip coating was used to incorporate the probe into the matrix. The probe used was a member of the chlorin family - octaethyl chlorin diol. The chlorins are related to the naturally occurring porphyrin group of molecules and are inherently non-toxic. Thus the test strip that was used as the sensor for measurement of concentrations in sucrose solutions was composed of the chlorin entrapped within the sol-gel film.

## 4.2 Materials and Methods

The specific chlorin used as the molecular optical probe was octa ethyl chlorin diol that was synthesized and provided by Chang [6]. The structure of the molecule is shown in Figure 4.1.

Titanium(IV)isopropoxide and valeric acid were obtained from Aldrich Chemical Company and used without further purification. Absolute ethanol was obtained from the Quantum Chemical Corporation. VWR microscope slides that were cut to fit 1 x 1 cm Cuvettes were used as substrates for films. An International Clinical Centrifuge (model CL 26802 M) was used for spin-casting films. Fluorescence spectra were taken with a SPEX

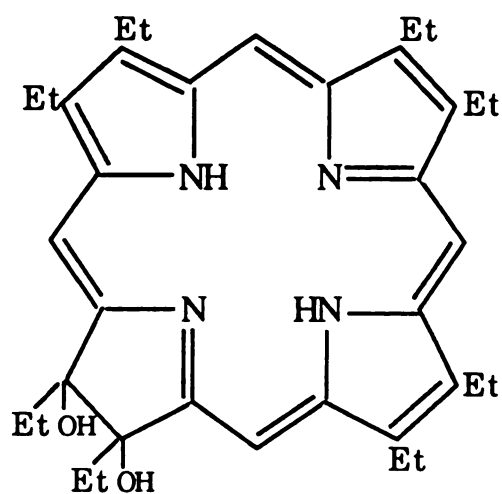


Figure 4.1 Chemical structure of Octaethyl chlorin diol.

FLUOROLOG spectrophotometer that was attached to PMT detector and a computer for recording and processing the data.

#### **4.2.1 Film preparation**

In a scintillation vial, 0.75 milliliters of valeric acid was added to 0.25 milliliters of titanium isopropoxide. Twenty microliters of distilled water was added to this mixture which was thoroughly mixed to give the film solution. Fifteen microliters of the solution was placed on to a clean glass slide. This was attached to the arm of the centrifuge and spun for 10 minutes. The sol-gel film thus formed on the slide was placed in a dust free chamber. The films were calcined in an oven at 250 °C for one hour primarily to drive off excess valeric acid that possesses an unpleasant odor. Calcination was started within one hour of the preparation of the film. This protocol gave films that were smooth, uncracked, and of uniform thickness.

#### **4.2.2 Entrapment of the chlorin**

Numerous screening experiments were conducted to determine the optimum concentrations to be used as well as the experimental protocol. As a result, the chlorin solution was prepared by dissolving 1 mg of octaethyl chlorin diol in 100 microliters of dichloromethane in a vial and mixing well. Four milliliters of 200 proof ethanol was added to the solution with constant stirring. Since chlorin is sensitive to ambient light, the vials were kept wrapped in aluminum foil.

The entrapment of the chlorin within the matrix was achieved by dip coating the titanium carboxylate thin film in the chlorin solution. The calcined films were dipped into the chlorin solutions two at a time for 15 minutes. This time duration was sufficient for the chlorin from the film solution to migrate into the sol-gel film. The resulting film was then rinsed with water and air dried with compressed air. All films were wrapped in aluminum foil and stored in a dust free environment.

The performance of the chlorin entrapped within the polymer matrix was evaluated using emission spectroscopy. Cast films supported on cut slides were placed vertically

inside quartz cuvettes. The glass slide with the film was placed against one wall of the cuvette such that the film was facing the incident light. Instead of the conventional right angle arrangement for recording emission, the cuvette was placed in the spectrophotometer cell compartment with a front face configuration (22 degree angle to incident light) to avoid stray incident light entering the detector. An excitation wavelength of 400 nm was used for the chlorin while emission was recorded from 600 to 750 nm.

## **4.3 Results and Discussion**

### **4.3.1 Sol-gel films**

After preparation using the protocol previously described, the films were calcined in an oven at 250 °C for one hour primarily to drive off excess valeric acid that possesses an unpleasant odor. The calcination also causes the transformation of the nature of the film from titanium carboxylate to a titanium oxide film [7].

### **4.3.2 Free chlorin in aqueous solutions**

Figure 4.2 shows the emission spectra of free octaethyl chlorin diol in aqueous sucrose solutions of 10, 30, and 50 wt %. As is evident, there is a marked change in the emission behavior of chlorin with an increase in solute concentration. The challenge was to obtain similar changes in the emission spectra from chlorin after it had been entrapped within the sol-gel matrix.

### **4.3.3 Entrapment of the chlorin**

Guest molecules can be entrapped within the porous matrix of sol-gel derived thin films either by dissolving them in the film solution prior to spin casting or by dip coating [8, 9]. This procedure requires the chlorin to be sufficiently soluble in a solution such that a functional amount of chlorin is available within the thin film to react with the target analyte. The dip coating technique used in this work provided films that were tested as a sensor with success.

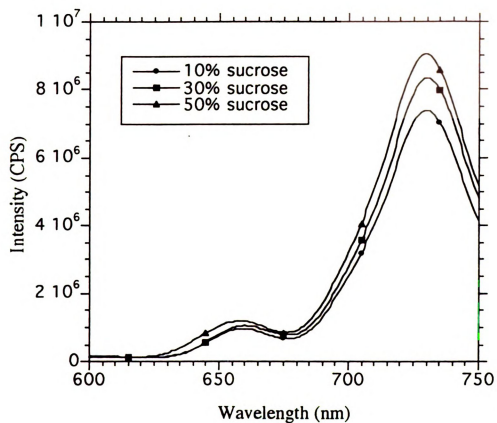


**Figure 4.2** Emission spectrum of free chlorin in solution in different sucrose solutions. All spectra collected at room temperature.

Although chlorins demonstrate a high degree of thermodynamic stability, there are some instability phenomenon associated with them. These are photodecomposition [10] and instability due to aggregation [11, 12, 13]. The first problem was taken care of by ensuring that the film and the precursor solutions were always stored in the dark. The second problem was taken care of by using controlled hydrolysis.

The role of controlled hydrolysis to produce sol-gel derived thin films and the important role played by modifying reagents has been reported [5]. Reagents such as alcohol can improve important properties of the film such as optical transparency, thermal stability, resistance to solvents etc. In the sol-gel process, alcohols are often used as the solvent. However, unlike most other solvents that are chemically inert, alcohols take part in reactions that take place during the sol-gel process. Therefore, alcohols are very effective in controlling the final structural properties of sol-gel derived materials. As a modifying reagent, ethanol, in addition to being a dispersive agent, can also participate in alcoholysis in sol-gel systems. This two fold effectiveness of ethanol renders it an ideal candidate for stabilization of the film.

We have demonstrated that chlorins can be entrapped within the porous matrix of sol-gel derived thin films by immersing the sol-gel film in a chlorin solution. In effect, we have a sensor made up of a fluorescent chlorin, which is entrapped within a titanium matrix that itself is bound to glass. The film is stable in aqueous solutions. The fluorescence intensity of the chlorin changes with respect to the solvent microenvironment in which it is placed. This effect is shown in Figure 4.3 which shows the changes in the emission spectra of chlorin in different aqueous sucrose solutions. This figure shows that the entrapped chlorin is still optically active and is available for sensing sucrose. A comparison with Figure 4.2 shows that while the wavelength's match quite well, the intensities of the peaks are quite different from that of the spectra of the free chlorin. The change in the intensities is to be expected because of the immobilized nature of the chlorin. The immobilization causes formation of secondary bonds within the sol-gel matrix. This

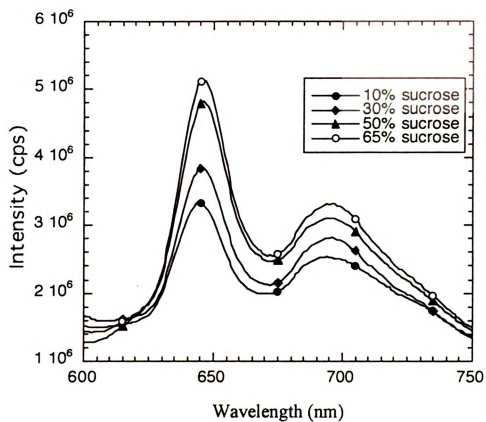


Figure 4.3 Changes in emission spectra of chlorin embedded in a titanium carboxylate thin film in various aqueous sucrose solutions; all spectra collected at room temperature.



chemistry causes changes in the photochemical behavior of the emitting species [14] and explains the observed change in the intensities of the emission bands of the chlorin in free solution and in the immobilized state.

Figure 4.3 also demonstrates the effect of sucrose on the emission spectrum of the entrapped chlorin. Even though the changes observed due to the sucrose is not too great in absolute numbers, the change observed is quite adequate for the measurement of the concentration in sucrose solutions. Also, as the figure shows, a change is seen in the spectrum with sucrose concentration through the ranges of high concentration where crystallization is expected. The potential of this sensor to be used in a crystallizer, where high concentrations of the solute are to be expected, has been established. A calibration curve can be created using the information in Figure 4.3 relating a normalized parameter from the emission spectrum. As an internal standard, the ratio of the peak intensities at two wavelengths is calculated that takes care of variations in the absolute intensity numbers. In this case, the ratio is taken of the intensities of the two peaks at 646 nm and at 673 nm. This peak intensity ratio is the parameter that is plotted against the sucrose concentration to generate the calibration curve that is shown in Figure 4.4. A linear curve fit gives an  $R^2$  value of 0.995. Thus, the concentration of an unknown concentration of an aqueous sucrose solution can be determined using this calibration curve.

Since the intensities of the two peaks are dependent upon the relative amounts of water present in the vicinity of the probe molecules, the relative intensity of the two emission peaks of chlorin can be used effectively as a sensor for measurement of the concentration of solute in a crystallizing solution. Thus, this technique of combining sol-gel technology with fluorescence spectroscopy can be used as a sensor to measure the concentrations of sucrose solutions.

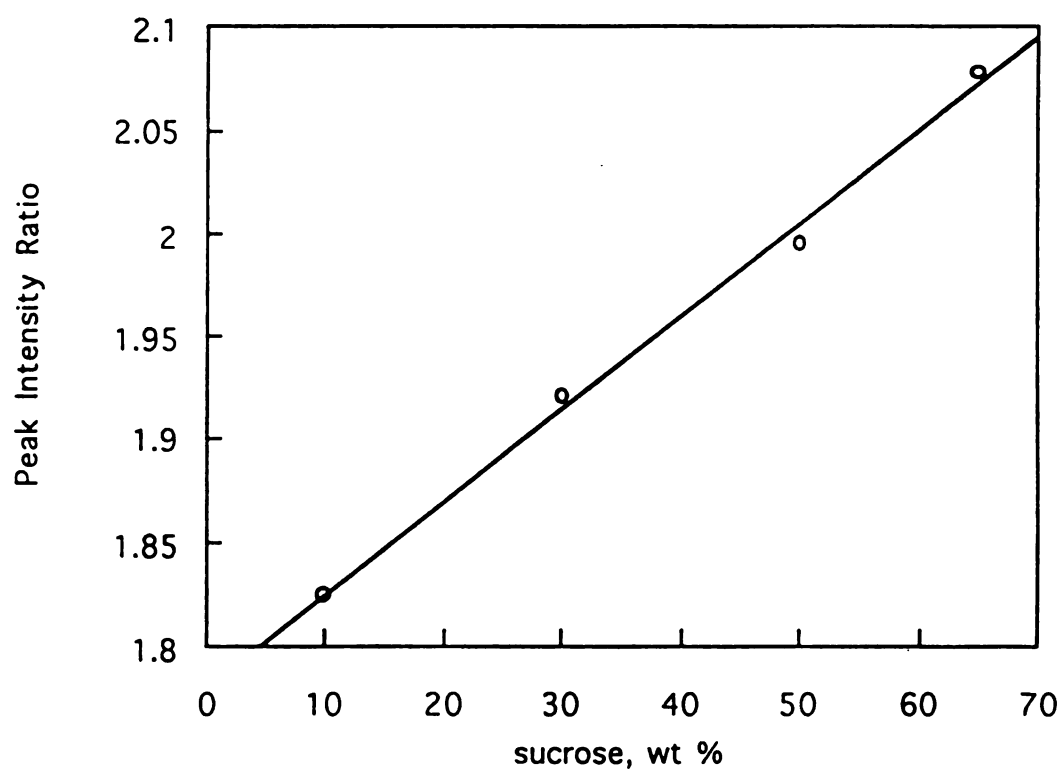


**Figure 4.4** Calibration curve showing a linear relationship between the Peak Intensity Ratio (defined as the ratio of the intensities of the peaks at 646 nm and 673 nm) and sucrose concentration.

## 4.4 References

1.
  - a. D. D. Dunuwila, B. A. Torgerson, C. K. Chang, and K. A. Berglund, *Anal. Chem.*, **66**, 2739, (1994).
  - b. K. G. Severin, J. S. Ledford, B. A. Torgerson, and K. A. Berglund, *Chem. Mater.*, **6**, 890, (1994).
2.
  - a. H. Reuter, *Adv. Mater.*, **3:5**, 258, (1991).
  - b. J. Livage, M. Henry, and C. Sanchez, *Progress in Solid State Chemistry*, **18**, 259, (1988).
  - c. H. Zheng, M. W. Colby, and J. D. Mackenzie, *Mat. Res. Soc. Symp. Proc.*, **121**, 537, (1988).
  - d. H. Schmidt, G. Rinn, R. Nab, and D. Sporn, *Mat. Res. Soc. Symp. Proc.*, **121**, 743, (1988).
  - e. F. Babonneau, A. Leautic, and J. Livage, *Mat. Res. Soc. Symp. Proc.*, **121**, 317, (1988).
  - f. S. M. Melpolder and B. K. Coltrain, *Mat. Res. Soc. Symp. Proc.*, **121**, 811, (1988).
3.
  - a. L. M. Ellerby, C. R. Nishida, F. Nishida, S. A. Yamanaka, B. Dunn, J. Selverstone-Valentine, and J. I. Zink, *Science*, **255**, 1113, (1992).
  - b. A. Slama-Schwok, M. Ottolenghi, and D. Avnir, *Nature*, **355**, 240, (1992).
  - c. I. Kuselman, B. I. Kuyavskaya, and O. Lev, *Anal. Chim. Acta.*, **256**, 65, (1992).
  - d. A. Schowk, D. Avnir, and M. Ottolenghi, *J. Am. Chem. Soc.*, **113**, 3984, (1991).
  - e. T. Haruvy and S. E. Webber, *Chem. Mater.*, **3**, 501, (1991).
  - f. R. Zusman, C. Rottman, M. Ottolenghi, and D. Avnir, *J. Non-Cryst. Solids*, **122**, 107, (1990).
  - g. B. Dunn, E. Knobbe, J. M. McKiernan, J. C. Pouxviel, and J. I. Zink, *Mat. Res. Soc. Symp. Proc.*, **121**, 331, (1988).
  - h. D. Avnir, D. Levy, Reisfield, *J. Phys. Chem.*, **88**, 5956, (1984).

4.    a. R. Chakraborty and K. A. Berglund, *AIChE Symposium Series no. 284.*, **83**, 114, (1991).  
      b. R. Chakraborty and K. A. Berglund, *J. Crystal Growth*, **125**, 81, (1992).  
      c. S. K. Yedur and K. A. Berglund, Accepted for publication in: *Appl. Spec.*, (1996).
5.    D. D. Dunuwila, C. D. Gagliardi, and K. A. Berglund, *Chem. Mater.*, **6**, 1556, (1994).
6.    C. K. Chang, Department of Chemistry, Michigan State University, personal communication, (1993).
7.    M. J. Waner, *Characterization of the Sol-Gel and MOCVD Processes for the Deposition of Aluminum Oxide Thin Films*. M.S. Thesis. Michigan State University, (1994).
8.    R. B. Lessard, M. M. Wallace, W. A. Oertling, C. K. Chang, K. A. Berglund, and D. G. Nocera, *Mat. Res. Soc. Symp. Ser.*, **155**, 109, (1989).
9.    C. D. Gagliardi, D. D. Dunuwila, C. K. Chang, and K.A. Berglund, *Mat. Res. Soc. Symp. Proc.*, **271**, 645, (1992).
10.   J. W. Buchler, In: *The Porphyrins: Structure and Synthesis, Part A*, Dolphin, D., Ed., Academic Press: New York, NY, Vol. 1, ch. 10, (1978).
11.   A. E. Alexander, *J. Chem. Soc.*, 1813, (1937).
12.   J. A. Bergeron, J. G. L. Gaines, and W. D. Bellamy, *J. Colloid Interface Sci.*, **25**, 97, (1967).
13.   W. I. White, In: *The Porphyrins: Physical Chemistry, Part C*, Dolphin, D., Ed., Academic Press, New York, NY. Vol. V, ch. 7. (1978).
14.   M. Bacci, F. Baldini, and S. Bracci, *Appl. Spec.*, **45**, 1508, (1991).

## **Chapter 5**

# **ON THE APPLICATION OF FLUORESCENCE SPECTROSCOPY TO MEASURE THE DESUPERSATURATION OF CITRIC ACID SOLUTIONS**

## **5.1 Background**

Desupersaturation studies are usually isothermal experiments conducted on seeded or unseeded supersaturated solutions to study the effects of various parameters such as seed size, seed surface area (or number of seeds), agitation, and supersaturation on the crystallization process. The desupersaturation studies also indicate the induction time and can give quantitative information about the growth and nucleation rates. The changes in the solution that occur during crystallization and affect the final product are of considerable interest for the design and control of a crystallizer.

Improved crystal size distribution is one of the most important concerns in any crystallization operation. Maintaining a constant supersaturation is recognized as the key for obtaining improved CSD's in batch crystallizers. In its most fundamental form, supersaturation is defined as the difference between the chemical potential of the solute on the crystal surface and that in solution. However, in all measurement techniques currently used, such as refractometry, supersaturation is approximated by the concentration difference of the solute in the supersaturated solution and its equilibrium solubility or by a ratio of the two concentrations. This approximation involves an underlying assumption of ideality that is strictly valid only for very dilute solutions [1]. For concentrated solutions,

such as those that might be expected in crystallization operations, this approximation can lead to serious errors in the measurement of supersaturation because of the high degree of nonideality of the solution [2]. A detailed discussion of these approximations and the errors caused by their use was presented in Chapter 2.

The nonideal behavior of a solution is reflected in the activity coefficient  $\gamma$ . The activity coefficient is strongly affected by the extensive intermolecular and intramolecular interactions between the solute and the solvent that define the solution structure of the whole system. It follows then, that the activity coefficient is strongly dependent on the solution structure at a molecular level. Thus, a technique for measuring the supersaturation that is reflective of the solution structure would be inherently more accurate than conventional systems that measure bulk properties that are not sensitive to the solution structure at a molecular level.

A novel analytical tool - the fluorescence probe technique - has been developed in our laboratory utilizing fluorescence spectroscopy to measure concentration and supersaturation of crystallizing solutions. This technology has been demonstrated to work exceedingly well for crystallizing solutions of various sugars and also of citric acid [3, 4, 5]. Fluorescence spectroscopy is fundamentally reflective of the intermolecular interactions and is thus strongly dependent on the solution structure. It has been shown that the solvatochromic nature of the fluorescent probe molecule pyranine, whose structure is shown in Figure 2.1, can be exploited to get a calibration curve correlating the solute concentration to a peak intensity ratio that is obtained from collecting the emission spectrum of the probe. In this work, we report on using the solvatochromic properties of pyranine to study the desupersaturation of citric acid.

## 5.2 Materials and Methods

Reagent grade anhydrous citric acid was obtained from Aldrich Chemical Co. and was used without further purification. The fluorescence probe Pyranine (chemically, the

trisodium salt of 8 - hydroxy, 1, 3, 6 - pyrene trisulfonic acid), was obtained from Lancaster, and was used as obtained. Distilled water was used in all experiments.

The desupersaturation experiments were carried out in a batch jacketed crystallizer that had a working volume of 1L. The temperature of the crystallizer was controlled by circulating water through the jacket from a water bath whose temperature was controllable to 0.1 °C. For each experiment, 300 mL of free solvent was used. To this, an appropriate amount of anhydrous citric acid was added to generate a supersaturation  $S$  of 1.2. Here,  $S$  is defined as the ratio of the amount of solute in solution to the equilibrium solubility at any given temperature. A constant stirrer speed of 400 rpm was used in all experiments. To get an exact amount of probe in the crystallizer for each experiment, a stock solution was prepared by dissolving 0.015 gm of pyranine in 50 mL of water. From this stock solution, 0.3 mL was carefully added to the crystallizer. This protocol generated a probe concentration of  $1.0 \times 10^{-5}$  M in the crystallizer which is an appropriate concentration for fluorescence experiments. In the experiments where the probe concentration was varied, a different amount of stock solution was added to the crystallizer to get the desired concentration.

The fluorescence spectrum of the probe in solution was recorded with the aid of a fiber optic cable that was introduced into the crystallizer through a port. The fiber optic was enclosed within a glass tube that was sealed at one end. The fiber tip was placed flush against this sealed end and was able to pick up the fluorescence emitted by the probe molecules through the glass barrier. For the pyranine molecules to emit light, they need to be excited at a fixed wavelength. The excitation light was provided by a hand held ultra violet light source marketed by Cole-Parmer Inc. The lamp generated light that had a primary wavelength of 365 nm. Since pyranine can be excited by light with a wavelength around 350 nm, this lamp was appropriate for exciting the pyranine molecules. The fiber optic was connected to a single channel spectrophotometer manufactured by Ocean Optics, Inc. The spectrophotometer comes equipped with a diode array detector that is optimized to

collect any light that comes through the fiber optic from a range of 225 to about 800 nm. The spectrophotometer itself was connected to a Pentium processor based computer that was used for data analysis.

Desupersaturation experiments at constant temperatures were conducted by first dissolving the appropriate amounts of anhydrous citric acid in the 300 mL of water at a slightly elevated temperature than the temperature of the experiment to generate a supersaturated solutions. After complete dissolution, the temperature was held at least 10 degrees higher than the saturation temperature for about 15 minutes to ensure the dissolution of all nuclei. The temperature was then brought down to the temperature of the experiment. All experiments were conducted isothermally.

Seeds were introduced into the crystallizer at time zero at which time the recording of the fluorescence spectra of pyranine commenced. The spectra were recorded at an interval of 1 minute for either ninety minutes or two hours. The seeds were of a monosized distribution with an average length of 780 microns unless otherwise noted. At the end of the experiment, the crystals that had grown in the crystallizer were filtered in a Büchner funnel, washed with a cold saturated citric acid solution and then washed again with ether to remove all water. For experiments at 25 °C, the effect of the amount of seed used was studied by using 3 gms, 15 gms, and 34 gms of seeds. In another series of experiments, desupersaturation was conducted at temperatures of 20 °C, 25 °C, and 30 °C to study the effect of temperature. In these latter experiments, a constant seed weight of 3 gms was used. To establish the effect of the probe concentration on the desupersaturation curve, identical desupersaturation experiments were conducted with three probe concentrations, 1e-05 M, 5e-06 M, and 1e-06 M.

### 5.3 Results and Discussion

The emission properties of pyranine have been well characterized [6]. In aqueous solution, pyranine exists with the sulfonate groups dissociated. Upon excitation with light



at wavelength around 350 nm, it has two excited states. One, emitting at around 440 nm, is due to the protonated form of the molecule, whereas the other, emitting at around 510 nm, is due to the deprotonated form. Whether the observed emission is from the protonated form or from the deprotonated form of pyranine depends on the molecular environment in its immediate vicinity. When surrounded completely by water molecules, pyranine exists solely in the deprotonated state, as water causes complete dissociation. The emission appears only at 510 nm. As the amount of solute in solution increases, the dissociated form starts getting protonated, and the emission spectra shows a shift in the peaks. The peak at 510 nm decreases, whereas the peak at 440 nm, which is due to the protonated form, increases. These observations are illustrated in Figure 2.3. Thus, solute-solvent interactions in solution can be studied by observing the relative changes in the emission peaks of pyranine.

The emission spectra in Figure 2.3 show that over the range from 0% citric acid to well above saturation, the two emission peaks change a lot. However, in an actual crystallization operation, the solution has to remain supersaturated. As soon as the solution concentration falls to saturation, crystallization is complete. Thus, under crystallization conditions, the relative change in emission peaks will not be as dramatic as is apparent in Figure 2.3. In fact, the peak at 510 nm, caused by the deprotonated state of pyranine, will hardly be visible as the solution concentration is very high. Although present, it will be dwarfed by the emission caused by the protonated form of pyranine that fluoresces at around 440 nm. As mentioned earlier, the use of fiber optics can cause a bathochromic shift in emission peaks. This is borne out in Figure 5.1 which shows the spectra obtained from a desupersaturation experiment. The emission peak appears at 449 nm. The experiment was carried out under the following conditions. Temperature = 25 °C, initial supersaturation ( $c/c^*$ ) = 1.2, agitator speed = 400 rpm, probe (pyranine) concentration =  $1.0 \times 10^{-5}$  M, seeds (average size 660 microns) = 3 gms. The excitation light for the pyranine molecules was provided from a UV light source that had a primary output

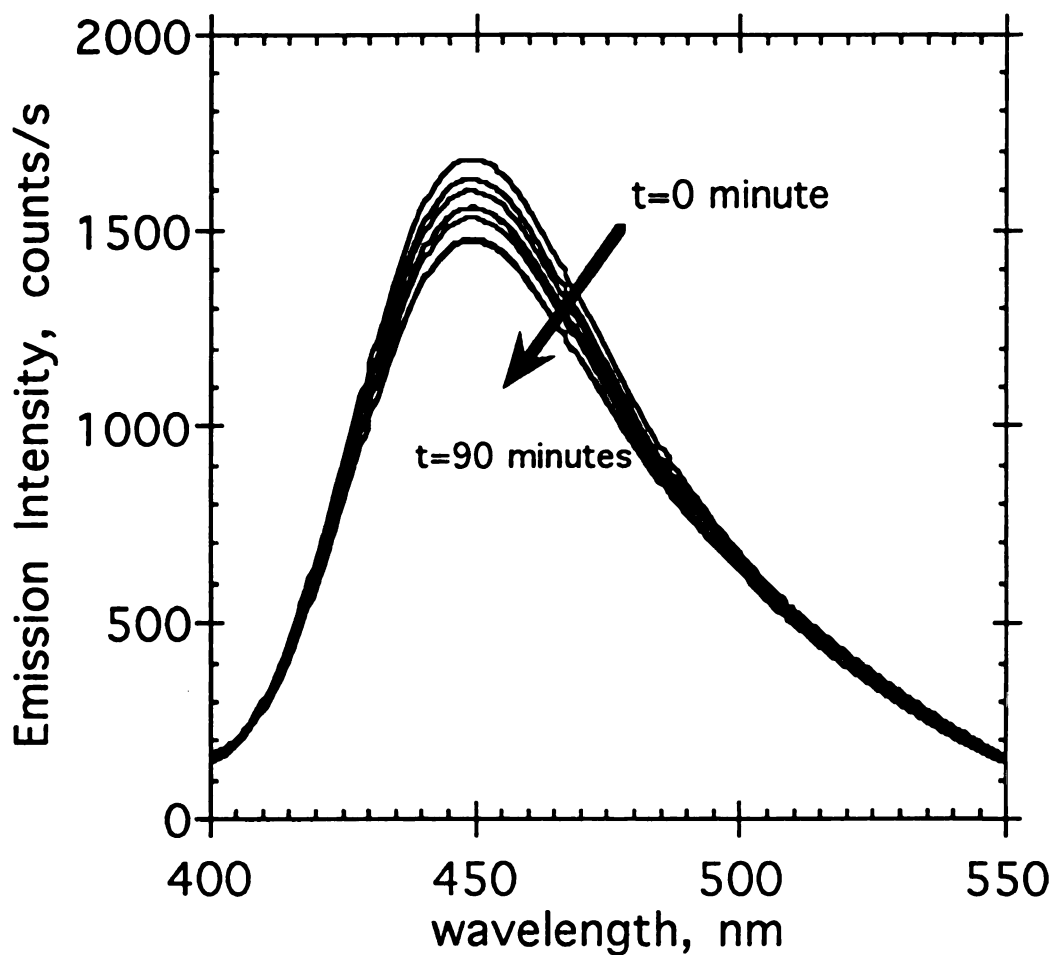


**Figure 5.1** Emission spectra of pyranine over the course of a seeded isothermal (25 °C) citric acid batch crystallization. Ten spectra are shown here, each at an interval of 10 minutes from  $t = 0$  minute to  $t=90$  minutes. These ten are culled from the ninety spectra collected at intervals of 1 minute.

wavelength of 365 nm. The emission spectra was collected over the whole range of the detector, i.e., from 225 to 800 nm. The spectrum was collected every minute for 90 minutes at which time the experiment was deemed complete. In this figure, only ten spectra at intervals of ten minutes each are shown for clarity. Note that a number of spectra, especially at the end of the experiment, fall on top of each other. There is an intense peak at 449 nm, but the peak at 510 nm is almost buried in the tail of the other. However, from a knowledge of the excited state kinetics of pyranine, we can infer that the peak at 510 nm, albeit extremely small, is present.

The absolute intensity of the emission peaks is influenced, among other things, by the excitation light intensity and the sensitivity of the spectrophotometer. To compare results of different experiments, it is more convenient to define and use a parameter that is not affected by variations in the instrument used. As an internal standard, then, we take a ratio of the two most intense peaks of pyranine and use that parameter, defined as the Peak Intensity Ratio (PIR), as the parameter that changes with time. In the experiments described, the PIR was defined as the ratio of the peak at 449 nm to that of the peak at 510 nm.

### **5.3.1 The desupersaturation curve**

From each of the spectrum obtained, a ratio of the peaks at 449 and 510 nm was calculated. This ratio was plotted against the time of the experiment and the result is shown in Figure 5.2. The shape of the curve matches a conventional desupersaturation curve remarkably well. In the initial, relatively flat part of the curve, the supersaturation decreases very slowly. In this region, the desupersaturation is dominated by the growth of the seed crystals. There is also a possibility of secondary nucleation, but this is not detectable in this initial portion. After an induction time,  $\tau$ , secondary nucleation causes the surface area of the crystals to reach a critical size that is capable of consuming all the excess mass in solution very rapidly. This phenomenon is reflected in a sudden increase in the desupersaturation rate. This increased desupersaturation rate continues to deplete all the

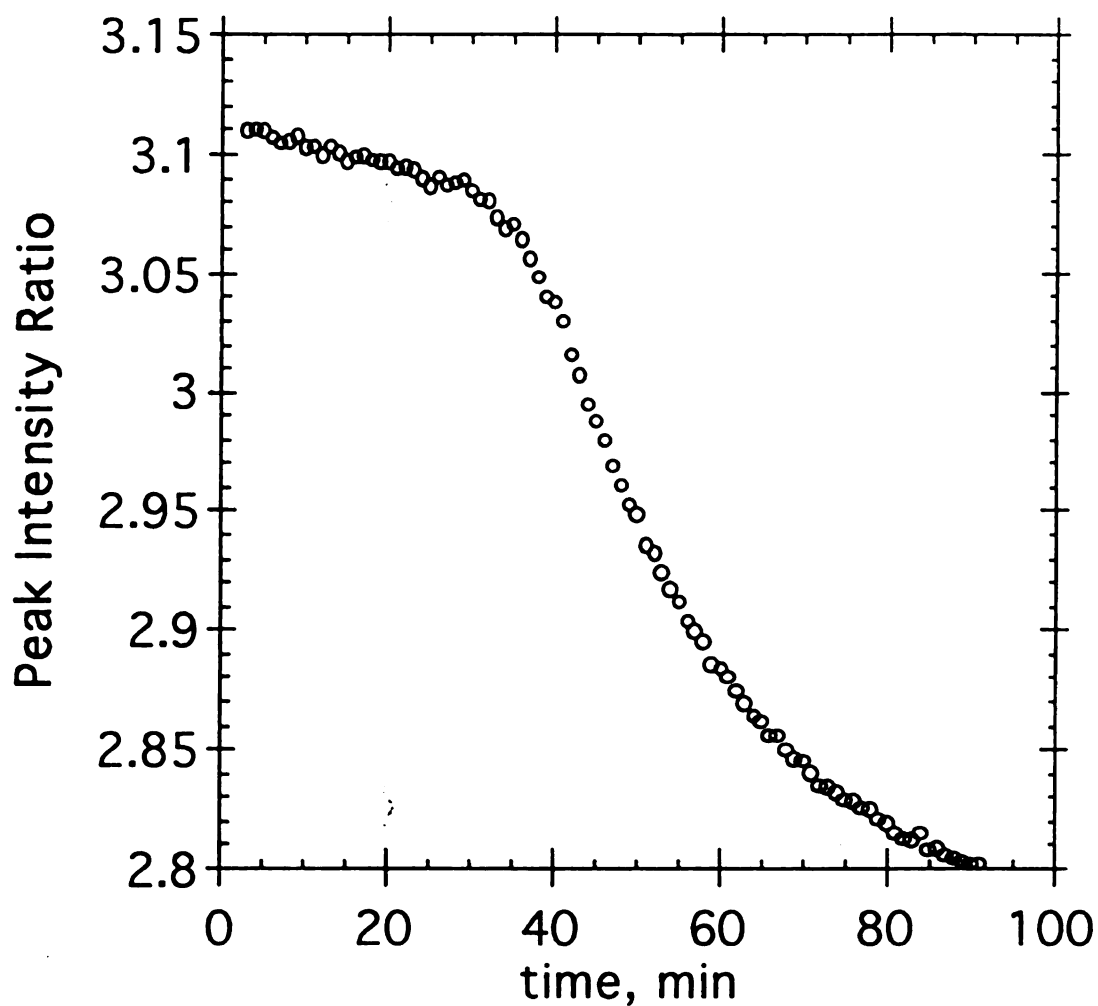


Figure 5.2 Typical desupersaturation curve of a seeded citric acid batch crystallization experiments. The experimental conditions were as follows: Temperature = 25 °C, initial supersaturation ( $c/c^*$ ) = 1.2, agitator speed = 400 rpm, probe (pyranine) concentration =  $1.0 \times 10^{-5}$  M, seeds (average size 660 microns) = 3 gms, excitation wavelength = 365 nm.

supersaturation and the solution eventually stabilizes to its saturation value. This end point is represented by the flat portion of the curve at the tail end. In this experiment, this point is reached in about 90 minutes.

The comment that growth of the seeds dominates in the relative absence of nucleation in the first flat part of the curve is borne out by observation, both visual and electronic. Visually, it is easy to observe that during the initial growth phase, the number of crystals (same as the number of seeds added) is almost constant and there is no appreciable change in the turbidity of the solution in the crystallizer, but after the induction period, a slew of nuclei appear, making the solution quite turbid. The cloudiness due to the new crystals steadily increases till the equilibrium saturation is reached.

Electronically, this phenomenon of nucleation is reflected by the backscattering of the incident light. The light from the UV lamp that is used to excite the probe molecules also provides information on nucleation. Before seeding, when no crystals are present in solution, none of this light is reflected, or 'backscattered' into the detector. However, after seeding, this incident light is picked up by the detector as a small peak at a wavelength of 370 nm. Again, the small shift in this wavelength from 365 nm to 370 nm is due to the use of the fiber optic that causes a small bathochromic shift. The intensity of this peak is dependent only on the amount of backscattered light which is very strongly dependent on the number of crystals in the crystallizer. Figure 5.3 shows a plot of the peak intensity at 370 nm as a function of time. Initially, the amount of backscattered light is relatively constant. After some time, which corresponds exactly to the induction time in Figure 5.2, the intensity increases rapidly. This increase in intensity is due to the formation of new crystals by secondary nucleation. This process of secondary nucleation continues until the supersaturation is totally depleted. Corresponding to this, the backscattering intensity also increases and reaches a saturation value after which there is no increase in intensity, indicating that nucleation is complete at this point. Thus, a comparison of Figures 5.2 and 5.3 serves to confirm the observation made that, in the desupersaturation experiment, there

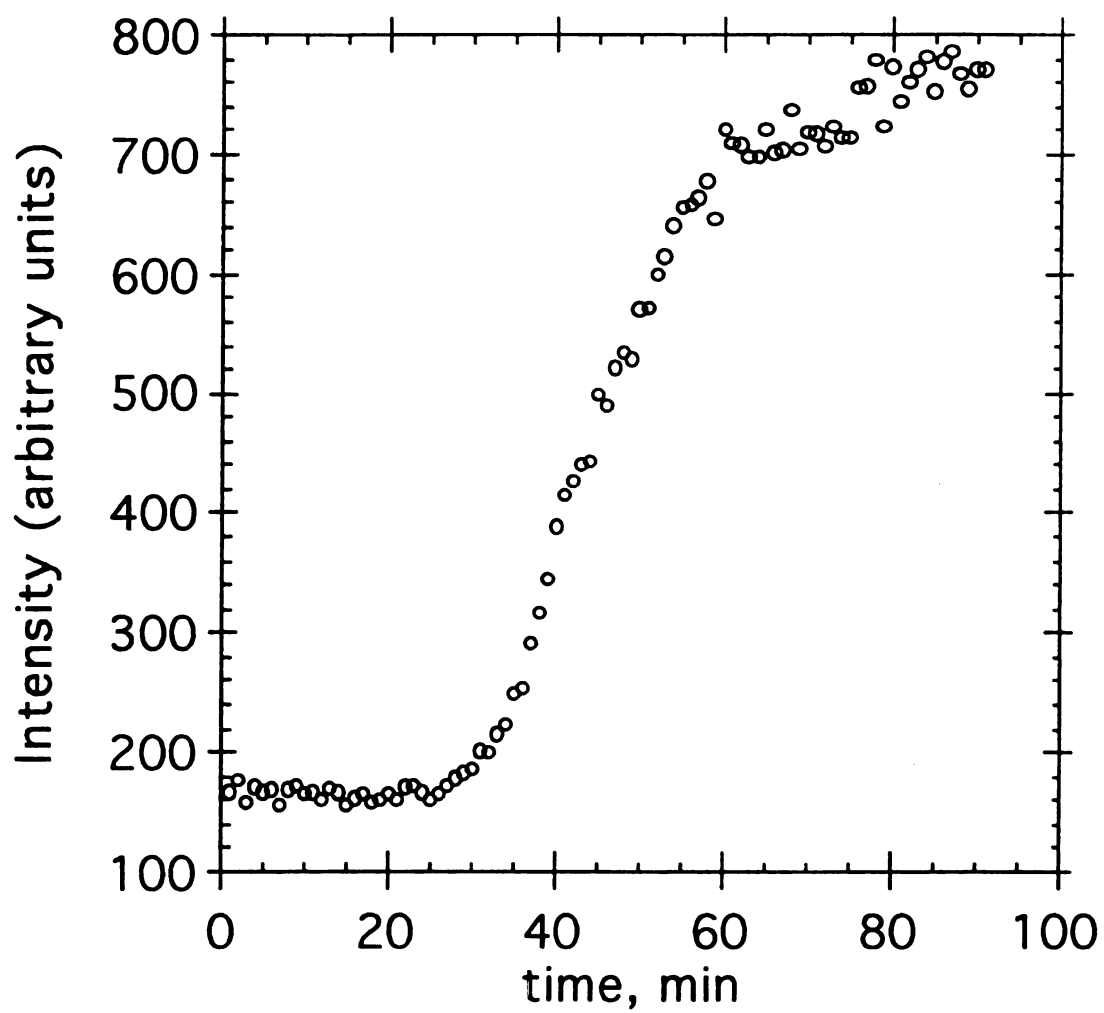


Figure 5.3 Backscattered excitation light during the desupersaturation experiment as a function of time. The experimental conditions are exactly the same as those described in Figure 5.2.

is an initial period of growth of the seeds, during which there is no detectable nucleation. After the induction period, secondary nucleation starts and the crystals, both old and new, continue to grow until the supersaturation is completely depleted and the system comes to equilibrium at the temperature of the experiment.

The combination of fluorescence and backscattering information that is simultaneously collected here makes this technique especially powerful. The hardware that makes this possible is the diode array detector that is part of the spectrophotometer used. The salient feature of this detector is that it is able to record the number of photons being entering the fiber optic over its entire operating wavelength range of 225 nm to 800 nm without discriminating between the backscattered incident light and the fluorescent light emitted by the probe molecules. As the incident light is known to be of a particular wavelength and the fluorescence is known to occur at longer wavelengths, it is easy to distinguish between the backscattered incident light intensity and the peaks due to fluorescence. Note that the backscattering information obtained does not require the presence of the probe at all. It simply gives a measure of the number of crystals reflecting the incident light back to the detector.

### **5.3.2 Effect of seed weight**

Figure 5.4 shows the desupersaturation curves for citric acid obtained with different seed weights of 3 gms, 15 gms, and 36 gms. All three curves were generated under isothermal conditions of 25 °C, and the initial supersaturation of 1.2 was identical for each case. Other experimental conditions, such as agitator speed (400 rpm), were also constant. The seeds used were of a monodisperse size with an average length of 780 micrometers. The seeds were generated by simply sieving a batch of anhydrous citric acid that was obtained from the manufacturer and were used without any pretreatment. The probe (pyranine) concentration was  $1\text{e-}06$  M for the runs with seed weights of 15 gms and 36 gms but was higher ( $1\text{e-}05$  M) for the experiment with 3 gms of seeds. Although this is an order of magnitude difference in the probe concentration, we have demonstrated that this

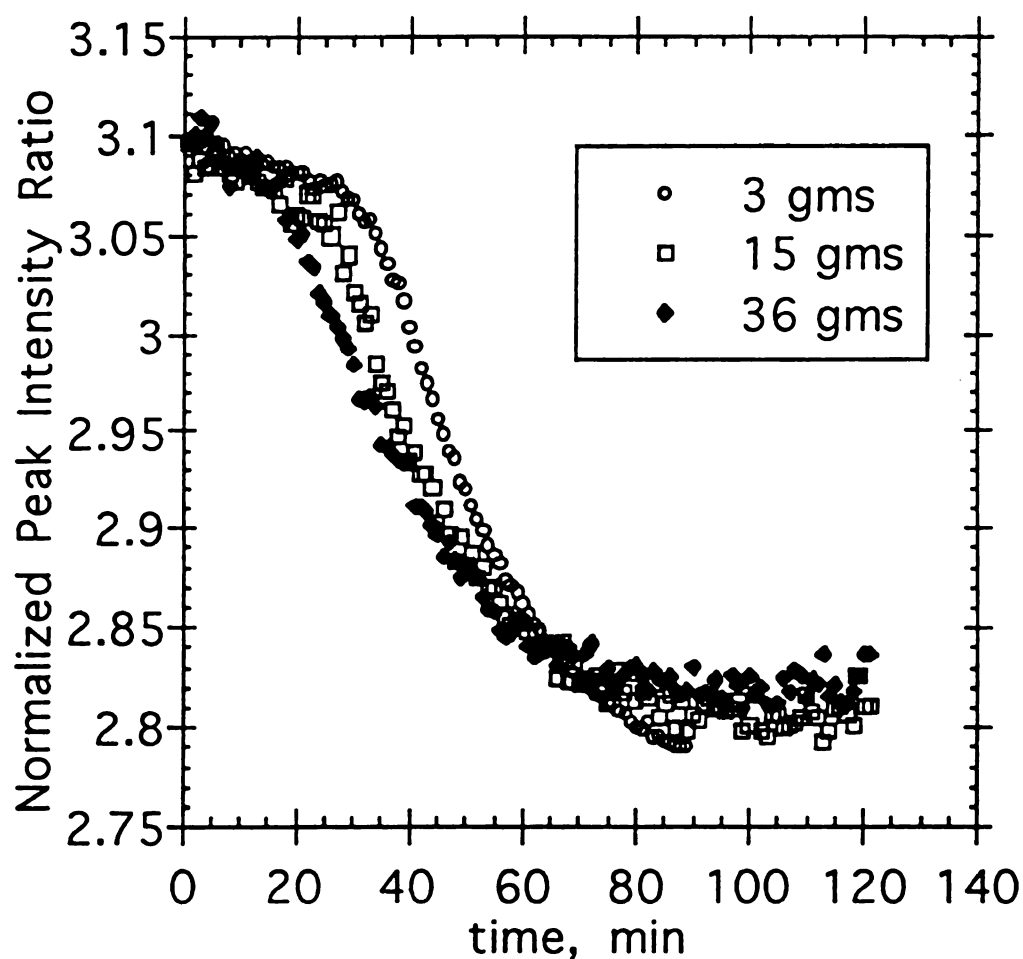


Figure 5.4 Effect of seed amount on the desupersaturation curve of seeded citric acid batch crystallization experiments. The ordinate are normalized so that all curves start at the same point, since initial supersaturation ( $c/c^* = 1.2$ ), is the same in all three cases. Other experimental conditions: Temperature = 25 °C, agitator speed = 400 rpm, probe (pyranine) concentration =  $1.0 \times 10^{-5}$  M, seeds (average size 660 microns) = 3 gms, excitation wavelength = 365 nm.



does not cause any appreciable change in the nature of the desupersaturation curve except for a very small increase in the overall intensity. This anomaly is corrected for by normalizing all curves so as to have the same initial value since the initial value has to be the same for all three cases. This normalization is discussed further in Section 5.3.4. Since the average size of the seeds is constant, it follows that the different seed weights used essentially translate to the different number of nuclei used.

The observed steep drop in supersaturation after a certain interval of time indicates the point where secondary nucleation causes the surface area of crystals in the crystallizer to exceed a critical value, at which point there is enough area available to rapidly desupersaturate the whole system. This drop in supersaturation continues till the solution comes near to its equilibrium saturation. A tail is observed in the desupersaturation curve at which time the crystallization is deemed complete. This was confirmed in all experiments by collecting all the crystals from the crystallizer at the end of the run. The dried crystals were weighed to confirm that the amount of solute in solution that was in excess of the solubility had indeed come out as crystals.

A standard protocol was used to obtain the final crystalline product. At the end of the experiment, the crystals were separated from the mother liquor by passing the slurry through a filter paper placed in a Büchner funnel that was attached to a water aspirator. The crystal mass was further washed with a cold saturated solution of citric acid to remove the minuscule amount of the probe that could possibly be sticking to the surface of the crystals. This washing step was repeated at least two times. The cold saturated solutions serves also to remove any mother liquor sticking to the crystals, while at the same time ensuring that none of the crystals dissolve in the wash solvent. After washing with the saturated solution, the crystals were washed with ether to remove any water that might be present. The crystals were then air dried at room temperature. While this protocol ensured the complete removal of solvent, it was not adequate to get dried crystals for CSD measurements. The problem with this protocol was the air drying step which caused the

agglomeration of crystals. Room temperature (about 25 °C) is not enough to properly dry the crystals. However, the use of high temperature (above 35 °C) is also not possible as that would drive away the water of crystallization associated with the citric acid product. In fact, prolonged exposure to room temperature has been known to cause the same problem. When that happens, fusion of crystals occur that renders the whole exercise of CSD measurement futile. The possible solution to this problem is to dry the crystals in an oven carefully controlled under 35 °C for as short a time as is necessary. Future experiments, where an attempt will be made to predict the CSD using the data presented in this paper, will involve using some such technique to solve this problem.

### **5.3.3 Effect of temperature**

The effect of temperature on the desupersaturation experiments was studied by conducting the experiment at temperatures of 20 °C, 25 °C, and 30 °C. In these three experiments, all other parameters were kept constant. The results are presented in Figure 5.5 as a scatter plot. The initial supersaturation in each case was 1.2, which led us to normalize the data at the initial point. The interesting observation here is the time taken for the surface area of the crystals to reach the critical size at which rapid desupersaturation takes place. At 20 °C, it takes almost an hour after seeding for the rapid drop to commence, whereas it is correspondingly lesser at the higher temperatures. This decrease in induction time with temperature can be explained by an inspection of the kinetic parameters which are a function of the temperature. The nucleation rate is usually higher at higher temperatures which causes nuclei to appear earlier. So, at the higher temperature, the critical surface area would be achieved earlier, causing the desupersaturation rate to increase earlier. This conclusion can be proven by obtaining the kinetic information from these plots. This exercise is the subject of Chapter 6.

One other point to note in this set of experiments is the small initial rise in the Peak Intensity Ratio for the experiment at 20 °C. The observation is almost certainly due to an experimental artifact in that the strong UV light source used to excite the probe molecules

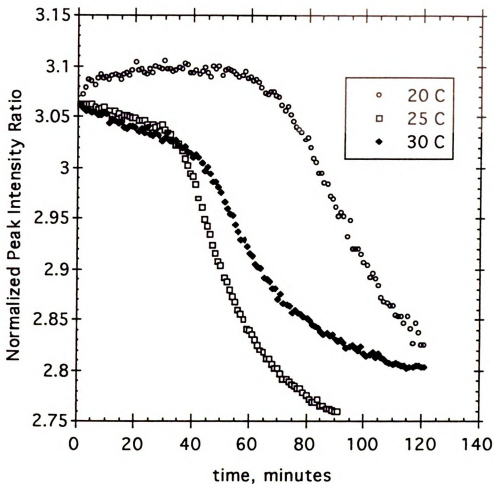


Figure 5.5 Effect of temperature on the desupersaturation curve of seeded citric acid batch crystallization experiments. The ordinate are normalized so that all curves start at the same point, since initial supersaturation ( $c/c^* = 1.2$ ), is the same in all three cases. Other experimental conditions: agitator speed = 400 rpm, probe (pyranine) concentration =  $1.0 \times 10^{-5}$  M, seeds (average size 660 microns) = 3 gms, excitation wavelength = 365 nm.

must have dissolved some of the fine nuclei at the beginning of the experiment causing the initial supersaturation to go up a little bit and then stabilizing. The normalization done (to match the initial supersaturation) serves only to match theory with experiment and should be viewed as such.

#### **5.3.4 Effect of probe concentration**

A valid question with the use of this technique is the effect of the probe on the system. The probe is usually added at an extremely small concentration of the order of  $1 \times 10^{-5}$  mols/liter. While this is a reasonably small amount of impurity, the quest for zero effect on crystal purity prompted us to check the effect of this small amount on the purity of the product. Two questions were posed: 1. Does the probe enter the crystal lattice of the citric acid product? 2. Does the concentration of probe have any effect on the results of the desupersaturation experiments?

The first question was answered by analyzing the crystal product obtained. A simple experiment was conducted by redissolving the washed crystals in water and taking the fluorescence spectrum of the solution. The spectrum obtained had absolutely no detectable fluorescence, which indicated that no appreciable amount of the probe enters the crystal lattice and that all the probe molecules stay in the mother liquor. This conclusion was further confirmed by analyzing the final crystal product by FAB-mass spectroscopy that looks for specific masses of fragments. If any amount of pyranine had entered the crystal lattice, it would be detected by this technique. Three samples of product crystals were analyzed. The results of the mass spectrometry corroborated the negative fluorescence result in two cases but showed a trace amount of pyranine in the third. This amount was probably left on the surface of the crystal due to poor washing and could definitely be removed by another washing of the crystal product with a saturated citric acid solution. These experiments conclusively prove that the pyranine does not enter the

crystalline product and that loss of crystal purity is not a concern when using this technique.

The second question, that of any effect of the concentration of probe on the desupersaturation experiments, was answered by conducting identical experiments with three different probe concentrations. The results are shown in Figure 5.6 by plotting the relative supersaturation,  $\sigma$ , against time. The relative supersaturation,  $\sigma$ , is defined by equation (5.1). The three probe concentrations used were 1e-05 M, 5e-06 M, and 1e-06 M, covering an order of magnitude. As is evident in the figure, there is no appreciable effect on the shape of the desupersaturation curve. In the raw data, the only difference is a slight increase in the ordinate numbers, which is consistent through the whole length of the experiment. This issue can be resolved very simply by normalizing each plot with respect to the initial point, knowing that the initial supersaturation was constant in all experiments and thus should have the same value ( if all other parameters are the same).

### 5.3.5 Measurement of kinetic parameters

The preceding sections demonstrated the ability of the fluorescent probe technique as a viable tool for the *in situ* measurement of supersaturation. Further, its utility in the measurement of desupersaturation experiments of citric acid was shown. In this section, a brief discussion is presented on the usefulness of these measurements in a control scheme and in measuring the kinetic parameters of a batch experiment.

It has been shown elsewhere [3, 4, 5] that the PIR can be correlated to the solution concentration with a high degree of confidence. The PIR is a parameter that is reflective of the solution structure and is inherently related to the activity. Thus, supersaturation in the solution can be alternatively defined in terms of this new parameter, the PIR. If PIR\* is defined as the Peak Intensity Ratio obtained at equilibrium saturation and PIR is the ratio at any other concentration, then the supersaturation can be defined either as a difference or as a ratio as follows:

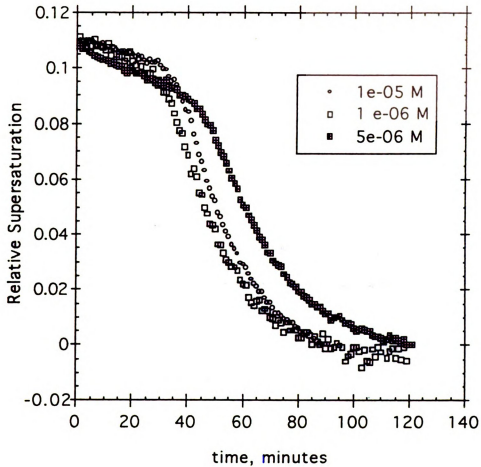


Figure 5.6 Effect of varying the probe (pyranine) concentration on the desupersaturation curve of seeded citric acid batch crystallization experiments. The ordinate shows the relative supersaturation  $\{(c/c^*)-1\}$  that is the same in all three cases. Other experimental conditions: temperature = 25 °C, agitator speed = 400 rpm, seeds (average size 660 microns) = 3 gms, excitation wavelength = 365 nm.

$$\text{Supersaturation} = \Delta\text{PIR} = \text{PIR} - \text{PIR}^* \quad (5.1)$$

$$\text{Supersaturation} = \sigma = \frac{\Delta\text{PIR}}{\text{PIR}^*}$$

Since PIR is a parameter that reflects the fundamental structure of the solution,  $\Delta\text{PIR}$  and  $\sigma$  will most likely contribute to a more accurate measurement of supersaturation. Maintaining a constant supersaturation is a requirement for attaining a CSD with a large average size in batch crystallizations. For this purpose, a set point for a control scheme that is designed to obtain such a CSD can be defined [7] as:

$\Delta\text{PIR} = \text{constant}$  , or

$\sigma = \text{constant}$

This idea is expressed pictorially in Figure 5.7. This definition is also a direct measurement of supersaturation that does not require calibrations and therefore is more practical as a set point for use in a control scheme. Thus, the accurate measurement of supersaturation that is defined in terms of the PIR can be an extremely valuable tool for use in the control of crystallizers.

## 5.4 Conclusions

The usefulness of the fluorescent probe technique to monitor the isothermal desupersaturation characteristics of a seeded batch crystallizer has been demonstrated. The probe molecule (pyranine) was added to the crystallizing mixture at the start of the experiment and its emission spectrum monitored over time. A ratio of two emission peaks was plotted against time to give rise to the desupersaturation curve. The effect of varying the seed weight on the desupersaturation curve was shown. With increasing seed size, the time required for secondary nucleation and the rapid desupersaturation to start decreases. An increasing temperature of experiment also caused the same effect. It was demonstrated that the relative amount of the probe in solution does not significantly alter the

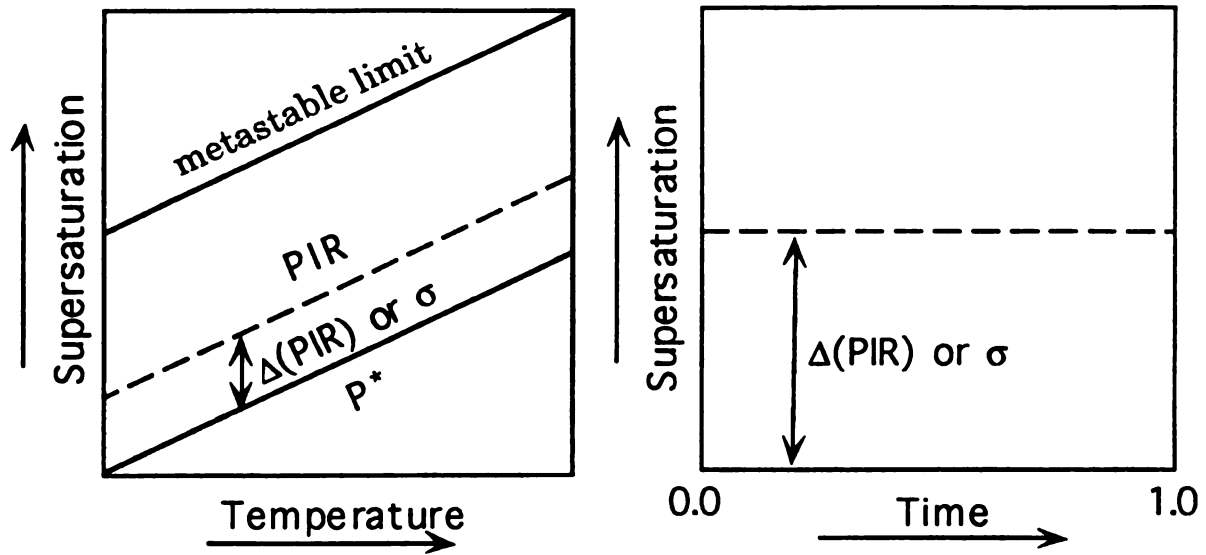


**Figure 5.7** Control policy projected to maximize the mean size of a crystal size distribution from a cooling batch crystallization process [7]. The policy is based on maintaining a constant supersaturation during the course of the crystallization. The supersaturation is defined by either of the following two equations:

$$\text{Supersaturation} = \Delta\text{PIR} = \text{PIR} - \text{PIR}^*$$

$$\text{Supersaturation} = \sigma = \frac{\Delta\text{PIR}}{\text{PIR}^*}$$

where PIR is the ratio of emission peaks of a probe such as pyranine in a supersaturated solution, and PIR\* is the same ratio in a saturated solution.



desupersaturation curve. Furthermore, the presence of the probe in the crystallizing solution does not affect the crystal purity.

## 5.5 References

1. J. Garside, *Chemical Engineering Science*, Industrial Crystallization from Solution. **40**, 3-26, (1985).
2. J. W. Mullin, O. Söhnel, *Chemical Engineering Science*, Expressions of supersaturation in crystallization studies. **32**, 683-686, (1977).
3. R. Chakraborty, K. A. Berglund, *Journal of Crystal Growth*, Steady State Fluorescence Spectroscopy of Pyranine as a Trace Extrinsic Probe to study structure in aqueous sugar solutions. **125**, 81-96, (1992).
4. R. Chakraborty, K. A. Berglund, *AIChE Symposium Series No. 284*, The Use of Pyranine as a Trace Fluorescent probe to Study Structure in Aqueous Sucrose Solutions. **83**, 114-123, (1991).
5. S. K. Yedur and K. A. Berglund, Accepted for publication in: *Appl. Spec.*, (1996).
6. H. Kondo, I. Miwa, and J. Sunamoto, *J. Phys. Chem.* **86**, 4826, (1982).
7. D. D. Dunuwila, An Investigation of the Feasibility of Using In Situ ATR FTIR Spectroscopy in the Measurement of Crystallization Phenomenon for Research and Development of Batch Crystallization Processes. PhD Thesis, Michigan State University. (1996).

## Chapter 6

### **MODELS FOR THE EXTRACTION OF KINETIC PARAMETERS FROM THE DESUPERSATURATION CURVES**

#### **6.1 Background**

In the previous chapter, the fluorescent probe was used to obtain information on the desupersaturation of citric acid solutions during isothermal batch crystallization experiments. The information obtained was in the form of curves that showed a parameter defined as the Peak Intensity Ratio changing during the time course of the experiment. A representative desupersaturation curve is shown in Figure 5.2. A number of parameters were varied to test their effect on the nature of the desupersaturation curves. These effects were shown in Figures 5.4, 5.5, and 5.6 and discussed in detail in Chapter 5.

The desupersaturation curves are ideal for studying the kinetics of batch crystallization parameters. These experiments are almost always conducted isothermally since the kinetic constants are temperature dependent. The process of crystallization can be divided into two parts: nucleation and growth. Nucleation refers to the birth of nuclei in solution and growth is the subsequent deposition of solid mass onto the nuclei. The nucleation and growth rates are expressed as

$$G = k_g S^n \quad (6.1a)$$

$$B = k_n S^m \quad (6.1b)$$

where  $G$  and  $B$  are the growth and nucleation rates respectively;  $k_g$  and  $k_n$  are the growth and nucleation rate constants,  $S$  is the supersaturation, and  $n$  and  $m$  are the 'order' to which the supersaturation is raised. These orders do not imply a reaction order, they are simply empirical constants that indicate the power to which the supersaturation is raised. Thus, the order has no fundamental significance. Typically,  $m > n$ , indicating that the nucleation rate is a much stronger function of supersaturation. For aqueous solutions,  $n$  is usually between 1 and 2, while  $m$  is usually between 2 and 5 [1]. A higher supersaturation will favor more nucleation and less growth whereas a lower supersaturation will favor the growth process with little nucleation. The relationship between all these parameters for a mixed suspension, mixed product removal (MSMPR) crystallizer is shown in Figure 1.1.

The expressions in equations 6.1a and 6.1b are rather simplistic. Each term is dependent on a number of parameters. Both the rate constants are dependent upon the temperature, the agitation rate (for batch crystallizers), and any impurities that might be present in the solution. Specifically,  $k_g$  may also be dependent on the crystal size  $L$ , and on the suspension voidage in the crystallizer, while  $k_n$  is also dependent on the suspension density  $M_T$ . The supersaturation  $S$  can be described in any convenient units that will in turn decide the units of the growth and nucleation rate. In the previous chapter, equations 5.1 gave two possible definitions for supersaturation.

In our work, we define the supersaturation as:

$$\sigma = \frac{\text{PIR} - \text{PIR}^*}{\text{PIR}^*} \quad (6.2)$$

Here, PIR is the Peak Intensity Ratio (as defined in Chapter 5) at any concentration and  $\text{PIR}^*$  is the same ratio at equilibrium conditions.

The kinetic constants together with the growth and nucleation rates describe the crystallization process. If these parameters are known for a particular system, the complete CSD and various crystal product properties such as total crystal area and mass can be

predicted. There have been numerous works that address this issue of obtaining the kinetic data from experiment.

The particle number-size distribution theory introduced by Randolph and Larson [2] and the fundamental supersaturation balance discussed by Mullin and Nyvlt [3, 4, 5] provide powerful models to evaluate crystallization processes. The model derived from the particle number-size distribution theory is based on the population balance (number of particles per unit volume per length range) and takes nucleation and growth of crystals into account. The fundamental supersaturation balance is derived taking into consideration that the driving force for all crystallization phenomena such as nucleation and growth is supersaturation. Thus, kinetic parameters for nucleation and growth are nested in these models giving them both predictive and descriptive capabilities. Another valuable set of equations commonly used in crystallization analysis is the moments of the particle number-size distribution [2]. The moments have been utilized to circumvent a basic dimensional incompatibility between the population balance and the transport equations for mass, momentum and energy.

The particle phase space consists of a set of internal coordinates in addition to the three spatial dimensions. This incompatibility complicates the simultaneous solution of the population balance with the transport equations. The most significant internal coordinate in the particle phase space is the particle size. Therefore, the population density distribution is integrated over the particle size internal coordinate reducing the dimensionality of the population balance to that of the transport equations. The moments 'm' that give the total particle properties upon integrating the population balance over the particle size coordinate are given by

$$m_j(t) = \int_0^{\infty} n(L,t) L^j dL, \quad j = 0, 1, 2, \dots \quad (6.3)$$

where  $n$  is the population density distribution and  $L$  is the particle size. The first moment gives the length, the second gives the area, and the third moment gives the mass of the crystals.

The application of these models in engineering simulations and process analysis and control has been limited by the unavailability of a reliable and sensitive technique to obtain kinetic data *in situ*. In crystallization processes, *in situ* measurement is extremely important since the hydrodynamic conditions set by the crystallizer dimensions, flow patterns induced by the propeller and the suspended crystal slurry can significantly alter kinetic parameters from that obtained under controlled laboratory experiments [6]. Theoretically, kinetic parameters can be extracted from the desupersaturation rate of the solution monitored by *in situ* fluorescence spectroscopy.

## 6.2 Development of the model

To obtain kinetic information from the desupersaturation curves that were generated by the fluorescent probe technique, we have modified the differential approach proposed by Mullin and Nyvlt [3]. The original model was intended to calculate the programmed cooling curve for a batch crystallizer. Here, the general model is presented as is, with appropriate substitutions where necessary.

Consider a batch crystallizer that contains a supersaturated solution that has 1 kg of free solvent. This solution is seeded with a mass  $W_s$  of seeds of a uniform size. The crystallizer is agitated at a constant speed and crystallization is accomplished by cooling the crystallizer.

The fundamental supersaturation balance is defined as:

$$\frac{d\sigma}{dt} = s - k_g A \sigma^n - k_n \sigma^m \quad (6.4)$$

where the derivative is with respect to time and  $A$  is the crystal surface area. The first term on the right hand side,  $s$ , is the supersaturation rate that corresponds to the creation of

supersaturation in the system, while the second and third terms correspond to the desupersaturation due to growth and nucleation respectively.

The supersaturation rate,  $s$ , can be expressed as

$$s = \frac{dc^*}{dt} = \frac{dc^*}{d\theta} \frac{d\theta}{dt} \quad (6.5)$$

As the temperature,  $\theta$ , goes down in a cooling crystallizer, equation (6.4) may be rewritten as

$$-\frac{d\sigma}{dt} = \frac{dc^*}{dt} + k_g A \sigma^n + k_n \sigma^m \quad (6.6)$$

This equation provides us with a general equation that can be used to fit the desupersaturation data. The experiment provides the left hand side of equation (6.6) while a fit can provide the relevant parameters on the right hand side of the equation.

As mentioned before, the terms on the right hand side are dependent on a number of parameters and any fit has to taken into account some of these. As with any model, it is desirable to fit the data with a minimum number of parameters, and that is the goal here. The following analysis considers the whole process from a fundamental viewpoint. We start with a mass of seeds and track their growth along with the formation of new nuclei due to nucleation over a fixed time interval. These growing nuclei and the newborn nuclei consume mass, and that is reflected in the desupersaturation rate. Thus, a relationship can be derived between the desupersaturation rate and the growth and birth of nuclei.

To obtain the relation between the cooling temperature  $\theta$  on time, the following analysis is made. The total number of crystals present at any given time  $N(t)$ , per kg of free solvent present in solution, is comprised of the number of seed crystals added at the start of the process and the number of crystals that are generated due to nucleation.

$$\begin{aligned} N(t) &= N_s + N_n \\ &= \frac{W_{s0}}{\alpha \rho_c L_{s0}^3} + \frac{k_n(\theta_0)[\sigma(\theta_0)]^m t}{\alpha \rho L_{n0}^3} \end{aligned} \quad (6.7)$$

where  $W$  is the weight of the crystals,  $\alpha$  is the volume shape factor,  $\rho_c$  is the density of the crystals, and  $L$  is the characteristic length of a crystal. The subscript 's' refers to the seed crystals, whereas 'n' refers to the nuclei formed.

All crystals that are present in the supersaturated solution grow in size according to the following equations:

$$L_s(t) = L_{s0} + \sum_{i=0}^{t-1} g_i(t) \Delta t \quad (6.8)$$

$$L_n(t) = L_{n0} + \sum_{i=t_0}^{t-1} g_i(t) \Delta t \quad (6.9)$$

where  $t_0$  denotes the time at which an individual nucleus first appeared and  $\Delta t$  is the time interval of growth.  $g_i$  is the linear crystal growth rate and is defined as

$$g_i = \frac{k_g(\theta_i, L_i) \beta \sigma^n}{3\alpha\rho_c} \quad (6.10)$$

where  $\beta$  is the surface shape factor. The crystal growth rate constant,  $k_g$ , is temperature dependent. It may also depend on the crystal size, the concentration of any impurity, and the voidage of the crystal mass.

The crystal surface area at a time 't' in a unit mass of solution is given by

$$A(t) = \beta N_s L_s^2(t) + \beta \sum_1^I N_n L_n^2(t) \Delta t \quad (6.11)$$

Combining equations (6.7), (6.8), (6.9), and (6.11), we obtain

$$A(t) = \beta N_s \left[ L_{s0} + \sum_{i=0}^{t-1} g(\theta_i, L_{si}) \Delta t \right]^2 + \beta N_n \sum_{i=0}^{t-1} \left[ L_{n0} + \sum_{j=1}^{t-1} g(\theta_i, L_{n(i-j)}) \Delta t \right]^2 \quad (6.12)$$

Substituting these equations into equation (6.4) and solving for the temperature drop with time, we obtain

$$\begin{aligned}
-\frac{d\theta}{dt} = & \frac{3W_{s0}}{\frac{dc^*}{d\theta} + \frac{d\sigma}{d\theta}} \frac{g(L_{st}, \theta_t)}{L_{s0}} \left[ 1 + \sum_{i=0}^{t-1} \frac{g(\theta_i, L_{si})\Delta t}{L_{s0}} \right]^2 + \\
& \frac{1}{\frac{dc^*}{d\theta} + \frac{d\sigma}{d\theta}} \left\{ k_n(\theta_0)[\sigma(\theta_0)]^m + 3 \sum_{i=0}^{t-1} \frac{k_n(\theta_0)[\sigma(\theta_0)]^m g(\theta_t, L_{ni,t})\Delta t}{L_{n0}} \left[ 1 + \sum_{j=1}^{t-1} \frac{g(\theta_j, L_{n(j-i)})\Delta t}{L_{n0}} \right]^2 \right\}
\end{aligned}
\tag{6.13}$$

This equation represents the theoretical cooling curve for a batch cooling crystallizer.

For the isothermal desupersaturation experiments, this equation can be modified very simply by moving all temperature derivatives to the left hand side and combining the terms. Since the temperature is constant throughout,  $dc^*/dt = 0$ . These manipulations result in the following equation:

$$\begin{aligned}
-\frac{d\sigma}{dt} = & \frac{3W_{s0}g(L_{st}, \theta_t)}{L_{s0}} \left[ 1 + \sum_{i=0}^{t-1} \frac{g(\theta_i, L_{si})\Delta t}{L_{s0}} \right]^2 + \\
& \left\{ k_n(\theta_0)[\sigma(\theta_0)]^m + 3 \sum_{i=0}^{t-1} \frac{k_n(\theta_0)[\sigma(\theta_0)]^m g(\theta_t, L_{ni,t})\Delta t}{L_{n0}} \left[ 1 + \sum_{j=1}^{t-1} \frac{g(\theta_j, L_{n(j-i)})\Delta t}{L_{n0}} \right]^2 \right\}
\end{aligned}
\tag{6.14}$$

This complex equation provides a basis for obtaining the kinetic parameters if the desupersaturation profile (the left hand side of equation 6.14) is known. The unknowns on the right hand side are  $g$ ,  $k_g$ ,  $k_n$ ,  $n$ , and  $m$ . Note that  $L$  is calculated from equations (6.8) and (6.9) using 'g' from equation (6.10). Once these are all known, the nucleation rate can be calculated by using a power model such as



$$B^0 = \frac{1}{\alpha \rho_c L_{n0}^3} \left[ k_{n,p} \sigma^{n_p} + k_{n,s} M \sigma^{n_s} \right] \quad (6.15)$$

where  $B^0$  is the nucleation rate,  $k_{n,p}$  is the primary nucleation rate constant,  $k_{n,s}$  is the secondary nucleation rate constant,  $n_p$  is the order of primary nucleation, and  $n_s$  is the order of secondary nucleation.

The first term on the right hand side of the equation (6.14) describes desupersaturation that is only due to growth of the seeds that are added, without any nucleation. From the desupersaturation experiments that were described in Chapter 5, (see for example Figure 5.2), this region of growth of seeds and no nucleation is given by the first flat part of the curve. In this region, the second term on the right hand side of equation (6.14) does not apply. By fitting the data to the reduced equation, the growth kinetics are obtained. With this information in hand, the entire data set can be fitted to the equation using the known growth parameters to provide the nucleation rates and rate constants. Thus, a successful fit will provide all the kinetic parameters of the crystallization such as the nucleation and growth rates and the respective rate constants.

Once the kinetic parameters are known, it is possible to predict the crystal size distribution at any time interval by simply integrating the equations for the length of the crystal at the desired time. These further analyses are part of the ongoing work in this area.

### 6.3 Conclusions

The desupersaturation experiments using the fluorescent probe technique are uniquely capable of providing kinetic information about the crystallization process. The utility of the fluorescent probe is in its ability to measure the continually changing conditions in the crystallizer with great sensitivity. While conventional techniques usually require the removal of a sample from the crystallizer to analyze it, this technique provides an *in situ* measurement tool of the crystallizing solution. Furthermore, the high sensitivity offered provides information of the changing conditions in the crystallizer within extremely

small time intervals. In the experiments conducted, the time interval chosen was one minute, but this can very easily be reduced to as low as one second. The high sensitivity obtained results in a larger number of data points that can be fit to the model with a much greater accuracy. Thus the fluorescent probe technique is convenient not only to measure the concentration and supersaturation in a crystallizer, but also to obtain valuable information on the crystallization kinetics.

## 6.4 References

1. P. C. Wankat. In: *Rate Controlled Separations*. Elsevier Applied Science. pp88. (1990).
2. A. D. Randolph and M. A. Larson. *Theory of Particulate Processes*, Academic Press, Inc., New York, USA, ch. 3, (1988).
3. J. W. Mullin and J. Nyvlt. *Chem. Eng. Sci.*, **26**, 369, (1971).
4. J. Nyvlt. *Colln. Czech. Chem. Commun.*, **30**, 2269, (1965).
5. J. Nyvlt and J. W. Mullin. *Chem. Eng. Sci.*, **25**, 131, (1970).
6. N. S. Tavaré, *Separation and Purification Methods*, **22:2**, 93, (1993).

## **Chapter 7**

### **CONTINUING INVESTIGATIONS AND RECOMMENDATIONS FOR FUTURE WORK**

#### **7.1 Background**

In chapters 2, 3, and 4, the utility of the fluorescent probes as a sensor for concentration and supersaturation measurements was demonstrated. In Chapter 5, the fluorescent probe pyranine was used to generate desupersaturation curves for seeded citric acid solutions in a batch crystallizer. Chapter 6 provided a predictive model to estimate the kinetic parameters of the crystallization of citric acid monohydrate in a batch crystallizer based on the desupersaturation curves. In most of these applications, the probe was allowed to be present freely in solution. The exceptions were the results presented with the immobilized probe in Chapters 3 and 4. These experiments with the immobilized probe showed that although the sensory properties of the probe can be preserved, the chemistry involved in the immobilization cause significant changes rendering the use of immobilized probes unsatisfactory. The problem of the probe serving as an interfering impurity remains to be addressed. Although Fast Atomic Bombardment (FAB) experiments on the citric acid monohydrates that was crystallized showed only trace amounts of residual probe in the final product, in many cases, it will still be unacceptable to add fluorescent probes of unknown toxicity into a crystallizer. Even if the probes are inherently safe, as is the case with the FD&C dyes, the possible inclusion of these probes into the crystals, thereby affecting the purity would undoubtedly cause reluctance on the part of current crystallization operations to use this technique. In the case where crystal purity is not a

serious concern, the question whether these probes affect the crystal habit would have to be answered. Although there is no indication that the habit is affected in any way by these probes; at this time, we are not in a position to make such a claim categorically.

For these myriad reasons, it is desirable that an alternate technology be developed that would use the same principles of fluorescent probes, but would be able to lay to rest any fears of possible contamination or habit modification. For this to be possible, it is necessary to contact the probe with the crystallizing solution *ex situ*. Such a configuration would involve drawing out a sample solution stream from the crystallizer, preferably with the crystals, contacting the probe with the sample in a flow cell where the fluorescence spectrum can be recorded, and then either returning the sample stream to the crystallizer after removing the probe, or by simply sending the sample stream to waste.

## **7.2 Continuing Investigations**

### **7.2.1 Estimation of kinetic parameters**

Based on the model provided in Chapter 6, work in ongoing to fit the experimental data to the model. A successful fit will provide the citric acid growth and nucleation rate, as well as the various kinetic parameters. These can potentially be used to predict the crystal size distribution.

### **7.2.2 *Ex situ* monitoring of concentration**

This proposed configuration of the experimental setup to solve the problems discussed in the section 7.1 is very similar to manifolds used in conventional Flow Injection Analysis (FIA). FIA is defined as a non-chromatographic flow analysis technique for quantitative analysis, performed by reproducibly manipulating sample and reagent zones in a flow stream under thermodynamically non-equilibrated conditions [1]. The basic components of FIA system and a variation of the conventional - reverse Flow Injection Analysis (rFIA) system are shown in Figures 7.1 and 7.2. There are certain basic differences between a conventional FIA system and an rFIA system. The most striking of

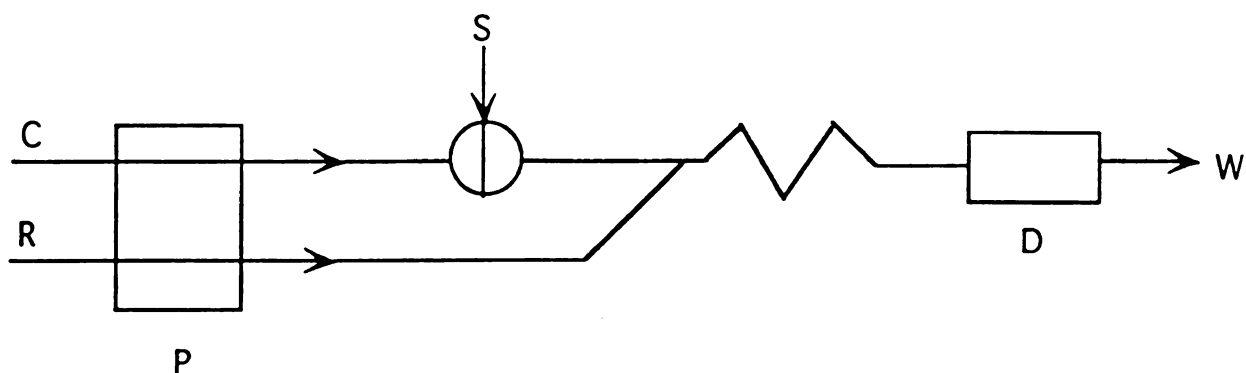


Figure 7.1 Schematic of a conventional Flow Injection System. C = carrier stream, R = reagent stream, S = sample, D = detector, P = pump, and W = waste stream.

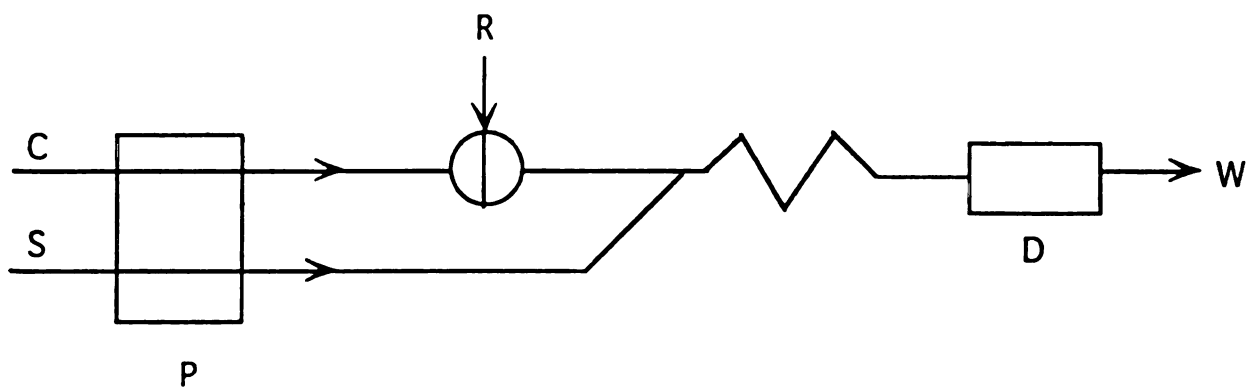


Figure 7.2 Schematic of a reverse Flow Injection System. C = carrier stream, R = reagent stream, S = sample, D = detector, P = pump, and W = waste stream.

these is in the nature of the mobile phase. In conventional FIA, the reagent (probe) stream moves continuously through the system along with the carrier while the sample is injected at fixed intervals. On the other hand, in rFIA, the sample and the carrier move continuously, while the reagent is injected intermittently. FIA techniques are used for a wide variety of applications [1, 2]. In crystallization too, FIA has been used for the determination of d- and l- glutamic acid [3], and for the determination of phylate and phytic acid during the crystallization of calcium oxalate [4, 5]. rFIA is generally of use in applications where there is an abundance of sample. An example where rFIA has been used is in the examination of ocean water chemistry aboard a ship [6]. In our case, we have a similar situation with an abundance of sample in the crystallizer making the use of rFIA quite appropriate. Furthermore, the use of a carrier stream is obviated in the proposed configuration.

Preliminary experiments with a working prototype of such a system were conducted in a batch crystallizer. Desupersaturation experiments with citric acid similar to those described in Chapter 5 were conducted. A schematic of the system used is shown in Figure 7.3. A supersaturated solution of citric acid was made by dissolving solute in excess of solubility at 25 °C. Dissolution was carried out at 35 °C and the resulting solution was cooled down to 25 °C. A supersaturation of 1.2 ( $=c/c^*$ ) was generated by this protocol. Pyranine was added to this solution to generate an overall probe concentration of  $1.0 \times 10^{-5}$  M in the crystallizer. A constant stirring rate of 400 rpm was used throughout. A sample stream was drawn out from the crystallizer with the aid of a peristaltic pump. The sample was directed through a flow cell. The flow cell was essentially a cylindrical disc with an O.D. of 2.54 cm and a height of 1 cm equipped with inlet and outlet port at its sides. A schematic depiction of the flow cell is presented in Figure 7.3. A fiber optic end was placed flush with the top of this flow cell to record the fluorescence spectrum of pyranine. After passing through the flow cell, the sample stream

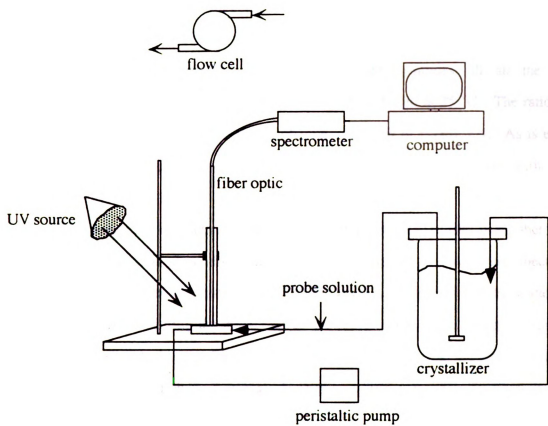


Figure 7.3 Schematic of the apparatus used to measure the concentration of a crystallizing solution *ex situ*. The top view of the flow cell is shown on the upper left hand corner.

was returned to the crystallizer. For the desupersaturation experiment, 3 grams of seeds (average size 780 nm) were added to the crystallizer at time zero.

The emission spectrum of the pyranine in the sample stream was recorded every minute for 2 hours. As expected, at the conditions maintained, the citric acid monohydrate crystals have an induction time of about 30 minutes, during which the seeds grow. After the induction time, secondary nucleation occurs that continues till all the excess supersaturation is depleted and the system comes to equilibrium at 25 °C. The ratio of the emission peaks of pyranine, as a function of time, is shown in Figure 7.4. As is evident, this sampling technique works very reasonably and the curve compares well with the one shown in Figure 5.2.

The important distinction with conventional techniques is that here, there is no separation of the solid phase from the solution necessary. The emission spectrum is collected in the presence of crystals and gives remarkably good results. The scattering of data points observed during the initial part of the curve is due to the changing number of crystals that are passing in front of the fiber optic end. As secondary nucleation commences and the number of crystals increases significantly, the flow cell is almost completely filled with crystals flowing past the fiber tip. Beyond a certain number, the emission spectrum is not affected by the number of crystals and there is a substantial reduction in the scattering of the data points. Work is ongoing in this area to improve the design so as to reduce this scattering.

### 7.3 Recommendations for future work

The utility of the experiment described in the previous section is manifold. It demonstrates that the emission spectrum of the probe can be collected *ex situ* by withdrawing a sample stream from the crystallizer without having to separate out the crystals. While in this experiment, the probe was added to the crystallizer, it would be relatively simple to change the experimental setup such that the probe is injected into the



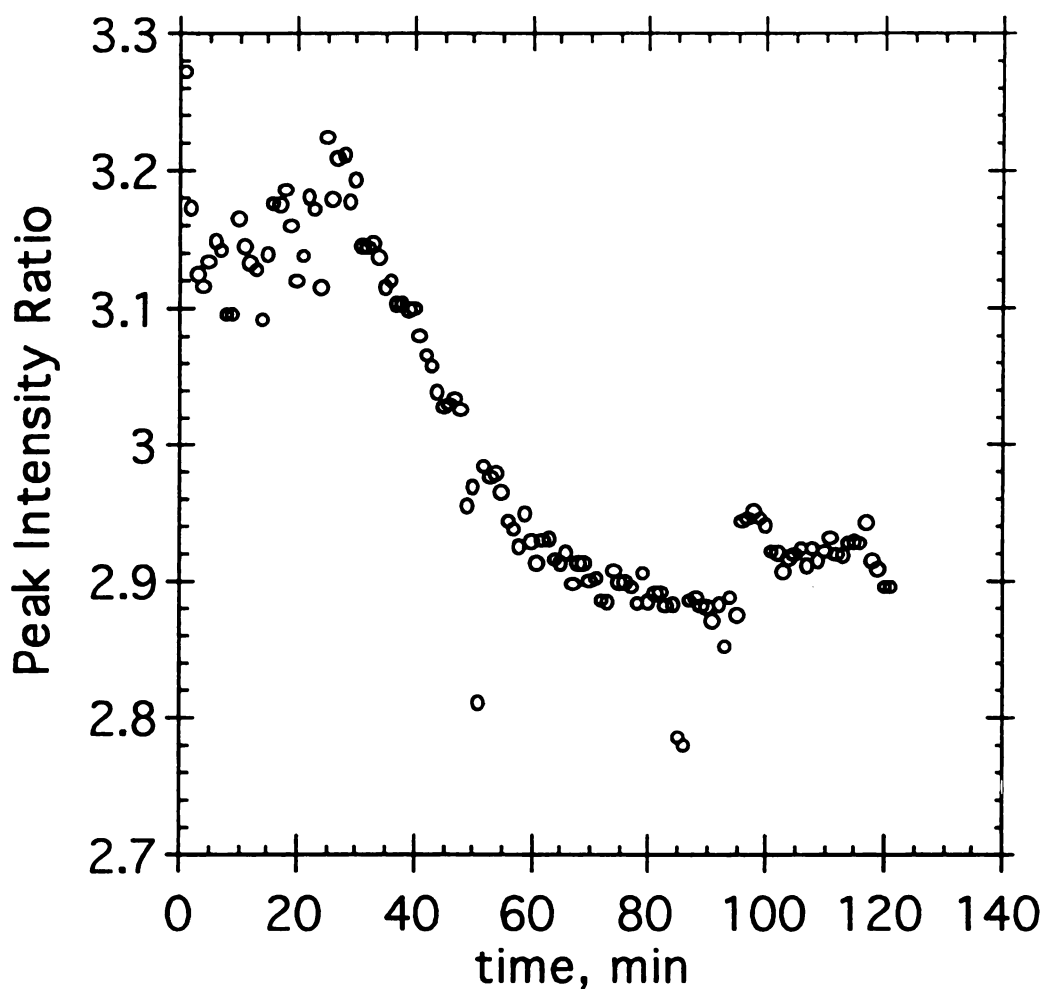


Figure 7.4 Typical desupersaturation curve of a seeded citric acid batch crystallization experiment using the apparatus shown in Figure 7.3. The experimental conditions were as follows: Temperature = 25 °C, initial supersaturation ( $c/c^*$ ) = 1.2, agitator speed = 400 rpm, probe (pyranine) concentration =  $1.0 \times 10^{-5}$  M, seeds (average size 660 microns) = 3 gms, excitation wavelength = 365 nm. The ordinate shows the Peak Intensity Ratio, defined as the ratio of the intensities of the emission peaks of pyranine at 449 nm and 520 nm.

flow cell directly by means of a syringe pump. This modification will be a primary focus of the continuing work in this area. Modifications in the design of the flow cell will also be required to incorporate an injection port for the probe solution. The design will also have to ensure adequate mixing of the probe with the sample stream before the emission spectrum is taken. This might require the probe to be injected first into some kind of a mixing chamber, either a mixing tee or a larger chamber with provision for physical agitation, that is placed before the flow cell. The overall objective being to incorporate this analytical technique into the control scheme for the crystallizer, it is important to miniaturize the whole technique as much as possible to shorten the lag times of the response. The miniaturization would require shortening the length of all the tubing to a minimum. The size of the tubing will have to be optimized very carefully, taking care that blockage of the lines from the crystals does not occur. Once all these parameters are optimized, it will be possible to incorporate this technique for measuring the concentration into a control scheme for the crystallizer.

The question of the further role of the sample stream exiting the flow cell has to be answered. Should the sample stream be returned to the crystallizer, or should it be sent to waste? The answer to this would depend on the scale of the crystallizer and the economics involved. In the case of a large scale crystallizer, where the sample volume is very small relative to the working volume, it may be preferable to send the sample to a waste stream. However, if the crystallizer is very small, it would not be possible to remove sample continuously without affecting the concentration inside the crystallizer. Also, if the compound being crystallized is quite expensive, the economics of the whole operation comes into the picture, and the sample stream cannot be discarded.

In these latter cases where the sample stream cannot be discarded, treatment of the sample stream to remove the probe molecules would be essential. The removal of the probe from the sample stream can be accomplished quite easily with the aid of ion exchange surfaces. As a pretreatment step, the sample stream should be heated so that all the crystals

dissolve. The dissolution can be achieved by passing the stream through a heater coil of sufficient length. The solution obtained has the probes in their anionic form. By passing this solution through a bed of anion exchange resins (such as those manufactured by Rohm and Haas under the trade name series IRA), the probe molecules can be exchanged onto the resin. The length of the bed and the residence time of the solution in the bed would have to be optimized keeping in mind the ion exchange capacity of the resin. The nature of the solute, the viscosity of the solution and the amount of probe in the sample stream would be other significant parameters to be considered for the design of the ion exchange bed. The only drawback to this technique would be the fact that the cationic sodium ions would still remain in solution (in the case of pyranine). If this is considered a problem, similar cation exchange material can be placed in the path of the stream to eliminate the cations. After this step, passing the sample stream through a heat exchanger to lower the temperature back to that in the crystallizer would complete the sample stream treatment necessary. The treated sample can be returned to the crystallizer with no effect other than the loss of a few crystals. As noted earlier, miniaturization of the whole process will significantly reduce such effects.

Once such a system is up and running, numerous experiments can be conducted that would be of interest in the field of crystallization. Preliminary experiments to expand the utility of this system would involve screening potential probe molecules for different crystallizing solutes. It has been our experience that there is no single fluorescent molecule that can be used for all solutes that might be of interest. It is essential to find probes that show a solvatochromic response in their emission spectra in the presence of the solution of the particular solute that is of interest. There is an extremely large number of fluorescent molecules that are used today for different applications. Only a few of those, though, will be suited any specific application. A comprehensive effort at screening this large number of fluorescent probes would be a necessary first step. It is envisaged that a list could be made of probes that are suited to be used with a particular class of compounds such as

sugars, carboxylic acids, amino acids, etc. Once such a list is available, it would be a simple matter for future researchers to pick a fluorescent probe that will work with a given solute.

An important area of interest is to study the effect of impurities on the crystallization process. When impurities are present in the mother liquor, it is well known that the kinetics of the process change that can result in an unspecified crystal size distribution. It is also quite likely that the habit of the resulting crystals change [7]. Studying the kinetics of such an impurity-affected system, along the lines of that described in Chapter 5 and 6, would give quantitative indications of the effect of the impurities.

### 7.3.1 ATR Fluorescence

Attenuated Total Reflectance (ATR) is a concept that is widely used with Infra Red and UV-Vis spectroscopies. Recently, ATR-FTIR spectroscopy has been very successfully used for the *in situ* measurement of supersaturation in maleic acid [8]. The use of ATR in fluorescence however, is quite limited. This is due to the inherent nature of fluorescence that requires the emitted light to be spatially separated from the incident light. This necessitates the introduction of a new light wave to carry the emitted light that has to cross a system boundary and enter the medium in which the internally reflected beam is passing through. Thus total internal reflection (that occurs in a single medium), which is the basis of ATR spectroscopy is not strictly possible. However, a slight variation has been used in which fluorescent molecules are coated onto the core of a fiber optic cable that is placed in the sample solution [9, 10]. The evanescent wave generated excites the fluorescent molecules and the emission is picked up either by the same fiber or by a different fiber placed alongside. This configuration has its advantages in that the probe is immobilized and the development of an analytical test kit of sorts is simpler. However, the immobilization procedure has to be optimized very carefully, as it is relatively easy to lose or alter the fluorescent properties of a molecule when it is immobilized. This aspect was

discussed in detail in Chapters 3 and 4. In spite of these concerns, ATR fluorescence holds tremendous promise in future research efforts.

## 7.4 Conclusions

With recent advances in fiber optic and spectrophotometer technologies, the development of an analytical sensor based on fluorescence for the measurement of concentration and supersaturation in a crystallizer has become a reality. Not only is the fluorescence technique capable of measuring the solution concentration, the kinetics of growth and nucleation can also be predicted. Once the kinetic parameters are known, the crystal size distribution can also be predicted using the theories of population balance. This predictive nature of the fluorescent probe technique makes it an extremely versatile tool in improving current crystallization operations and designing better control strategies for the future.

## 7.5 References

1. Z. Fang, In: *Flow Injection Separation and Concentration*. VCH, Weinheim, Germany. (1993).
2. B. Karlberg and G. E. Pacey. In: *Flow Injection Analysis A Practical Guide*. Elsevier, Amsterdam. (1989).
3. E. Ballesteros, M. Gallego, and M. Valcarcel. *Anal Chem*, **68**, 322-326, (1996).
4. F. Grases, A. Costa-Bauza, and J. G. March. *Analysis*, **21**, 95-99, (1993).
5. F. Grases and P. March. *Analytica Chimica Acta*, **219**, 89-95, (1989).
6. J. Thomsen, K. S. Johnson, and R. L. Petty. *Anal. Chem.*, **55**, 2378, (1983).
7. D. L. Klug. In: *Handbook of Industrial Crystallization*. Ed. Allan S. Myerson. Butterworth-Heinemann, USA. (1993).
8. D. D. Dunuwila, An Investigation of the Feasibility of Using In Situ ATR FTIR Spectroscopy in the Measurement of Crystallization Phenomenon for Research and Development of Batch Crystallization Processes. PhD Thesis, Michigan State University. (1996).

9. Cheng, Y. L., Lok, B. K., and Robertson, C. R. In: *Surface and Interfacial Aspects of Biomedical Polymers*. Ed. J. D. Andrade. Vol 2., Plenum Press, New York. (1985).
10. Hlady, V., Van Wagenan, R. A., and Andrade, J. D. In: *Surface and Interfacial Aspects of Biomedical Polymers*. Ed. J. D. Andrade. Vol 2., Plenum Press, New York. (1985).

## Chapter 8

### CONCLUSIONS

The fluorescence probe technique is shown to be well suited for accurately measuring the supersaturation in aqueous solutions of citric acid and in sugar solutions. The measurement is more sensitive than those obtained by conventional analytical techniques such as refractometry. The nature of the measurement also facilitates the *in situ* measurement of supersaturation in a crystallizer without separation of the solid crystals from the solution. The relative supersaturation is defined in terms of a parameter ( the Peak Intensity Ratio), that is generated by monitoring the fluorescence of probe molecules placed in contact with the crystallizing solution.

Pyranine is currently the best choice for use as a fluorescent probe. This recommendation is based partly on its strong solvatochromic behavior and partly on its high quantum efficiency and long shelf life.

Three of the seven colors listed by the FDA as food grade are well suited for use as supersaturation sensors in sucrose solutions. These are FD&C Blue No. 1, FD&C Red No. 40, and FD&C Green No. 3.

Anionic ion exchange membranes can be used to immobilize these probe molecules for use in immersible sensors. However, the immobilization procedure causes a reduction in sensitivity and performance.

The kinetic parameters of crystal nucleation and growth can be estimated by modeling the desupersaturation curve that is generated by monitoring the fluorescence of

pyranine during the course of an isothermal batch crystallization experiment. The changing supersaturation in the crystallizer is reflected by the change in the fluorescence behavior of pyranine. The desupersaturation curve generated is then modeled to fit theoretical equations of crystal nucleation and growth to give the various kinetic parameters such as growth and nucleation rate constants and the growth and nucleation orders.

Although the presence of the probe in contact with the solution does not appear to affect the crystallization process in general, it is still desirable to contact the probe with the crystallizing solution in an *ex situ* manner, so that no contamination of the crystals is possible. A system is set up based on the principle of Reverse Flow Injection Analysis, that is well suited to make the necessary measurements by drawing out a sample of the slurry from a crystallizer and contacting the probe with it in an *ex situ* manner. Results obtained show a very close correspondence with the experiments where in the measurements were made *in situ*. Future research efforts will attempt to modify and perfect this new setup as a first step in expanding the scope of the fluorescence probe technique.



## APPENDIX

## Appendix

Table A1      Raw data for Figure 2.4

Citric acid concentration wt%	Peak Intensity Ratio
10	0.34835
20	0.58491
30	0.90729
40	1.3249
50	1.9628
65	3.1494

Table A2      Raw data for Figure 2.5

Supersaturation	Peak Intensity Ratio
0.081917	3.93
-0.072643	3.02
-0.2272	1.99
-0.38176	1.35
-0.53632	0.903
-0.69088	0.589
-0.84544	0.354
- 1	0.0512

Table A3 Raw data for Figure 2.6

Citric Acid Concentration (wt%)	pH
10	1.51
20	1.24
30	1.06
40	0.78
50	0.51
65	0.09

Table A4 Raw data for Figure 2.7

pH of HCl-NaOH solutions	Peak Intensity Ratio	pH of citric acid solutions	Peak Intensity Ratio
0.12	1.3364	1.54	0.34835
0.3	0.90244	1.28	0.58491
0.5	0.70972	1.06	0.90729
0.74	0.60671	0.78	1.3249
1	0.4647	0.51	1.9628
1.26	0.28647	0.09	3.1494
1.5	0.19378		

Table A5 Raw data for Figure 2.8

Citric Acid concentration wt%	Peak Intensity Ratio
10	1.54
20	1.28
30	1.06
40	0.78
50	0.51
65	0.09

Table A6 Raw data for Figure 3.6

Sucrose Concentration, wt%	Peak Intensity Ratio
30	0.26825
50	1.0721
65	5.5909

Table A7      Raw data for Figure 3.7

Sucrose Concentration, wt%	Peak Intensity Ratio
0	1
10	1.9709
30	4.4627
50	9.4343
65	22.281

Table A8      Raw data for Figure 3.9

Sucrose Concentration, wt%	Peak Intensity Ratio
10	1.6064
30	2.3278
50	3.2114
65	4.5053

Table A9      Raw data for Figure 4.4

Sucrose Concentration, wt%	Peak Intensity Ratio
10	1.825
30	1.925
50	1.99
65	2.08

Table A10 Raw data for Figure 5.2

Time (minutes)	Peak Intensity Ratio	Time (minutes)	Peak Intensity Ratio (contd.)
3	3.1094	36	3.0642
4	3.1104	37	3.0559
5	3.1096	38	3.0485
6	3.1069	39	3.0401
7	3.1044	40	3.038
8	3.1051	41	3.0297
9	3.1074	42	3.0157
10	3.1022	43	3.0066
11	3.1033	44	2.9946
12	3.099	45	2.9877
13	3.1031	46	2.9794
14	3.1003	47	2.9686
15	3.0969	48	2.9608
16	3.0985	49	2.9523
17	3.0993	50	2.9483
18	3.0973	51	2.9358
19	3.0969	52	2.9322
20	3.0964	53	2.9238
21	3.0937	54	2.9168
22	3.0942	55	2.9116
23	3.0934	56	2.9037
24	3.0899	57	2.8991
25	3.0863	58	2.8947
26	3.0903	59	2.8853
27	3.087	60	2.8839
28	3.0881	61	2.88
29	3.0893	62	2.8743
30	3.0845	63	2.869
31	3.0812	64	2.8638
32	3.0803	65	2.8617
33	3.0736	66	2.8555
34	3.0689	67	2.8556
35	3.0703	68	2.8498

Table A10 Continued

69	2.8455
70	2.8451
71	2.84
72	2.8345
73	2.8341
74	2.8315
75	2.8288
76	2.8279
77	2.8252
78	2.8248
79	2.8205
80	2.8187
81	2.8147
82	2.8122
83	2.8116
84	2.8146
85	2.8073
86	2.8082
87	2.8052
88	2.8044
89	2.803
90	2.8021
91	2.8021



Table A11 Raw data for Figure 5.3

Time (minutes)	Peak Intensity	Time (minutes)	Peak Intensity (contd.)
3	157.66	36	253.11
4	170.87	37	289.93
5	165.76	38	315.91
6	168.41	39	344.63
7	155.07	40	387.39
8	168.33	41	414.74
9	171.12	42	426.07
10	164.46	43	439.59
11	165.06	44	442.67
12	159.94	45	498.79
13	169.08	46	489.39
14	165.8	47	521.19
15	155.34	48	533.19
16	160.37	49	527.12
17	164.55	50	569.66
18	157.77	51	570.59
19	159.69	52	598.47
20	164.41	53	613.42
21	159.6	54	639.81
22	170.12	55	654.97
23	171.34	56	657.33
24	165.27	57	662.58
25	159.62	58	676.91
26	164.06	59	644.88
27	171.19	60	720.57
28	177.51	61	708.97
29	182.05	62	707.28
30	184.91	63	696.55
31	200.43	64	697.01
32	199.85	65	720.27
33	214.55	66	700.43
34	222.9	67	703.04
35	248.56	68	736.31

Table A11 Continued

69	703.48
70	718.11
71	717.17
72	706.62
73	723.05
74	713.09
75	713.4
76	755.45
77	756.91
78	778.23
79	722.21
80	772.34
81	743.05
82	759.7
83	770.6
84	780.55
85	751.93
86	777.68
87	785.93
88	766.53
89	754.09
90	770.1
91	770.1

Table A12 Raw data for Figure 5.4

Time (minutes)	3 gms	15 gms	36 gms
1	3.096	3.096	3.096
2	3.097	3.081	3.0994
3	3.0962	3.0874	3.1085
4	3.0935	3.083	3.0996
5	3.091	3.0847	3.106
6	3.0917	3.0888	3.0955
7	3.094	3.0837	3.0864
8	3.0889	3.0803	3.0737
9	3.0899	3.0767	3.0827
10	3.0856	3.0829	3.0883
11	3.0898	3.0864	3.0799
12	3.087	3.0799	3.08
13	3.0836	3.0769	3.0883
14	3.0852	3.0731	3.0728
15	3.0859	3.0738	3.074
16	3.084	3.0727	3.0751
17	3.0835	3.0652	3.076
18	3.083	3.0771	3.0571
19	3.0804	3.0554	3.0601
20	3.0809	3.059	3.0479
21	3.0801	3.0581	3.0506
22	3.0766	3.0699	3.0366
23	3.073	3.0693	3.0336
24	3.077	3.0562	3.0203
25	3.0737	3.0553	3.0159
26	3.0748	3.0493	3.0093
27	3.076	3.0609	3.004
28	3.0712	3.0307	2.9978
29	3.0679	3.0394	2.993
30	3.067	3.0208	2.9842
31	3.0604	3.015	2.966
32	3.0557	3.0051	2.9658

Table A12 continued

33	3.057	3.01	2.9675
34	3.051	2.9845	2.963
35	3.0427	2.9749	2.9429
36	3.0354	2.9707	2.942
37	3.027	2.9612	2.9376
38	3.0249	2.9466	2.9351
39	3.0166	2.9528	2.9349
40	3.0027	2.9338	2.933
41	2.9936	2.939	2.911
42	2.9817	2.928	2.9103
43	2.9748	2.9279	2.9084
44	2.9666	2.9203	2.9013
45	2.9558	2.9031	2.8965
46	2.948	2.9092	2.8855
47	2.9396	2.8973	2.893
48	2.9356	2.883	2.8845
49	2.9232	2.8956	2.8753
50	2.9196	2.8811	2.8816
51	2.9112	2.8878	2.8762
52	2.9043	2.8746	2.8768
53	2.899	2.8807	2.8651
54	2.8911	2.8691	2.8592
55	2.8866	2.8708	2.8574
56	2.8822	2.862	2.8488
57	2.8729	2.856	2.845
58	2.8714	2.8515	2.8474
59	2.8676	2.854	2.8542
60	2.862	2.8519	2.8542
61	2.8566	2.8483	2.8409
62	2.8515	2.8483	2.8356
63	2.8493	2.84	2.842
64	2.8432	2.8403	2.8384
65	2.8433	2.8403	2.8401
66	2.8375	2.8243	2.8313
67	2.8332	2.8421	2.8408

Table A 12 continued

68	2.8329	2.8237	2.8403
69	2.8278	2.8331	2.8359
70	2.8223	2.8225	2.8252
71	2.8219	2.8254	2.837
72	2.8193	2.8229	2.8422
73	2.8166	2.8259	2.8236
74	2.8157	2.8184	2.8248
75	2.813	2.8129	2.8299
76	2.8126	2.8177	2.8189
77	2.8084	2.8287	2.8246
78	2.8066	2.8173	2.8271
79	2.8025	2.8205	2.8301
80	2.8001	2.8138	2.8308
81	2.7995	2.8172	2.8266
82	2.8025	2.8148	2.8185
83	2.7952	2.8217	2.8285
84	2.7961	2.8058	2.8246
85	2.7931	2.8117	2.8232
86	2.7923	2.8158	2.8256
87	2.791	2.7998	2.8189
88	2.79	2.813	2.8159
89	2.79	2.7976	2.8189
90		2.8067	2.8305
91		2.8035	2.8169
92		2.8127	2.8171
93		2.8146	2.8158
94		2.8098	2.824
95		2.8106	2.8156
96		2.8086	2.8136
97		2.8098	2.8261
98		2.8129	2.8216
99		2.7987	2.8098
100		2.8009	2.8258
101		2.8157	2.8175
102		2.7983	2.8202

Table A12 continued

103	2.7954	2.8125
104	2.806	2.8114
105	2.8065	2.8122
106	2.7991	2.825
107	2.8007	2.8179
108	2.8031	2.8292
109	2.8053	2.8261
110	2.8158	2.8145
111	2.8082	2.8242
112	2.805	2.8222
113	2.792	2.8372
114	2.7976	2.8161
115	2.8089	2.8215
116	2.8103	2.8129
117	2.8073	2.8118
118	2.8014	2.8184
119	2.8265	2.8259
120	2.8109	2.837
121	2.8109	2.837

Table A13 Raw data for Figure 5.5

Time (minutes)	20 deg C	25 deg C	30 deg C
1	3.062	3.062	3.062
2	3.0713	3.062	3.059
3	3.0785	3.062	3.0556
4	3.0871	3.063	3.0565
5	3.0859	3.0622	3.0541
6	3.0812	3.0596	3.0545
7	3.0884	3.057	3.0522
8	3.0924	3.0578	3.0516
9	3.0883	3.06	3.0551
10	3.0889	3.055	3.0526
11	3.0862	3.056	3.0437
12	3.0905	3.0517	3.0482
13	3.0925	3.0558	3.0468
14	3.0912	3.0531	3.0438
15	3.0871	3.0497	3.0448
16	3.0926	3.0513	3.0402
17	3.0937	3.052	3.038
18	3.0901	3.0501	3.0415
19	3.0961	3.0497	3.0413
20	3.1036	3.0492	3.0403
21	3.0958	3.0465	3.0354
22	3.0976	3.047	3.0389
23	3.093	3.0462	3.034
24	3.0925	3.0428	3.0404
25	3.0973	3.0392	3.0326
26	3.0939	3.0432	3.0317
27	3.1	3.0399	3.0342
28	3.0987	3.0411	3.0315
29	3.0973	3.0422	3.0263
30	3.1047	3.0375	3.0288
31	3.0968	3.0342	3.0348
32	3.0978	3.0333	3.0269
33	3.095	3.0267	3.0267

Table A 13 continued

34	3.0957	3.0221	3.0279
35	3.0988	3.0235	3.0223
36	3.098	3.0175	3.0193
37	3.1028	3.0093	3.0206
38	3.1011	3.0021	3.0153
39	3.0934	2.9938	3.015
40	3.0937	2.9917	3.0106
41	3.0964	2.9835	3.0126
42	3.0919	2.9697	3.0101
43	3.0942	2.9608	3.0054
44	3.0984	2.9489	2.9972
45	3.0932	2.9422	3.0005
46	3.0895	2.934	2.9947
47	3.0998	2.9234	2.9866
48	3.0974	2.9156	2.9862
49	3.1006	2.9073	2.9808
50	3.0902	2.9033	2.9756
51	3.0963	2.8911	2.9658
52	3.0968	2.8875	2.9594
53	3.0955	2.8792	2.9542
54	3.0943	2.8724	2.9524
55	3.0924	2.8672	2.9441
56	3.09	2.8594	2.9374
57	3.0907	2.8549	2.9291
58	3.0944	2.8505	2.9285
59	3.0881	2.8414	2.9221
60	3.0887	2.8399	2.9151
61	3.0851	2.8361	2.9124
62	3.0861	2.8305	2.9055
63	3.0837	2.8252	2.9019
64	3.0786	2.8202	2.9004
65	3.0726	2.818	2.8912
66	3.0725	2.812	2.8898
67	3.0743	2.8121	2.8877
68	3.0742	2.8063	2.8815



Table A 13 continued

69	3.07	2.8021	2.8815
70	3.0698	2.8018	2.8701
71	3.0619	2.7967	2.8753
72	3.0559	2.7913	2.8663
73	3.0595	2.7909	2.8643
74	3.0524	2.7883	2.8631
75	3.0451	2.7857	2.8568
76	3.0403	2.7848	2.86
77	3.0373	2.7821	2.8567
78	3.034	2.7817	2.8559
79	3.0274	2.7775	2.8531
80	3.0289	2.7758	2.8516
81	3.0198	2.7717	2.8489
82	3.0092	2.7693	2.8451
83	3.0047	2.7687	2.8434
84	2.9947	2.7717	2.8426
85	2.9942	2.7645	2.8381
86	2.9851	2.7654	2.8356
87	2.9843	2.7624	2.8374
88	2.972	2.7617	2.8341
89	2.9693	2.7603	2.836
90	2.96E+00	2.7594	2.8309
91	2.95E+00	2.7594	2.8291
92	2.9562		2.8304
93	2.9515		2.8273
94	2.9323		2.8218
95	2.9484		2.8229
96	2.9202		2.8248
97	2.9194		2.8221
98	2.9192		2.8194
99	2.9144		2.8236
100	2.9058		2.8164
101	2.9037		2.8147
102	2.8916		2.8149
103	2.8963		2.8184

Table A13 continued

104	2.8909		2.813
105	2.8834		2.8165
106	2.8715		2.8123
107	2.8682		2.8121
108	2.8661		2.8086
109	2.8639		2.8079
110	2.8638		2.8063
111	2.8546		2.808
112	2.8534		2.8064
113	2.8525		2.8054
114	2.8459		2.8053
115	2.8536		2.8023
116	2.8407		2.8031
117	2.8264		2.803
118	2.846		2.8043
119	2.8366		2.8048
120	2.8255		2.80E+00
121	2.8255		2.80E+00

Table A14 Raw data for Figure 5.6

Time (minutes)	Probe Concentration 1e-05 M	Probe Concentration 1e-06 M	Probe Concentration 5e-05 M
1	0.10967	0.11121	0.1077
2	0.10967	0.10913	0.10688
3	0.10968	0.10914	0.10673
4	0.11003	0.10941	0.10586
5	0.10975	0.10784	0.10539
6	0.10878	0.11007	0.10442
7	0.10787	0.1077	0.10388
8	0.10814	0.10789	0.10332
9	0.10894	0.10709	0.10263
10	0.10712	0.10628	0.10275
11	0.10749	0.10899	0.10233
12	0.10594	0.10418	0.10148
13	0.10743	0.1068	0.10192
14	0.10643	0.10502	0.1009
15	0.10521	0.10399	0.10036
16	0.10578	0.10404	0.10054
17	0.10605	0.10248	0.099034
18	0.10535	0.10327	0.098181
19	0.1052	0.10599	0.099819
20	0.10502	0.1023	0.098767
21	0.10407	0.10077	0.098087
22	0.10425	0.10337	0.098167
23	0.10395	0.10026	0.098093
24	0.1027	0.098061	0.097186
25	0.10141	0.097969	0.095737
26	0.10285	0.098122	0.095713
27	0.10166	0.09956	0.095962
28	0.10208	0.094771	0.095597
29	0.10251	0.093509	0.095885
30	0.10077	0.094063	0.094662
31	0.099596	0.091146	0.093684
32	0.099271	0.091321	0.095483

Table A 14 continued

33	0.09689	0.088795	0.093888
34	0.095207	0.087261	0.092571
35	0.095703	0.083709	0.092878
36	0.093525	0.080677	0.092145
37	0.09057	0.077522	0.089994
38	0.087942	0.076777	0.090251
39	0.084946	0.071783	0.08973
40	0.084185	0.068865	0.088926
41	0.081217	0.061886	0.088048
42	0.076223	0.063919	0.087402
43	0.072975	0.060907	0.085479
44	0.068687	0.055243	0.085241
45	0.066235	0.054482	0.083549
46	0.063271	0.049691	0.08136
47	0.059427	0.047704	0.079779
48	0.056619	0.043834	0.079439
49	0.053612	0.043321	0.077496
50	0.052169	0.042043	0.074042
51	0.047728	0.036495	0.072315
52	0.046432	0.036011	0.069782
53	0.043414	0.033315	0.068222
54	0.040943	0.030909	0.065834
55	0.03906	0.029658	0.063187
56	0.036241	0.028249	0.060506
57	0.03461	0.028183	0.058478
58	0.033037	0.026749	0.056458
59	0.029708	0.023613	0.052827
60	0.029182	0.022186	0.0508
61	0.027818	0.021666	0.049971
62	0.025784	0.017177	0.04718
63	0.023862	0.015301	0.045373
64	0.022024	0.014004	0.043529
65	0.021257	0.01578	0.041518
66	0.019074	0.016397	0.039014
67	0.019086	0.012273	0.038187

Table A 14 continued

68	0.017013	0.013063	0.036181
69	0.015476	0.012175	0.03357
70	0.015356	0.0097865	0.033309
71	0.01354	0.0095951	0.030608
72	0.011573	0.0071082	0.029635
73	0.011417	0.0089512	0.028983
74	0.010477	0.0078827	0.028515
75	0.0095228	0.0045987	0.025755
76	0.0091971	0.0081414	0.02443
77	0.0082284	0.0052404	0.022689
78	0.0081023	0.0053052	0.021888
79	0.006582	0.0054979	0.021205
80	0.0059395	0.0027778	0.019377
81	0.0044793	0.002612	0.01911
82	0.0036083	0.0046615	0.017858
83	0.0033799	0.0046215	0.017196
84	0.0044541	0.0036372	0.016076
85	0.0018657	0.0002051	0.014865
86	0.0021626	0.0032405	0.014629
87	0.0010999	0.0013043	0.013513
88	0.00082795	0.00031779	0.014106
89	0.00033224	0.0041843	0.012281
90	1.68E-06	-0.0013255	0.011172
91	1.68E-06	0.0020082	0.011556
92		-0.0013985	0.0090085
93		-0.00092809	0.010012
94		0.00090257	0.010171
95		-7.98E-05	0.010284
96		-0.00090817	0.0091739
97		-0.0058984	0.0078122
98		-0.0039394	0.0078776
99		-0.0033395	0.0072616
100		-0.00071599	0.0058647
101		-0.00073313	0.0048532
102		-0.0021225	0.0056013

Table A 14 continued

103	-0.0080443	0.0060486
104	-0.0018527	0.0054515
105	-0.0055465	0.0047842
106	-0.0060348	0.0049872
107	-0.00151	0.0037122
108	-0.0040607	0.0029977
109	-0.00066716	0.0029724
110	-0.0025145	0.0024399
111	0.0012106	0.001629
112	-0.0046223	0.0021135
113	-0.0022702	0.0034755
114	-0.0013974	0.0013731
115	-0.0046406	0.0024117
116	-0.0014245	0.0017937
117	-0.0050638	0.00055298
118	-0.00068145	0.0020173
119	-0.0058775	0.00013278
120	-7.84E-06	2.23E-06
121	-7.84E-06	2.23E-06

MICHIGAN STATE UNIV. LIBRARIES



31293015550464